

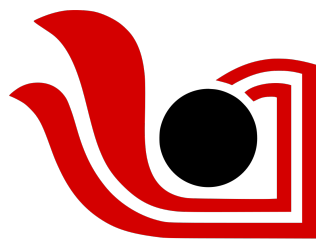
Mechanics of Single Flexible Polymer Chains using AFM Nanorheology

A thesis submitted in partial fulfillment of the
requirements for the degree of
Doctor of Philosophy

by

Vikhyaat Ahlawat

20142033



IISER PUNE

Indian Institute of Science Education and
Research Pune-411008

August, 2021

Abstract

In this thesis, I investigate the role of Atomic Force Microscope (AFM) nanorheology in quantitative estimate of stiffness for neutral flexible polymers and biopolymers. A major part of my thesis explores the possibility of bias in traditional pulling experiments with single molecule techniques of Atomic Force Microscope (AFM). In past, AFM based pulling experiments produces force-extension relation for polymers which have extensively reported unphysically low value of persistence length, a key and fundamental elasticity parameter.

The thesis advances the current state-of-the-art in measuring single polymer elasticity in two aspects. First, it proposes active oscillatory rheology as a method to accurately measure entropic elasticity of polymer. Second, it further validates the methodology of active rheology with a home-built fiber-interferometer AFM. By active oscillation the AFM cantilever at off-resonance frequency and slow pulling on polymer, we directly estimate stiffness of polymer. The active oscillations of AFM cantilever-probe with sub-nm amplitudes and off-resonance (< 1 KHz) frequencies, ensured that overall response is linear and dominated by elastic response. By simultaneous oscillations and slow pulling on polymer, I found that stiffness measured from oscillatory response showed significant deviation from pulling force-extension curves. This was true only in good solvent whereas polymer in poor solvent showed no deviation. Analysis of stiffness with entropic WLC model yielded a large and physical persistence length in good solvents. The value also matched with constant force measurements done with magnetic tweezers. An additional free energy contribution explains no deviation in poor solvent. The results were rationalized with statistical mechanics of combined cantilever-polymer system and hints at importance of coupling between AFM cantilever-probe and intrinsic polymer response.

We also performed oscillatory measurements with home-built fiber-interferometer AFM. The fiber-interferometer assembly measures cantilever deflection directly at a local point in contrast to commercial beam deflection methods. This becomes important while oscillating the cantilever base in liquids. A local detection at a point provides a straightforward interpretation of stiffness, independent of complications from cantilever hydrodynamics and further validated our methodology. In addition, fluctuations about measured stiffness showed expected dependence on the size of polymer chain. This was also not observed in traditional pulling experiments.

The last part of my thesis deals with role of mechanical forces in proteins. In this regard, I pursued to understand how mechanical forces dictates the function and self-assembly of proteins. Specifically, I compared protein Titin with mechanical role inside cardiac muscle and a non-mechanical membrane protein using thermal fluctuations. Using fluctuation-dissipation relation, the power spectral density (PSD) of AFM thermal deflection reproduces the elastic response of protein. Compared to active method, we showed that fluctuations are not sensitive to the response of polymer due to dominance of viscous and elastic stiffness of a large AFM cantilever.

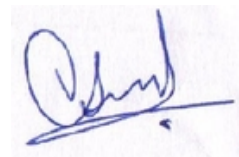
Dedication

To my family

Declaration

I declare that the thesis submitted is record of original research work carried out by me. I also declare that I have adhered to all academic and research ethics and have not represented a fabricated or falsified idea/data/source in my submission. Wherever other's ideas have been included, I have adequately cited the original sources. I understand that violation of the above will be cause for disciplinary action by the Institute and can evoke penal action from the sources which have thus not been properly cited or from whom prior permissions have not been taken.

Place: Pune

A handwritten signature in blue ink, appearing to be 'Vikhyat', written over a horizontal line.

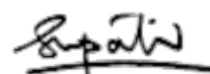
Date: April 13, 2022

Vikhyat

Certificate

This is to certify that the thesis entitled **Mechanics of Single Polymer Chain Using AFM Nanorheology** submitted by **Vikhyaat Ahlawat** is a record of bonafide work carried out by the candidate, under my supervision. The contents of this report have not been submitted and will not be submitted either in part or in full, for the award of any other degree or diploma in this institute or any other institute or university.

Date: April 13, 2022



(Supervisor)

Acknowledgements

I express sincere thanks to my supervisor **Dr. Shivprasad Patil**, for his motivation and continuous encouragement. He has been instrumental in shaping my research work. Freedom to chose problems in the lab and facing up to the challenges has i think made us better at our research.

I am grateful to my advisory committee members , **Dr. Arijit Bhattacharyay** and **Dr. Apratim Chatterjee** for their critical input and want to thank IISER Pune for the fellowship and many other resources needed for my research.

I like to acknowledge the support rendered by my colleagues and especially Dipti throughout my research work. It would have been difficult without her.

I wish to extend gratitude to my parents for all their support during my research.

Vikhyaat

Contents

| | | |
|----------|--|-----------|
| 1 | Introduction | 14 |
| 1.1 | Historical Perspective | 14 |
| 1.2 | Polymers and Biopolymers | 16 |
| 1.2.1 | Basic definitions and types | 16 |
| 1.2.2 | Polymer flexibility and conformations | 17 |
| 1.2.3 | Synthetic Polymers | 19 |
| 1.2.4 | Proteins | 20 |
| 1.3 | Statistical mechanics of linear polymer chains | 21 |
| 1.3.1 | Configurational statistics of ideal polymer chains | 21 |
| 1.3.2 | Real Chains-Excluded volume | 24 |
| 1.4 | Statistical mechanics of real polymer chains under force | 27 |
| 1.5 | Review of single molecule mechanical experiments | 30 |
| 1.5.1 | Atomic Force Microscopy(AFM) | 31 |
| 1.5.2 | Optical Tweezers | 32 |
| 1.5.3 | Magnetic Tweezers | 33 |
| 1.6 | Linear response and fluctuations - Active and Passive Rheology | 34 |
| 1.7 | Motivation and Objective | 37 |
| 1.8 | Scope and Thesis outline | 38 |
| 2 | Force Spectroscopy using Atomic Force Microscope | 42 |
| 2.1 | General overview and chapter organisation | 42 |
| 2.1.1 | Chapter Organisation | 43 |
| 2.2 | Fundamentals of AFM | 43 |
| 2.2.1 | Principle of AFM- a force measurement device | 43 |
| 2.2.2 | Tip-sample interactions | 45 |
| 2.2.3 | Force-distance curves | 47 |
| 2.2.4 | Interpretation of force-distance curve | 50 |
| 2.3 | Cantilever mechanics | 52 |
| 2.4 | AFM system components | 54 |
| 2.4.1 | Deflection Detection Methods | 55 |
| 2.4.2 | Piezoelectric Positioners | 57 |
| 2.4.3 | Feedback loop | 59 |
| 2.5 | Experimental calibrations | 60 |
| 2.5.1 | Spring constant calibration | 60 |
| 2.6 | Dynamic-AFM | 61 |
| 2.6.1 | Cantilever Dynamics | 61 |
| 2.6.2 | Hydrodynamics of cantilever | 63 |
| 2.6.3 | Cantilever excitation methods | 63 |

| | | |
|----------|---|------------|
| 2.6.4 | Analytic theory of Dynamic AFM in liquids | 64 |
| 2.6.5 | Lock-in Technique | 66 |
| 2.7 | Chapter Summary | 66 |
| 3 | Active Rheology of Single Flexible Synthetic Polymer Chain in Different Solvents | 68 |
| 3.1 | Introduction | 68 |
| 3.1.1 | Poly(ethylene)glycol | 73 |
| 3.1.2 | Polystyrene | 78 |
| 3.1.3 | Deconvolution Principle | 80 |
| 4 | Active Rheology Measurements on Flexible Polymers using Interferometer based AFM | 89 |
| 4.1 | Introduction | 89 |
| 4.2 | Materials and Methods | 90 |
| 4.2.1 | Sample preparation | 90 |
| 4.2.2 | Fiber-Interferometer AFM | 91 |
| 4.2.3 | Modelling cantilever-polymer dynamics | 93 |
| 4.3 | Results and Discussion | 93 |
| 4.3.1 | Polyethylene Glycol (PEG) | 93 |
| 4.3.2 | Polystyrene | 95 |
| 4.4 | Fluctuations about mean | 96 |
| 4.5 | Explanation of Deviation | 97 |
| 4.6 | Chapter Summary | 98 |
| 5 | Passive Rheology measurements on Protein Molecules | 105 |
| 5.1 | Introduction | 105 |
| 5.2 | Materials and Methods | 107 |
| 5.3 | Results and Discussion | 109 |
| 5.3.1 | Bacteriorhodopsin | 109 |
| 5.3.2 | I27 repeats | 112 |
| 5.3.3 | Explanation | 113 |
| 5.4 | Comparison between Active and Passive Rheology | 116 |
| 5.5 | Chapter Summary | 116 |
| 6 | Conclusion | 119 |
| 6.1 | Summary and Conclusions | 119 |
| 6.2 | Future Direction | 120 |

List of Figures

| | | |
|------|--|----|
| 1.2 | Random coil conformations of polymer chain | 17 |
| 1.3 | Torsion angle Ψ of zero about the C-C bond represent a trans conformer while 120° represent a gauche conformer for the repeat unit of polyethylene. | 18 |
| 1.4 | Synthetic polymers of polyethylene(glycol)(PEG) and polystyrene . . . | 19 |
| 1.5 | In the <i>ttg</i> conformation of repeat unit O-CH ₂ -CH ₂ -O, it is possible to form two hydrogen bonds (red line) with adjacent oxygen's(blue) with water molecule. For <i>ttt</i> or all-trans conformation, there is possibility of only one hydrogen bond with water. As a result of hydrogen bonding, <i>ttg</i> is shorter in length and more energetically stable. | 19 |
| 1.6 | Globular and Membrane protein used in this thesis. | 21 |
| 1.7 | Flexibility mechanism of a polymer | 22 |
| 1.8 | Excluded-volume interaction. On the left is the ideal chain configurations with allowed self-intersectiopns. On the right is the real chain configuration with excluded spherical shell representing each segment of the chain. | 24 |
| 1.9 | In Flory theory, an assumption of uniform concentration of polymer segments in spherical volume $V \sim R^3$ is made. A connected chain on the left in volume V is viewed as being made up of disconnected segments spread uniformly in volume V | 26 |
| 1.10 | A Worm like chain | 29 |
| 1.13 | A basic setup of a magnetic tweezer experiment. It includes a DNA molecule tethered between a paramagnetic bead and glass surface. Paramagnetic bead is trapped in a gradient of magnetic field with a net force acting in upward direction. | 34 |
| 2.1 | The principle of AFM operation | 44 |
| 2.2 | The graph shows distance variation of tip-sample interaction forces. The variation has both short range repulsive and long range attractive contributions. | 45 |
| 2.4 | The conversion of a force distance profile to force-displacement profile. | 49 |
| 2.6 | The enlarged view of a section of cantilever at position x before and after the bending due to force. A thin segment of the cantilever with thickness dy is located at a distance $+y$ from the neutral axis. After bending through an angle $d\theta$, the length of the segment changes from l to $l + dl$ | 54 |
| 2.7 | A schematic for components that form an AFM system. 1 AFM head and piezoelectoc stage. 2 HV electronics. 3 DSP and computer software. | 55 |

| | | |
|------|---|----|
| 2.9 | Optical-fiber based AFM deflection detection | 57 |
| 2.10 | The top panel shows the interference pattern where X-axis is separation between fiber-tip and cantilever backside and Y-axis is intensity. In this, quadrature point are shown by a green square. The bottom panel is just the double derivative signal to intensity pattern in top panel, to locate the maximum slope position (quadrature points) on the interference pattern. | 58 |
| 2.11 | | 58 |
| 2.12 | The feedback controller | 59 |
| 2.13 | | 62 |
| 2.14 | Piezo and Magnetic excitation modes of oscillating the cantilever . . . | 64 |
| 3.1 | A schematic of experimental setup shows in-phase (X) and quadrature (Y) amplitude components of lock-in amplifier with a polymer attached between the tip and sample surface. A small piezo drive oscillates the cantilever with off resonance frequency ($\sim 1KHz$) and deflection amplitude from photodiode forms an input channel of lock-in amplifier. | 71 |
| 3.2 | Drive amplitude A_b calibration against an externally applied drive voltage using home-built fiber-interferometer detection. A drive frequency of 1 KHz was chosen for calibration. | 72 |
| 3.3 | a) Force-extension curves for PEG in 2-propanol and b) its rescaling with apparent contour lengths. | 73 |
| 3.4 | a) Normalized force-extension curves in 2-propanol fitted to WLC. Persistence length estimated is $l_p = 0.13$ nm. b) Normalized force-extension curves in water fitted with Two-state FJC model. The estimated Kuhn Length is 0.24 nm. | 74 |
| 3.5 | Expected versus Measured stiffness-extension behavior in good solvent. | 75 |
| 3.6 | The raw profiles for PEG in water which include force-extension curve in constant velocity(~ 60 nm/sec) experiment (black) and lock-in amplifier's in-phase X-signal amplitude (red) and quadrature Y signal amplitude (green). | 76 |
| 3.7 | The figure shows comparisons between stiffness-extension data for PEG obtained by oscillatory response and simultaneously measured force-extension curve a) For PEG in water, derivative of WLC which was fitted to force-extension data in pulling experiments(blue dash) with $l_p = 0.13$ nm and stiffness-extension data from oscillatory response(black) when fitted with WLC (red) gives $l_p = 0.65$ nm. The green data regime between 100 and 300 pN (or between 80 and 100 nm) was excluded when fitting to WLC with both methods. b) For PEG in 2-propanol, WLC derivative (blue dash) with $l_p = 0.13$ nm again obtained from fitting the force-extension data and stiffness-extension data by oscillatory response (black) when fitted with WLC (red) gives $l_p = 0.64$ nm. | 77 |
| 3.8 | Polystyrene force-extension curves in water modelled with WLC having persistence length $l_p = 0.23$ nm. | 79 |

| | | |
|------|---|-----|
| 3.9 | a) Measurements with polystyrene in water. It shows stiffness measured using dynamic oscillatory method in black which is then fitted with WLC in red. For comparison, derivative of WLC obtained from fitting to force-extension curve is shown with blue dash. b) The same measurements with Polystyrene in 8M urea. | 80 |
| 3.10 | Parallel coupling between spring constant of cantilever(k) and polymer(k_i). | 82 |
| 4.1 | A schematic diagram of AFM used in experiment. It consist of three major components 1) fiber-interferomer 2) 5-axis nanopositioner and 3) sample-stage assembly. A lock-in amplifier is used to detect amplitude and phase changes from signal photodiode(PD) output. | 92 |
| 4.2 | A photograph of interferometer based AFM setup. | 92 |
| 4.3 | (a) Force-extension curve for PEG in water fitted with WLC with a persistence length $l_p = 0.12 \pm 0.02$ nm. A region between 100 and 300 pN does not fit and is also excluded. (b) Force-extension curve fitted with two-state FJC model with Kuhn segment length 0.24 ± 0.02 nm. | 94 |
| 4.4 | (a) The raw amplitude A and phase δ profiles measured using fiber based interferometer for PEG in water. (b) Comparison of stiffness-extension curve measured from amplitude signal (black) with derivative of force-extension curve (blue-dash). It also shows fitting of stiffness-extension curve with WLC (red) while excluding region between 50 and 70 nm is shown in green. A similar behavior is seen in fig. 2a for force-extension curves. Persistence length estimated is 0.5 ± 0.1 nm. | 95 |
| 4.5 | (a) Polystyrene stiffness-extension curve in water (black) measured using interferometer based AFM and fitted with WLC model (red). It is compared with derivative of force-extension curve with l_p 0.23 nm (blue-dash). (b) Polystyrene stiffness-extension curve taken in 8M Urea (black) fitted with WLC (red) of $l_p = 0.88 \pm 0.02$ nm and compared with force-extension derivative (blue-dash) of l_p 0.23 nm. | 96 |
| 4.6 | (a) and (c) shows force-extension and stiffness-extension curves for PEG in water. Similarly, (b) and (d) are force-extension and stiffness-extension curve for Polystyrene in water respectively. Fluctuations about mean stiffness are strong in PEG with molecular weight 10 kDa than a longer polymer of Polystyrene with molecular weight 200 kDa. No size dependent variation in fluctuation is observed for force-extension curve. | 97 |
| 5.1 | | 107 |
| 5.2 | The I27 domain from protein Titin consisting of beta-sheet secondary structure connected with hydrogen bonds (not shown). | 108 |
| 5.3 | The unfolding force profile of Bacteriorhodopsin (BR) as a function of extension. The protein is pulled from C-terminal end and seven helices of secondary structure unfolds in pair as depicted with three main force peaks. | 110 |

| | | |
|-----|---|-----|
| 5.4 | a)Time series data collected as various locations along the unfolding protein marked by arrows. The time series corresponding to blue and red arrow point are shown in an enlarged view. b) The Power Spectral Density (PSD) estimate for free cantilever (green arrow) and cantilever plus protein (blue and red arrow) | 112 |
| 5.5 | The pulling force-extension curve shows five unfolding events corresponding to unfolding of each I27 domain. | 113 |
| 5.6 | Time series for thermal deflection of cantilever are recorded as the protein is pulled and power spectral density was calculated for free cantilever (green arrow point) and cantilever plus protein (red arrow point) | 114 |
| 5.7 | The changes in frequency of PSD peak as a function of force on the I27 domain. | 114 |

List of Tables

| | | |
|-----|-------|-----|
| 5.1 | | 111 |
|-----|-------|-----|

Chapter 1

Introduction

1.1 Historical Perspective

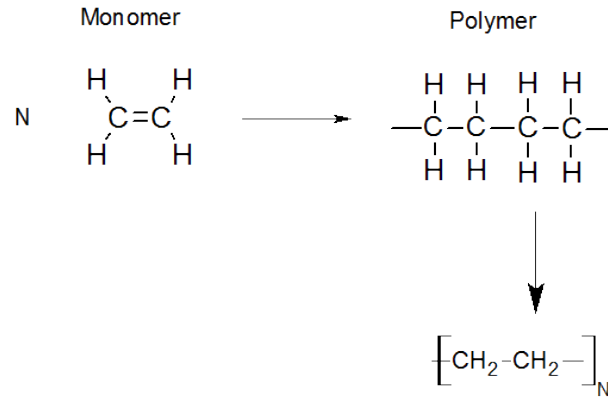
In 1920, seminal work of Hermann Staudinger[1] established polymer or a "Makromolekel" as long chain-like molecule consisting of monomer units that are linked together by covalent bonds. It was long debated that this large size molecule was just aggregated together by secondary forces of aggregation and its properties similar to colloids arise due to its overall size. Staudinger took a contrary view that colloidal properties of this large molecule arise from its internal microstructure formed covalently rather than external forces of aggregation. In the decade following 1920, this debate between macromolecule/colloid was finally put to rest by Staudinger through his work on rubber-molecule and thus began the era of polymer science. Polymers forms a prominent and an indispensable part of our everyday life. Synthetic polymers are ubiquitous in articles of commerce and technological importance with wide range of applications in processing industry, healthcare, agriculture, cosmetics and construction industry. In our human body, there are biological polymers like proteins and DNA that perform functions essential to our survival. They are an important building blocks of life on earth performing diverse regulatory and receptor functions due to participation in evolutionary processes.

Early work on polymers was primarily concerned with the polymerization chemistry and its characterization. However, understanding the behavior of polymers based on physical principles was essential to consider the study of polymers as a well-established field of science. In this regard, Paul Flory's name and his efforts are synonymous with various fundamental concepts in polymer science. Flory's scientific quest led to development of polymer science as well-accepted branch of science with the help of statistical mechanics and thermodynamics[2]. In his early work, Flory worked on the problem of 'molecular-weight distribution' expected in the process of condensation polymerization[3]. Polymer of different lengths are generally produced in a polymerization process resulting in a distribution. At the time, it was prevailing view that reactivity of a given functional group to form a polymer decreases with increasing molecular weight. Contrary to this notion, Flory assumed that reactivity is a function of local structure and not the overall molecular size. Applying statistical methods based on this assumption, he predicted the distribution, which later became a norm to describe polymers products in general. This work and from comparison between colloids and macromolecules emerges a common theme wherein 'local structure' takes precedence over 'overall size'. Polymer theories therefore aim

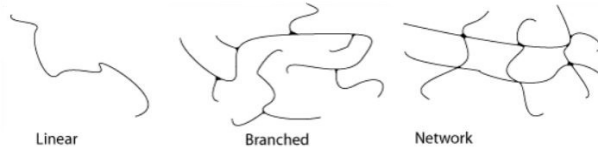
to relate this local detail to physical properties of polymers. As we will see, this local information dictates the shape of isolated polymer in dilute solution. Shape of a polymer is an important parameter based on which general theories describing constitutive properties of polymeric systems could be constructed[3]. A polymer shape is not rigid as that of a rod but is some sort of a random coil that keeps on fluctuating. Thermal fluctuations from the surroundings continuously affect the shape of polymers in liquid solutions and modeling their effect requires using principles from statistical mechanics. In the next section we discuss statistics associated with configuration or shape of a randomly coiled polymer in dilute solutions.

Investigation of polymer's statistical configurations (or conformations as in chemistry) acquire importance in developing a physical understanding of amorphous materials like rubber. The work of K. H Meyer, W. Kuhn and E. Guth made first attempts to understand unusually high elasticity of rubber[4, 5, 6]. It was known through the work of Staudinger that amorphous polymer system like rubber are made up of large network of single polymer chain units. In 1932, K. H Meyer first pointed out that, to a large extent, elasticity of rubber stems from polymer units ability to accommodate large deformations due to vast configurational space accessible to randomly shaped polymer coil. It is not due to dense packing of one polymer unit with another, but instead is simply a consequence of statistical behavior of a randomly coiled polymer. For details see [ref 2]. Simple ideas such as this, finally brought about the realization that physical properties of polymer materials must be formulated in terms of statistical configurations of individual polymer molecules. In this regard, development of single molecule techniques greatly helped in establishing fundamental understanding of polymer chain. Such techniques have allowed tracking a single polymer molecule in real time and manipulate polymer by application of mechanical force. The elasticity of a polymer chain under mechanical force was one of the first fundamental property addressed using such techniques. Understanding elasticity of simple polymer chains have permitted a greater understanding of more complex polymeric structures including biological polymers[7, 8]. In biology, for instance, almost all biological polymers are subjected to mechanical force and have evolved to diverse functions and structures in response to this selection pressure. The interplay of force, function and structure has advanced our understanding of molecular biophysics.

To conclude, polymer science with its primitive beginning has come in its current form primarily from developments of advanced experimental and theoretical methods. Although many facets of polymers still need to be understood, the basic physics principles are now well established. It is however important to point out that their experimental verification is still in a development stage. For instance, the problem of excluded volume, where part of the chain cannot coincide with other already occupied part was only recently verified in magnetic tweezer experiments. This provides immense opportunity for advanced experimental techniques to test basic principles of polymer science. [3]



(a) A basic polyethylene polymer formed by reaction of individual monomer units



(b) Architectures of polymer chains with different level of hierarchical complexity

1.2 Polymers and Biopolymers

1.2.1 Basic definitions and types

A polymer or a macromolecule is a long chain molecule formed from structural sub-units called monomers that are linked together via covalent bonds. It is produced by a polymerization process, during which monomer sub-units are covalently linked together. The number of units N that are eventually linked is called the degree of polymerization. Fig 1.1a shows the structure of a basic polymer called polyethylene. It consists of a long chain of covalently bonded carbon atoms called the backbone. In most synthetic polymers, the backbone is made of carbon atoms. Attached to this backbone is a regular pattern of other atoms or groups of atoms called side groups. The simplest possible side groups are single hydrogen atoms, as in polyethylene. The chemical identity of sub-units and their organization along the chain is fixed during the synthesis and determines most of the properties of polymers. Monomer units can be sequenced differently to produce a microstructure with significantly different properties for the polymer. Similarly, as depicted in fig 1.1b, a polymer could also be synthesized in different architectures of the backbone ranging from a simple linear chain to more complex random branched chains formed by cross-linking linear chains. For instance, a further cross-linking of chains ultimately results in formation of a polymer network or gel which is commonly used in everyday life. Due to the random nature of polymerization processes, polymer chains of different degrees of polymerization are generally produced. Therefore, a sample of synthetic polymers is poly-disperse with distribution in degree of polymerization or chain length. However, this is not the case for naturally synthesized polymers like proteins and DNA which are produced with a precise degree of polymerization. A main motivation to study simple synthetic polymers is also to understand this very important and interesting class of biological polymers[9]. The physical properties of biopolymers

defines essential structure and function of all biological systems at the molecular level and provide a basis for their evolution. A polymer like polyethylene that is formed from monomers of the same type are called homopolymers. Biopolymers on the other hand are essentially heteropolymers made with combination of different types of naturally occurring monomers such as amino acids. This inherent heterogeneity in composition is the key distinguishing property of these biopolymers from their simple synthetic counterparts. It not only allows a large permutation and combinations for evolutionary feedback to be maintained (natural selection), but also endows them with different three dimensional structures, giving rise to an ability to perform diverse functions in face of adaptability to external environment.

1.2.2 Polymer flexibility and conformations

We begin by addressing some essential properties of an ideal polymer chain[10]. In such a chain, all interactions with itself and surrounding medium are screened and chain structure is set only by thermal energy $k_B T$. After the synthesis processes, the chemical organisation of various atoms and groups remains fixed unless covalent bonds are broken, however a polymer backbone can still adopt multiple conformations. A conformation is defined by relative location of sections of polymer backbone in space. A flexible polymer chain adopts random coil conformations as sketched in fig 1.2. The fact that chain have random conformations and not a straight(almost stretched) conformations is due to inherent flexibility associated with long flexible chain polymer. A long chain molecule can be flexible due to its large length. To understand this, consider the straight-stretched conformation of the polymer which looks like a thin homogeneous string. This can be well approximated as an elastic filament that obeys Hooke's law under deformation. As we know, an ideal Hooke's spring is more flexible as its overall length increases and therefore polymer chain is flexible because of its large linear length. Furthermore, close inspection suggest that a small bending of tiny segments of polymer chain in different random direction(due to thermal fluctuation) is sufficient to coil it into random conformations.

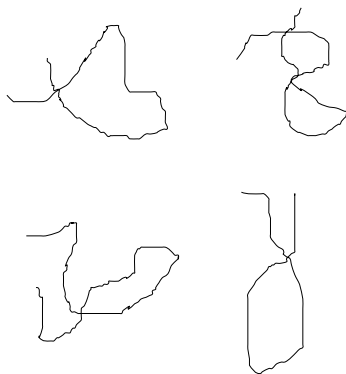


Figure 1.2: Random coil conformations of polymer chain

This ability of tiny segment of chain to randomly bend essentially arises because of flexibility mechanism operating at a molecular level[10]. Consider a segment of three consecutive C-C bond of polyethylene as shown in fig 1.3. The spatial location of atoms or groups in this unit is defined by bond lengths, bond angles between adjacent C-C bond and torsion angle Ψ . Due to covalent bonding, the bond length and

bond angle almost remain fixed but a torsion angle around a C-C bond is relatively easy to rotate. At room temperature, the energy barrier between stable torsion angles is close to thermal energy. This means that relative positions of the atoms and groups can change due to flexibility of rotation around C-C bond. Rotation of torsion angle is not completely free but is subjected to a potential that comes from the interaction of side groups on adjacent carbon atoms in the chain. This potential energy varies as torsion angle is changed and goes through minima and maxima, as side groups move relative to each other. Torsion angle corresponding to minimum potential energy are stable and designated as trans ($\Psi = 0$), gauche + ($\Psi = +120$) and gauche - ($\Psi = -120$) as shown in fig 1.3. The conformations, that a chain will eventually adopt, are combinations of these three rotational angles. One notices that trans state is more stable than gauche state because of lesser possibility of steric interactions from side groups. Therefore, successive C-C bond tries to retain trans state under thermal energy, which makes the chain look like a zig-zag as shown in fig 1.3. However, at room temperature, the energy difference between gauche and trans state is close to thermal energy and therefore, a gauche state frequently appears at different locations along the chain. This alters the zig-zag conformation of the chain and gives flexibility to the chain[10]. As a consequence, polymer chain

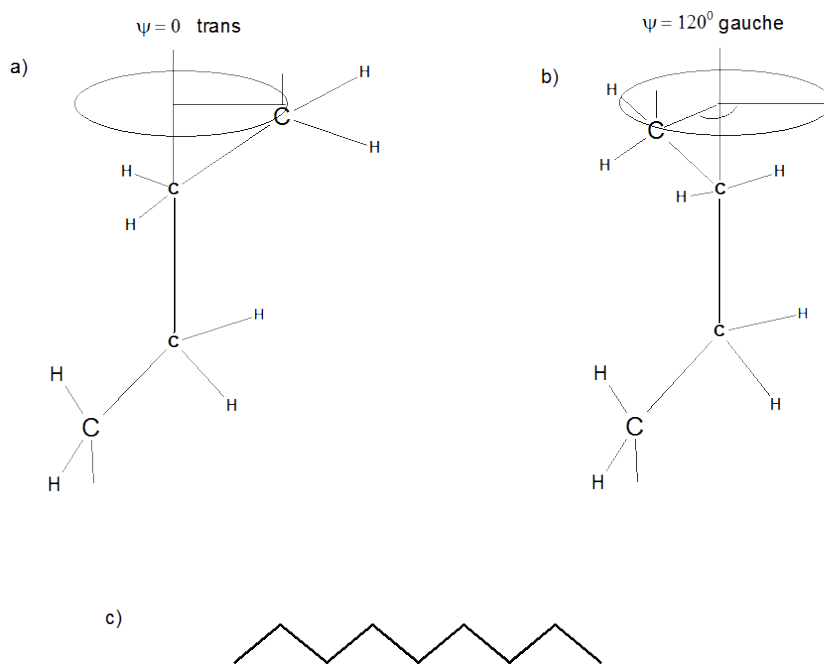


Figure 1.3: Torsion angle Ψ of zero about the C-C bond represent a trans conformer while 120° represent a gauche conformer for the repeat unit of polyethylene.

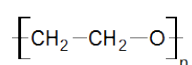
possesses a property where, on an average, any two C-C bonds that are sufficiently far apart along backbone will be oriented randomly to each other. The correlation in orientation at a shorter separation is because of restricted bond angles and steric hindrances from side groups to torsion rotation. This orientational independence gives rise to different random coil conformation for the whole polymer chain. The number of random coil conformations that chain can access are enormously large. This is because of large possibility of rotational states as chain length increases. There are three stable rotational conformations for each C-C bond, 6 for two consecutive C-C bond and 9 for three consecutive C-C bonds and so on. In this way,

chain as a whole has a huge possibility of rotational states and all these states are accessible in thermal equilibrium. In a nutshell, a polymer physically behaves as a statistical random coil.

In the following two subsections, we will review various conformations or chemical structure that synthetic and biological polymers can adopt. In particular, emphasis will be on the conformations of synthetic polymers like PEG and polystyrene and proteins like titin and bacteriorhodopsin, since single molecule AFM experiments on them forms much of the work in this thesis.

1.2.3 Synthetic Polymers

Poly(ethyleneglycol)



Polystyrene

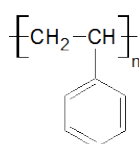


Figure 1.4: Synthetic polymers of polyethylene(glycol)(PEG) and polystyrene

Polyethylene(glycol)(PEG) is a model linear polymer which is non-toxic, biodegradable and water soluble. It has wide applications in drug delivery and tissue engineering including commercial applications, such as antifouling surfaces, lubrication and cosmetics[11]. PEG has both polar(hydrophilic) and non-polar(hydrophobic) groups in its structure, which contribute to its solubility and properties in both organic and aqueous solvents. Most important property, that makes PEG useful in various applications, stems from its exceptional solubility in water[11]. In this

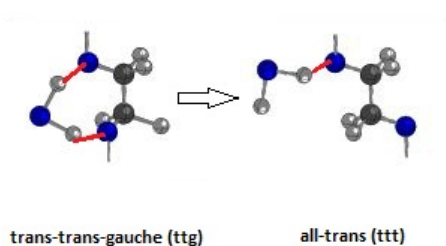


Figure 1.5: In the *ttg* conformation of repeat unit $\text{O}-\text{CH}_2-\text{CH}_2-\text{O}$, it is possible to form two hydrogen bonds (red line) with adjacent oxygen's(blue) with water molecule. For *ttt* or all-trans conformation, there is possibility of only one hydrogen bond with water. As a result of hydrogen bonding, *ttg* is shorter in length and more energetically stable.

regard, micro-structure of PEG in water plays a decisive role. PEG in solid crystal form is known to exist in two microstructural forms - Helical and Planar[12]. The

helical form is further retained when PEG is dissolved in aqueous solvent and corresponds to trans-trans-gauche conformations of monomers. They are retained in water because trans-trans-gauche(ttg) state is energetically favourable due to possibility of two hydrogen bonds (red) as sketched in fig 1.5. The helical form is more stable compared to planar form(ttt) in which the possibility of hydrogen bonds (red) is just one as seen in fig. 1.5. In addition, (ttg) state is shorter compared to (ttt) state. As we discuss later in the thesis, the stretching the polymer under force results in conformational transition from helical(ttt) conformations to planar(ttg) conformations with a characteristic signature.

Polystyrene is another simple and essential polymer used in everyday practice. It has bulky hydrophobic side group of benzene which makes it a model hydrophobic polymer to study more complex biological heteropolymers like globular proteins. In contrast to PEG, polystyrene in water collapses to form a globule rather than a random coil making water a poor solvent for polystyrene. The stretching under force of polystyrene and PEG in good and poor solvents will form a part of this thesis.

1.2.4 Proteins

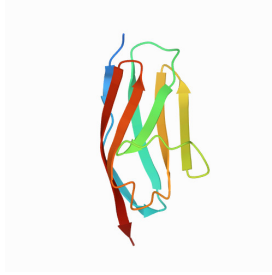
The main feature of biopolymers like proteins that distinguishes them from simple synthetic polymers is specific biological function that they perform[9]. A protein is regarded as an automated machine capable of performing diverse biological functions including regulation of nutrients, mechanical function in contractions of muscles and passage pathway across cell membrane. They are able to perform these diverse function due to their ability to fold into unique 3-D conformational structure[9].

Primary Structure Initially, a protein is a simple linear polymer chain formed from the set of 20 amino acids. A basic repeating unit for the protein $-(C^\alpha - C = N - C^\alpha)-$ results from the formation of bond ($C = N$) between carbon of one amino acid and nitrogen from another amino acid, where amino acids are distinguished by a different side chains at C^α position. The linear sequence of amino acids on the chain is strictly determined during the biological synthesis from DNA and is called the primary structure of protein. From this point of view of biology, primary structure is a consequence of biological evolution[9].

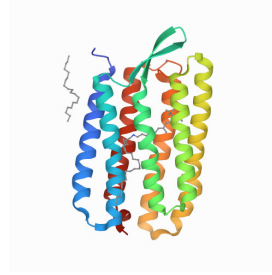
Secondary Structure Next, amino acids that make up a protein can be charged, polar and hydrophobic. Due to these differences in physical character, they tend to interact with each other. In presence of thermal energy, a polypeptide chain continuously explores various contacts until stabilized energetically, for example, by hydrogen bond. The intra-chain hydrogen bonds stabilizes the contacts into small size structure of alpha-helices and beta sheets of about 10-20 amino acids. The structures generate a short-range order in linear arrangement of polypeptide chain and are called secondary structure of protein.

Tertiary Structure Lastly, an overall 3-D structure for the whole chain appears due to long range interactions between chains elements. This is the tertiary structure. In conclusion, protein in its native state is folded into a hierarchical structure and is far different from simple random coil nature of synthetic counterparts. So, instead of the mechanism of flexibility, other specific interaction like hydrogen bonding, hydrophobic and electrostatic interactions become important[9].

Figure 1.6a shows the of beta-sheet rich domain or subunit I27 of a giant muscle



(a) I27 domain of protein Titin found in muscles.



(b) Membrane protein Bacteriorhodopsin

Figure 1.6: Globular and Membrane protein used in this thesis.

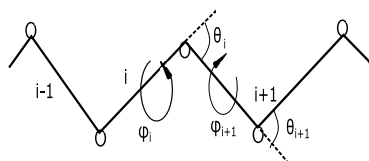
protein titin. The beta strands (shown using arrows) are connected in a sheet arrangement through hydrogen bonds with each other(not shown). This protein is considered to play a dominant role in muscle contractions[13]. This is achieved by the same domain repeated one after another (say 10-20) times and let all of them simultaneously fold and unfold under external stress. This unfolding and refolding generates a mechanical power that supports muscle contractions. It is known that beta-sheet rich secondary structure is commonly found in proteins responsible for mechanical functions because of larger mechanical stability provide by beta-sheets compared to alpha helices[13]. In figure 1.6b is shown an alpha-helix rich protein bacteriorhodopsin. This protein is a part of cell's lipid membrane and used to transport or pump proton ions across the membrane. Since the function performed is not mechanical in nature, this protein is less stable and unfold easily under force. The study of protein under mechanical force but with different function and therefore structures can give crucial insights into the interplay between force, function and structure.

In the present thesis, we will mainly be interested in the protein stretched under high force so that secondary and tertiary structure will not be relevant and only polypeptide backbone with its associated flexibility mechanism will play a role. Just as the flexibility of polymer chain is determined by torsion angle Ψ , polypeptide backbone flexibility is determined from torsion angles ϕ around $(C^\alpha - N)$ bond and ψ about $(C^\alpha - C)$.

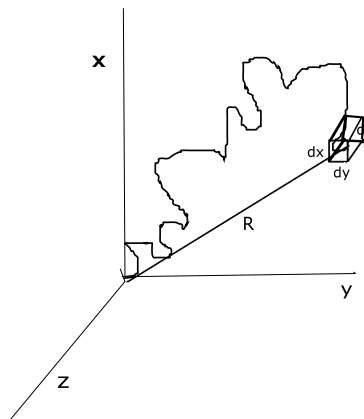
1.3 Statistical mechanics of linear polymer chains

1.3.1 Configurational statistics of ideal polymer chains

Polymer configuration(or conformation as in chemistry) is the relative positions of repeating units or monomers in space. During polymerization process of a polymer, local architecture and chemical composition remains fixed, however, polymer in thermal environment can adopt large number of configurations[2]. As discussed already, this is due to molecular flexibility mechanism determined mainly by torsional angles φ as shown in 1.7a. A chemical bond in each repeating unit is almost always free to rotate producing enormous configuration(or conformations) for the total length of polymer. Since polymer chain takes large number of configurations, its calculation requires averaging over all available configurations and must rely on



(a) Skeletal representation of a polymer with bonds i , bond angles θ and torsional rotations φ . A given configuration for the polymer corresponds to fixed values of these parameters.



(b) End-to End distance R for a given polymer configuration

Figure 1.7: Flexibility mechanism of a polymer

methods of statistical mechanics. In polymer science, it is important to know the spatial configuration or shape of isolated polymer in solution. It is a good starting point as many basic properties of polymeric systems, at a fundamental level, are intimately related to their microscopic constituents and to this characteristic parameter. For example, elasticity of rubber-like material is directly related to the ability of random polymer coils that constitutes a rubber, in accommodating large changes in their spatial configurations. A configuration that a polymer can adopt depends mainly on two factors:

- Short-range interaction of monomer with another bonded monomer along the polymer chain
- Long-range interactions between two distant monomers that are physically separated in space(not bonded together) .

Based on this, a polymer chain can be broadly divided into two types: "ideal" chain, and "real" chain. In this section, we discuss ideal chain configuration which assumes only short-range interactions between chain monomers and long-range interactions are ignored. For this, one considers a condition for the surrounding solvent called 'Theta Point'. In such a case, long range interactions are effectively cancelled out by polymer-solvent interactions. In a real chain, both long-range and short-range interactions are considered. We discuss this in detail in the next section. As shown[3, 2], long-range interactions does not distinguish between polymer with different short-range features such as local structure geometry, chemical constitution and rotational hindrances of adjacent bonds. Modelling ideal conformations thus allow for rationalizing differences between different polymer systems in terms of their local structure property. Now we derive the distribution for end-to-end distance of ideal polymer chain as shown in Fig 1.7b, characterizing its shape or size. With this, other configuration-dependent properties can be obtained by averaging over the distribution.

A simplest description of polymer is that of freely-jointed chain[9]. In this model, chain is represented as series of rigid rods(monomers) that are joined together such that each rod is free to adopt any orientation without being constrained by the

adjacent rod. With this assumption, configuration of a polymer can be mapped to trajectory of a simple random walk. We first map a polymer conformation to 1D-random walk and later generalise to 3D. Starting with origin, the number of possible ways in which polymer end could be at position x after n steps of unit length is given by binomial coefficient:

$$W(n, x) = \frac{n!}{n_+!n_-!} \quad (1.1)$$

where n_+ is the steps in forward direction and n_- in backward direction such that $x = n_+ - n_-$ and $n = n_+ + n_-$. Also the probability of taking both forward and backward step is $1/2$. Therefore, probability of finding the polymer end at position x is :

$$P_{1D} = \frac{W(n, x)}{2^n} = \frac{n!}{\left(\frac{n-x}{2}\right)!\left(\frac{n+x}{2}\right)!} \frac{1}{2^n} \quad (1.2)$$

The above expression is the binomial probability distribution for a random walk. Under approximation $x \ll n$ which amounts to taking continuum limit, the above expression for discrete binomial distribution reduces to a continuous Gaussian distribution. In other words, under the limit of large number of steps in a random walk, the position x is Gaussian distributed. This is an expected consequence of central limit theorem. To see this, one takes a logarithm on both sides of equation 2 and use Stirling approximation for large n : $\ln n! \sim n \ln n - n + \frac{1}{2} \ln(2\pi n)$

$$\begin{aligned} \ln P_{1D} &= n \ln n - n + \frac{1}{2} \ln(2\pi n) \\ &\quad - \left[\left(\frac{n+x}{2}\right) \ln\left(\frac{n+x}{2}\right) - \frac{n+x}{2} + \ln 2\pi \left(\frac{n+x}{2}\right) \right] \\ &\quad - \left[\left(\frac{n-x}{2}\right) \ln\left(\frac{n-x}{2}\right) - \frac{n-x}{2} + \ln 2\pi \left(\frac{n-x}{2}\right) \right] - n \ln 2 \quad (1.3) \end{aligned}$$

Rewriting the logarithms

$$\ln\left(\frac{n \pm x}{2}\right) = \ln\left(\frac{n}{2}\right) + \ln\left(1 \pm \frac{x}{n}\right) \quad (1.4)$$

and making a Taylor expansion as

$$\ln\left(1 \pm \frac{x}{n}\right) = \pm \frac{x}{n} - \frac{1}{2} \left(\frac{x}{n}\right)^2 \quad (1.5)$$

Combining last three equations, we have

$$\ln P_{1D}(n, x) = -\frac{1}{2} \ln(2\pi n) - \left(\frac{x^2}{2n}\right) \quad (1.6)$$

Therefore,

$$P_{1D}(n, x) = \frac{1}{\sqrt{2\pi n}} e^{-\frac{x^2}{2n}} \quad (1.7)$$

note that x now should be treated as continuous variable. One can generalize the above equation to 3D after standardizing with length l of each step in random walk.

$$P_{3D}(n, R) = \left(\frac{1}{2\pi n l^2}\right)^{\frac{3}{2}} e^{-\frac{3R^2}{2nl^2}} \quad (1.8)$$

One immediately notes from the above distribution that mean square end-to-end distance is $\langle R^2 \rangle = nl^2$. Thus, root mean square end to end distance ($\sqrt{\langle R^2 \rangle}$) i.e the size, scale as square root of degree of polymerization \sqrt{n} . It immediately implies that polymer takes the shape of a coil rather than a straight extended shape, which would be the case if size scaled as n . This estimate is fairly good approximation to the size of polymer chain. It turns out that ideal chain models although at the outset looks artificial or nonphysical, their successes in explaining scaling proprieties is unparalleled. As we will see, apart from scaling of size with n other scaling relations like for external applied force with size or n can be reasonably obtained well supported by experiments. More level of sophistication can be added in modelling a ideal chain that incorporates actual bond angles and rotational hindrances. However, all such correlations can be accommodated such that mean square end-to-end distance is:

$$\langle R^2 \rangle = Cnl^2 \quad (1.9)$$

where C , for a sufficiently long chain is a constant characterizing the short range correlation along the chain. One last point, all ideal chain models which follow the above relation can recast into an 'equivalent' free-jointed chain in such a manner that

$$\langle R^2 \rangle = Nb^2 = Cnl^2 \quad (1.10)$$

where N and b are equivalent number of Kuhn segments and length of Kuhn segments respectively. Therefore, n and l can be substituted with N and b respectively in eq (1.8) for all future discussions.

1.3.2 Real Chains-Excluded volume

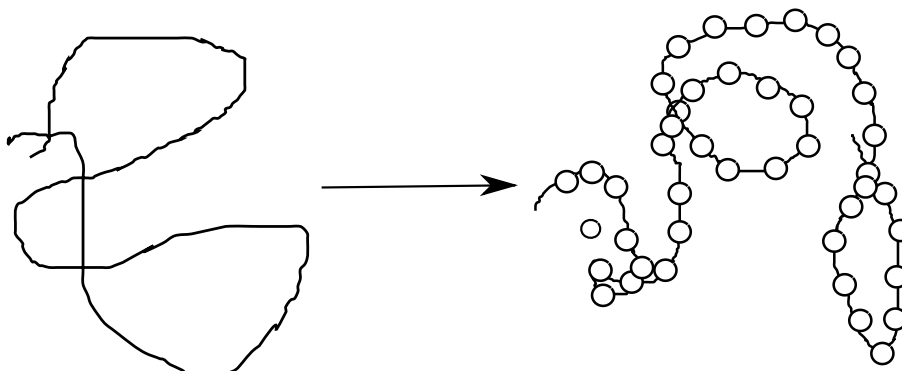


Figure 1.8: Excluded-volume interaction. On the left is the ideal chain configurations with allowed self-intersections. On the right is the real chain configuration with excluded spherical shell representing each segment of the chain.

In the last section, we considered a random walk configuration which allowed for intersection within parts that are separated by some distance. However, in real physical situation, a chain does not allow for such self intersections within its own parts. This means that two parts of the chain cannot occupy the same space and there must be an exclusion of some volume for each local section of the chain as depicted in fig 1.8. To access the influence of such exclusion on polymer conformation it is important to know the contacts between two or more monomers that

need to be included. At the outset such a calculation seems intractable. However, it is shown that for long linear polymer overlap/contacts between only two monomers that are far separated along the polymer contour suffices[10]. It is these long-range interactions, called excluded-volume interaction that predominantly affect the polymer conformations. To quantitatively understand such interaction, two essential points need to be examined

- First, excluded-volume interaction depend on the surrounding solvent or its temperature. This is because excluded volume interaction is between two non-bonded monomers that are physically separated in space unlike short range interaction between bonded monomers considered previously. This means that excluded-volume is an effective interaction between a pair of monomer determined by direct interaction with each other and also their interactions with solvent medium.
- Second, excluded volume is not always exclusion in the sense that effective interaction can be attractive or repulsive depending on the quality of solvent. A solvent is a good solvent when the effective interaction is repulsive and poor solvent when it is attractive. It is natural therefore to expect that the chain is more expanded or swollen in case of good solvent and collapsed or contracted in poor solvent.

To make these ideas mathematically precise, we define excluded volume interaction between a pair of monomer as

$$U_{int} = k_B T \bar{v}(r_m - r_n) \quad (1.11)$$

For this interaction energy to significantly change the polymer configuration, $U \gg k_B T$. Therefore, dimensionless parameter \bar{v} must be $\bar{v} \gg 1$. This parameter depends on physical separation between monomers m and n and will decay rapidly as a function of distance $r_m - r_n$. It is hence approximated by a delta function $\bar{v} = v\delta(r)$ where $r = r_m - r_n$ and v is excluded-volume parameter with dimensions of volume and delta function has dimensions of 1/volume. Excluded volume parameter v can thus be visualized as some effective volume of a sphere around local segments of the chain as seen in Fig 1.8. Summing this pair interaction all over the polymer length we get,

$$U_{int} = k_B T \frac{v}{2} \int dm \int dn \delta(r_m - r_n) \quad (1.12)$$

A factor of $\frac{1}{2}$ is because each pair is counted twice for the integration over m and n . Writing $\delta(r_m - r_n) = \int dr \delta(r - r_m) \delta(r - r_n)$ and identifying $c(r) = \int dm \delta(r - r_m)$ (dimensions of concentration) as a measure of number of local segments of the chain per unit volume at some r distance from the center of molecule, we have

$$U_{int} = k_B T \frac{v}{2} \int dr \int dm \delta(r - r_m) \int dn \delta(r - r_n) \delta = \frac{1}{2} k_B T v \int dr [c(r)^2] \quad (1.13)$$

In Paul Flory treatment, $c(r)$ is considered uniform such that in some volume

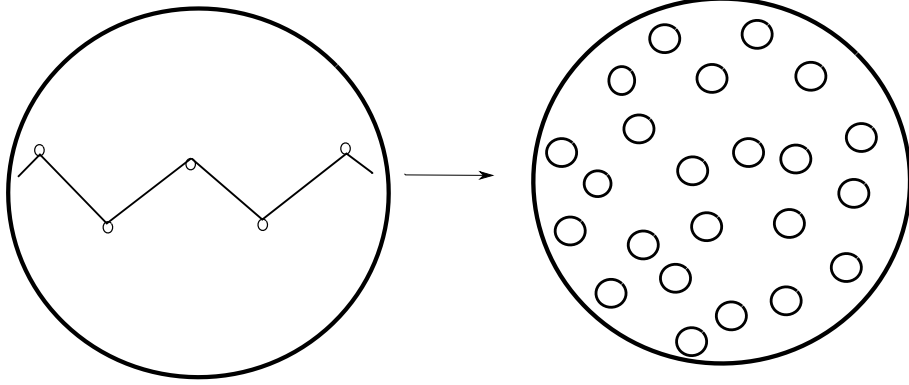


Figure 1.9: In Flory theory, an assumption of uniform concentration of polymer segments in spherical volume $V \sim R^3$ is made. A connected chain on the left in volume V is viewed as being made up of disconnected segments spread uniformly in volume V .

$V \sim R^3$, such that $c(r) \sim c \sim \frac{N}{R^3}$ as depicted in Fig 1.9. In addition, entropic elasticity stored in the conformations of the polymer is (apart from a constant) is negative logarithm of eq (1.8) $\sim \frac{R^2}{Nb^2}$. Adding the two without the prefactors, we have total interaction free energy as

$$U_{total} \sim k_B T \left[v \frac{N^2}{R^3} + \frac{R^2}{Nb^2} \right] \quad (1.14)$$

Minimizing this by taking a derivative $\frac{\delta U_{total}}{\delta R} = 0$ and assuming $v > 0$, we have end to end distance $R \sim N^{\frac{2}{3}}$. Therefore, in good solvent in which case effective interaction between monomers is repulsive i.e $v > 0$, set of configuration are spanning a relatively larger domain implying a larger average size of the polymer compared to an ideal chain. By considering three body interactions, it can further be shown that for poor solvent ($v < 0$) it is $R \sim N^{\frac{1}{3}}$ and chain is relatively collapsed than an ideal chain. Summarizing,

| | |
|--------------------------|--------------------------------|
| $R \sim N^{\frac{1}{2}}$ | Ideal chain (Theta solvent) |
| $R \sim N^{\frac{2}{3}}$ | Swollen chain (Good solvent) |
| $R \sim N^{\frac{1}{3}}$ | Collapsed chain (Poor solvent) |

The above treatment along the lines of 'Flory theory' overestimates the excluded volume energy U_{int} by assuming concentration of local segments to be uniform. It also underestimates elastic energy by assuming ideal chain conformation. For real chain the polymer will be more stretched than an ideal case. Due to mysterious

reasons, errors due to underestimation of elastic energy and overestimation of excluded volume energy cancel out and one gets final results in good agreement with experiments and elaborate theories such as renormalization theory[10].

1.4 Statistical mechanics of real polymer chains under force

In the last section, investigation of polymer's statistical configurations acquire added importance in quantitative understanding of amorphous polymeric materials like rubber. Mechanical elasticity of rubber had been a major focus of research in the past[5]. A rubber is unusually elastic which can be stretched very far before it breaks. Furthermore, it is observed that a rubber gives off heat when stretched with a force and a rubber stretched against a predefined force gets contracted when heated. This was quite unusual since most materials expand upon heating. These common observation remained a puzzle for quite some time in history and a quantitative understanding was missing[4, 6]. It was known from Staudinger work that amorphous rubber is made up of large network of single polymer chain units. In 1932, K. H Meyer added a key insight by pointing out that elasticity of rubber, to a large extent, stems from constituent polymer units ability to have large deformations. They can accommodate these deformations because of vast configurational space accessed by them[ref 2]. During the stretching of a rubber, the constituent polymer molecule uncoil and straighten out from a randomly coiled configurations to a more extended one. In this process entropy naturally diminishes since there is only one straight configuration and many coiled ones. This lead to the idea of entropic elasticity of polymer chain that determine complex physical properties of polymeric materials.

The next step was to quantify the entropic elasticity and in this regard work taken by W. Kuhn, E. Guth, H. Mark is important. Let us suppose that we try to fix the ends of the polymer to some end-to-end distance R , which amounts to applying a small deformation to the chain. In absence of this deformation, the end to end distance R has a probability distribution given by eq (1.8). Due to the deformation, polymer will suddenly have less number of available end-to-end configurations and hence low entropy with current end-to-end distance R becoming less probable. However according to second law of thermodynamics polymer has the natural tendency to maximize its entropy, it results in generation of force, an entropic force. This entropic force arise from decrease in vast number of configurations of the polymer as it is stretched or extended under deformation. Polymers are therefore also considered as 'entropic springs'.

To quantify entropic spring nature of a random polymer is simple. It is asserted that free energy $F = U - TS$ for the polymer is entropy dominated $F = -TS$ and in the limit of very small deformation is given by,

$$F(N, R) = -T\Delta S = -k_B T \ln P_{3D} = -\frac{3}{2}k_B T \frac{R^2}{Nb^2} \quad (1.15)$$

For large deformation or end-to-end distance R probability distribution will be quite different and above equation is not valid. Entropic force which is required to hold the polymer at some end-to-end distance R is then, $f = \frac{\delta F}{\delta R} = \left(\frac{3k_B T}{Nb^2}\right)R$ with spring

constant $k = \frac{3k_B T}{Nb^2}$. This temperature dependence of spring constant qualitatively explains why rubber gives off heat when stretched and a stretched rubber contracts upon heating.

The above relation between force and extension suffers from the obvious defect that the chain can be extended infinitely without any constrain. A chain, however, cannot be extended beyond the average extension $\langle R \rangle = Nb = L$, called the contour length of polymer. This does not limit the validity of eq (1.15) which in any case valid only for very small deformation but a more accurate relation between force and extension valid for large deformation is required. In the next section we discuss the statistical behavior of polymer chain in high force regime and derive WLC and FJC force versus end-to-end distance relation.

Freely-jointed Chain

To begin with, it is essential to discuss the influence of external force on the thermodynamics of single polymer. A single polymer chain is always in contact with a heat reservoir with temperature T and has an entropy S and available free energy is F . These quantities are related via well known thermodynamic relation $F = U - TS$ where U is energy of polymer. Now, suppose that we choose a thermodynamic ensemble in which polymer is held at a constant force f to which the polymer responds by changing its end-to-end distance to some R . This is in contrast to 1.15 where constant end to end distance ensemble was assumed. Then the work done on polymer is fR and amount of heat transferred to reservoir is $-Q$ lead to increase in entropy of reservoir S_R so that $-Q = -TS_R$. Energy conservation then implies $U = -TS_R + fR$. It is clear from above that in single polymer thermodynamics the traditional role played by pressure and volume variable is replaced by force and end-to-end distance. Combining the expression of F with U , we have, $F - fR = -(S + S_R)$. The $F - fR$ is the effective free energy under force which is minimized while approaching equilibrium because total entropy $S_0 = S + S_R$ is maximized by second law of thermodynamics. Thus, under constant force $F - fR$ is free energy of interest compared to just F in case of constant end-to-end distance ensemble. Based on above considerations, we seek a probability distribution for end to end distance R from which various average quantities can be calculated. According to basic postulate of statistical mechanics the probability of being in a macro-state is proportional to the number of available micro-states. But since entropy is defined as logarithm of number of micro-states, the probability distribution is proportional to exponential of entropy:

$$p(R) \propto e^{S_0/k_B} = \frac{1}{Z} e^{-(F-f.R)/k_B T} \quad (1.16)$$

The normalization factor $Z = \int e^{-(F-f.R)/k_B T} dR$ is called the partition function which allows to calculate average end-to-end distance R as a function of external force f as

$$R = k_B T \frac{d(\ln Z)}{df} \quad (1.17)$$

Hence, calculation of partition function for FJC polymer chain is crucial. A FJC chain, as discussed, previously, is assumed to be made of series of N rigid links of length b called Kuhn length. Links are connected end to end spanning its entire

contour length and are completely independent in their orientation with each other. Because of this partition function factorizes into product of N terms. Thus, we only need to calculate the partition function for only one rigid link. Writing in spherical polar coordinates we have :

$$Z = \left(\int_0^{2\pi} \int_0^\pi e^{fb \cos \theta / k_B T} \sin \theta d\theta d\phi \right)^N = \left(\frac{4\pi \sinh \beta f b}{\beta f b} \right)^N \quad (1.18)$$

It is noted that we set F to zero since its is a constant for each configuration of polymer and the radial part is neglected because segments are considered rigid. By using equation 1.17 force versus end-to-end distance relation is :

$$R = L \left(\coth \beta f b - \frac{1}{\beta f b} \right) \quad (1.19)$$

where $L = Nb$ is contour length and $\beta = 1/k_B T$. In the limit of low forces $f \ll K_B T/b$ the above relation reduces to $f = \frac{3k_B T}{Nb^2} R$ that corroborates well with low deformation behavior outlined in previous section 1.15. In the high deformation, high force regime $f \gg k_B T/b$, the end-to-end distance is $R = L(1 - \frac{k_B T}{fb})$ and asymptotically approaches its contour length as $1/f$. This large force behaviour to a large extent explained the rubber elasticity at high deformation.

Wormlike Chain

Yet another class of model called worm-like chain treats the polymer as a continuous homogeneous string in contrast to a discrete set of rigid links as in FJC[14]. As shown in fig 1.10, a section of this continuous string is designated by a space curve $r(s)$ with respect to origin O and a unit tangent vector $t(s)$, where coordinate s is the distance along the polymer contour. The string can bend locally with bending energy penalty

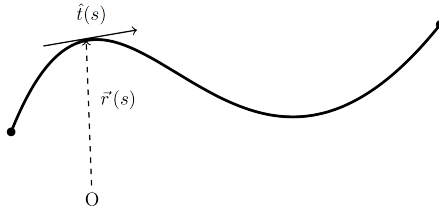


Figure 1.10: A Worm like chain

proportional to curvature $k = d^2 r / ds^2$ times bending constant $A = K_B T l_p$ (Nm^2). Here l_p is a characteristic length-scale of polymer chain called the persistence length which defines how rapidly correlation between tangent vectors decay exponentially $\langle t(s)t(s') \rangle = e^{|s-s'|/l_p}$. Thus, it signifies the local bending ability of polymer chain, with larger persistence length means chain is stiffer locally and vice-versa. The total energy under external constant force f is then :

$$U = \int_0^L \frac{A k^2}{2} ds - f R \quad (1.20)$$

The partition function in this constant force ensemble $e^{-U/k_B T}$ is not exactly solvable. But under approximation of high force, $f \gg k_B T/l_p$, an approximate solution for end-to-end distance was calculated by Marko-Siggia[14] as :

$$R = L \left(1 - \sqrt{\frac{k_B T}{4fl_p}} \right) \quad (1.21)$$

The end-to-end distance approaches its contour length as $1/\sqrt{f}$ which is slower than $1/f$ for FJC model. The universal low force regime follows a linear relationship between force and end-to-end distance and combining the two relations produces an interpolation formula for WLC which is valid for all force regime:

$$f = \frac{k_B T}{l_p} \left(\frac{1}{4 \left(1 - \frac{R}{L} \right)^2} - \frac{R}{L} + \frac{1}{4} \right) \quad (1.22)$$

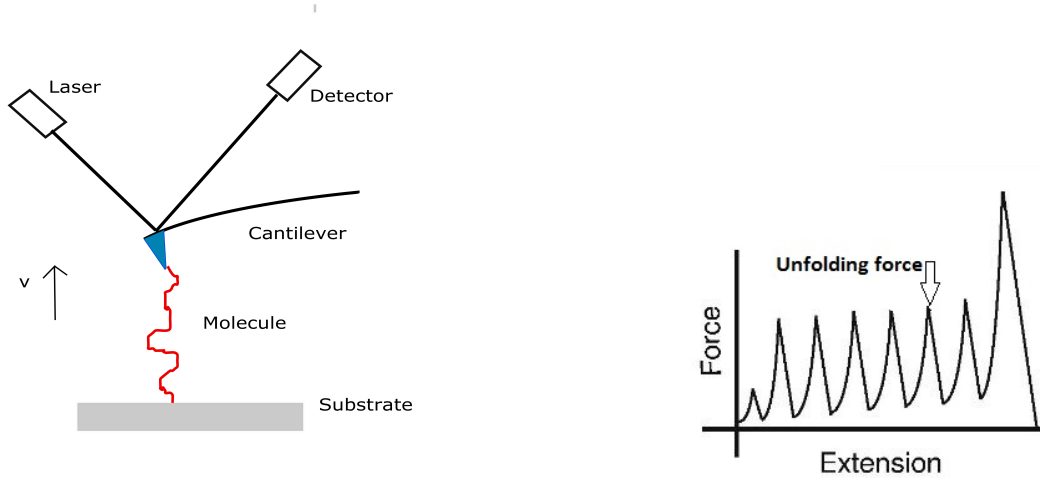
A key difference between FJC and WLC is the way bending of chain is treated in two models. It can be shown that a WLC model can be mapped to a statistically equivalent FJC with Kuhn length $b = 2l_p$ [15]. However, b is no longer a rigid link of the chain but there exist bending within the length scale with various bending modes. This, in turn, is responsible for exponential correlation of orientation correlation along the chain than an nonphysical delta correlation of rigid links. In conclusion, WLC chain represent a more physical picture of a polymer chain although still operating at an average backbone level without regards to side groups.

1.5 Review of single molecule mechanical experiments

Development of experimental tools that allows precise application and measurement of minute forces has opened up new perspectives in polymeric and biological systems. Using these tools, it is possible to make mechanical measurements on single molecules and study fundamental intramolecular and intermolecular interactions at the molecular level. Apart from measurement of elasticity of polymers and biopolymers, these tools have made possible observations of biological processes that could not otherwise be directly detected in ensemble average assays. This includes, for example, protein folding pathways[13], mechanical work generated by motor proteins[16] and mechanics of biological molecules such as DNA[17], actin-filaments[18, 16] and receptor-ligand pairs[19] In all the examples mentioned above, various intermolecular and intramolecular interaction dictate their complex mechanical behavior and hence a measurement under force would reveal these interaction with high precision. The knowledge obtained through single-molecule experiments is primarily fundamental in nature, and provides essential evidence for existing principles. Therefore, study of single molecules have attracted the interest of researchers, and in turn stimulated new developments in instrumentation. Today, a number of techniques differing in force and dynamical ranges are available, the most prominent of which are optical tweezers, magnetic tweezers and AFM(atomic force microscopy). They are generally referred to as single molecule force spectroscopy techniques.

Besides them, there are single molecule tools such as optical techniques of FRET(fluorescence resonance energy transfer) and FCS(fluorescence correlation spectroscopy) in which no external force is applied. In these techniques, fluorescence signal of a molecule is used to probe its fast internal dynamics in picosecond to microsecond range. In this overview, we only focus on force spectroscopy techniques that are relevant to the current thesis work.

1.5.1 Atomic Force Microscopy(AFM)



(a) A basic AFM schematic with molecule tethered between AFM cantilever and the substrate.

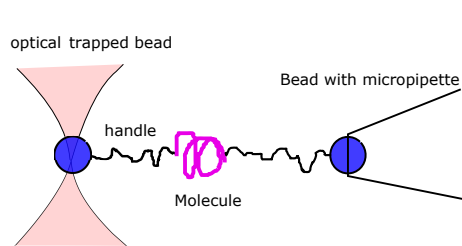
(b) Force-extension curve for a standard multi-domain protein which consist of tandem repeats of I27 domain present in muscle protein titin.

AFM was invented by G. Binnig and H. Rohrer[20] as an extension to scanning tunneling microscopy (STM), which was used to image metallic surfaces with Angstrom resolution. It is no surprise that initial use of AFM were restricted to imaging applications but was soon refined to measure and apply force to single molecules[8]. Development of atomic force microscope(AFM) have been instrumental in studying single molecule under force. AFM is perhaps one of the most straightforward technique to understand and implement experimentally. In this, a molecule of interest which is on a substrate is tethered to a force sensing probe(Figure 1.11a). This is done by approaching the probe in the vicinity of the substrate and molecule is attached to the probe by some specific or nonspecific interaction. A cantilever with a sharp tip, which acts as a force probe moves away from the substrate at constant velocity and both deflection of the cantilever and separation between cantilever and substrate are monitored. Considering the cantilever as a mechanical spring, the small deflection δx are converted into force via harmonic approximation $F = k\delta x$. This results in generation of force-versus extension curves for the molecule. AFM is a very versatile technique and one of the few techniques that can perform both imaging and manipulation under force. Force and spatial resolution in the AFM are limited by thermal fluctuations. At a given constant position of the cantilever, the force acting on it and the extension between tip and substrate fluctuate. The fluctuations are given by $\langle \delta x^2 \rangle = k_B T/k$ and $\langle \delta F^2 \rangle = k_B T k$ where k_B is the Boltzmann constant, T is the absolute temperature of the environment and k is the stiffness of the cantilever. At room temperature for $k \sim 100 \text{ pN/nm}$, $\sqrt{\langle \delta F^2 \rangle} = 20 \text{ pN}$, $\sqrt{\langle \delta x^2 \rangle} = 0.2 \text{ nm}$. This shows that force resolution for a typical AFM is 20 pN. AFM experiments covers force range in between 20 pN-10 nN depending on the

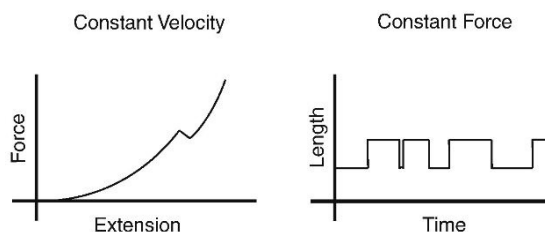
stiffness of the cantilever. The operational principle and instrumentation will be discussed in more detail in the next chapter.

Herman Gaub and Mathias Rief performed some of the initial force spectroscopy experiments with AFM[21]. Force spectroscopy was performed on simple polymer chains as well as biomolecules. Domains of titin protein were first to be studied under force, which later became a standard for single molecule force spectroscopy experiments. Using protein engineering the immunoglobulin(I27) domains are repeated in a concatamer to get fingerprint of a single molecule event. This results in a characteristic force extension curve with sawtooth pattern seen in fig 1.11b. The peak in the pattern correspond to unfolding of a single domain out of the concatamer of I27 protein domains. The unfolding force is a measure of mechanical stability of the protein and is generally related to structural topology of the protein molecule. The distance between the peaks represent the fully stretched length of I27 domain and the rising slope is a measure of entropic elasticity of unfolded domain.

1.5.2 Optical Tweezers



(a) A basic schematic of optical tweezer setup consisting of optically trapped bead attached to one end of the molecule via handles. Another end of molecule is attached to a different bead sucked in an micropipette.



(b) Two standard experimental protocol i.e. constant velocity and constant force implemented in a optical tweezer.

Optical tweezers or optical traps have become a sensitive tool to manipulate single molecules in a precise and controlled manner. They were developed by Arthur Ashkin and coworkers at Bell Labs as a result of their work related to trapping objects using focused laser beams[22, 23]. They showed that a spherical dielectric bead of about a micron-size could be held and manipulated in solution by using optical forces. Trapping is due to the radiation pressure of focused laser beams that creates a stable three-dimensional potential well for the bead. For details on the principle physics of the technique see[ref 24]. In a typical optical tweezer setup, the molecule of interest is tethered via DNA handle to a micron sized bead which is ultimately held in an optical trap fig 1.12a. Since the trapping potential is harmonic, force acting on the bead is directly proportional to the displacement between the bead and the center of the trap, $F = kx$ where k is the stiffness of the trap. The other end of the molecule is attached via a handle to another bead, which is held by a micropipette or by another optical trap Fig 1.12a. Mechanical force on the overall system is then applied by controlling the bead attached to micropipette. The force-extension profile are usually generated using two different protocols albeit

yielding the same information fig 1.12b. One protocol applies force by changing the position of the micropipette bead at constant velocity and measure the resultant force on the optically trapped bead. In another protocol, the force on the molecular system is held constant using an active feedback control and extension is monitored in real time. Constant force measurements are simple to interpret compared to constant velocity protocol but the active feedback with finite time response (~ 1 ms) complicates the interpreting of events faster than a millisecond. The force resolution of optical tweezers is atleast 10 times better than AFM. This is because the stiffness of the optical trap is about $10^2 - 10^4$ times smaller than an AFM probe. The force range accessible in an OT setup is in the range [0.5 pN - 65 pN].

OTs have been predominantly used to investigate nucleic acids and molecular motors[7]. DNA and RNA molecules have been widely studied in force spectroscopy experiment using optical tweezers. Generally both constant velocity and constant force mode are employed to generate force-extension curves. Figure 1.12b shows the stretching of a single RNA riboswitch aptamer molecule in a constant velocity experiment. It shows sawtooth pattern on either of the sides of a kink. This kink represent the unfolding of structure within the molecule which results in effective increase in the length or extension of the molecule. A constant force experiment on a protein is shown in Figure 1.12b. At a fixed force the protein is populated in both folded and unfolded state. It shows the active folding and unfolding of the protein as a function of time which manifest as a hop or a abrupt length changes between two or more states. The resulting probability distribution for both folded and unfolded state allows to extract protein free energy landscape and other kinetic parameters of folding reaction.

1.5.3 Magnetic Tweezers

A basic setup for magnetic tweezer experiments is shown in fig 1.13. The working principle involve tethering one end of molecule, typically a DNA, to a paramagnetic bead via some specific chemistry with other end fixed to a glass surface. The paramagnetic bead is held at a constant force in the gradient of magnetic field generated by the two magnets. This gradient applies a net upward force proportion to the change in magnetic field, $F = \mu\Delta B$ and the force can be changed by moving the magnets upward or downward. Force-extension curves are recorded by measuring the force using transverse fluctuation of the bead with force $F = k_B T l / \langle \delta x^2 \rangle$. Here, l is the position of the bead from the glass surface which is independently measured using precise image analysis of the bead. In the last decade, advances in magnetic tweezer(MT) have provided several advantages compared to optical tweezer and AFM[25]. MT has enabled molecule manipulation at very low forces which are not accessible with OT and AFM. Typical stiffness of the probe in MT is about 10^{-4} pN/nm which allows forces in the range 0.05 - 20 pN to be easily accessible. For experimental configuration of MT, the constant force measurement are naturally suited without the need of any feedback circuit. This is because the gradient of magnetic field are almost constant for range of position of the bead. It is also possible to rotate and twist the molecule by rotation of the magnets. MT experiments have been predominantly performed on DNA.

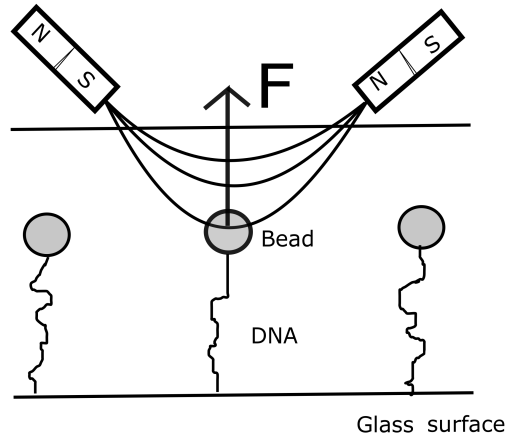


Figure 1.13: A basic setup of a magnetic tweezer experiment. It includes a DNA molecule tethered between a paramagnetic bead and glass surface. Paramagnetic bead is trapped in a gradient of magnetic field with a net force acting in upward direction.

| | AFM | Optical Tweezers | Magnetic Tweezers |
|---|------------|------------------|-------------------|
| Spring Constant (pN nm^{-1}) | 10-500 | 0.05-1 | 0.0001 |
| Force range (pN) | 20 -> 1000 | 1-100 | 0.05-20 |
| Force resolution (pN) | 10 | <1 | <1 |
| Time resolution (μs) | < 100 | <10 | <10 |

1.6 Linear response and fluctuations - Active and Passive Rheology

Linear Response

The term rheology encompasses the tools and techniques that are used to measure the response of a system to external perturbation. A dynamical observable $R(t)$ of a system evolves in time following a differential equation $DR(t) = 0$ where D is a linear differential operator. Now suppose that the system is subjected to a general time dependent force or stimulus $f(t)$ such that $DR(t) = f(t)$. Then, average

response $R(t)$ which is linear in external force for small strength of forcing is defined as :

$$R(t) = \int_{-\infty}^t \Phi(t-t')f(t')dt' \quad (1.23)$$

In most physical situations the properties of system do not change with time and linear response does not depend on the when the external force is applied but rather on retarded time or time lapse from the application of force. The response function $\Phi(t-t')$ which characterizes the response is therefore a function of retarded time $t-t'$ only. On physical grounds, response is also expected to be causal which means that it only depends on past history of force and response function is zero for $t > t'$. This condition is easily accommodated by limiting the integration limit to just t .

In many situation one is interested in response to oscillatory force with a particular frequency ω . In any case, the general time dependent force can be written through fourier analysis in terms of frequency components with continuous range of frequencies ω . Since the response is linear, each frequency component could be superimposed to yield a response to general frequency ω . This is easily done by taking the fourier transform on both sides of equation 1.24 and rearranging the terms to get :

$$R(\omega) = \chi(\omega)F(\omega) \quad \text{with} \quad \chi(\omega) = \int_0^{\infty} d\tau e^{i\omega\tau} \Phi(\tau) \quad (1.24)$$

where $R(\omega)$ and $F(\omega)$ are fourier transforms of $R(t)$ and $f(t)$ respectively. In general, frequency response function $\chi(\omega)$ is a complex quantity with both real $\chi(\omega)'$ and imaginary part $\chi(\omega)''$. From the definition in eq 1.24, the real part has cosine term and imaginary part has a sine term so that response s finally written as;

$$R(\omega) = [\chi'(\omega) \cos \omega t + \chi''(\omega) \sin \omega t]F(\omega) \quad (1.25)$$

If we are driving the system with oscillatory force $f_0 \cos(\omega t)$ than the real part of response function $\chi'(\omega)$ measures the in-phase or elastic response of the system and out-of-phase imaginary part $\chi''(\omega)$ measures the dissipative response of system.

Another way of writing the response is in terms of green function $G(t-t')$ so that

$$R(t) = \int_{-\infty}^{+\infty} G(t-t')f(t')dt' \quad (1.26)$$

where green function is response to delta function $DG(t-t') = \delta(t-t')$. Taking fourier transform on both sides of eq. reveal that a simple fourier transform of green function is the frequency response function $\chi(\omega)$.

Fluctuations

Uptil now we discussed the response of system in presence of external force. Now let us look at a system subjected to spontaneous fluctuation or noise, say a polymer/ brownian particle in a fluid. We develop tools that quantify noise or a fluctuation in both its time dependence and frequency domain. If random variable $R(t)$ defines a random process due to fluctuations, then average of the product of random variable at two different instant of time is aptly called the autocorrelation function : $\langle R(t_0)R(t_0+t) \rangle$. Under simplification of stationary processes when overall behavior

of system does not change with time, autocorrelation can be written as a function of time interval $t - t_0$ only and given as :

$$\langle R(t_0)R(t_0 + t) \rangle_{eq} = \langle R(0)R(t) \rangle_{eq} = \Phi(t) \quad (1.27)$$

The Wiener-Khintchine theorem than shows that fourier transform of autocorrelation function $\int_{-\infty}^{+\infty} dt \Phi(t) e^{i\omega t}$ is equal to power spectral density $S_R(\omega)$ defined as;

$$S_R(\omega) = \lim_{T \rightarrow \infty} \frac{|\int_0^T dt R(t) e^{i\omega t}|^2}{T} \quad (1.28)$$

This allows us to calculate power spectrum directly from autocorrelation function. I have deliberately used the same notation for autocorrelation as that for response function. Next, we argue that there is deep connection between response to external force and equilibrium fluctuation quantified through its autocorrelation in absence of external force. Stated differently, frequency spectrum in power spectral density is related to the frequency response function $\chi(\omega)$ in presence of external forcing. This is the essence of famous fluctuation-dissipation theorem. To illustrate the connection, let us take the model of overdamped simple harmonic oscillator in presence of stochastic noise $\eta(t)$. This gives a stochastic differential equation that governs the dynamical evolution of variable $R(t)$ in time. The equation is a good description of a polymer represented by a dumbbell with spring k and dashpot γ connected in parallel and in contact with a heat bath.

$$\gamma \frac{dR}{dt} + kR = \eta(t) + f(t) \quad (1.29)$$

Based on this we explicitly calculate the autocorrelation, power spectral density and frequency response in presence of force $f(t)$.

It is easy to show that autocorrelation in equilibrium without the external force $f(t)$ is $\Phi(t) = \frac{1}{\gamma} e^{-t/\tau}$, where $\tau = \gamma/k$ is the relaxation time. Thus, correlation between $R(t)$ at different times just decays exponentially with relaxation time τ . It means that autocorrelation describes the relaxation of the system which is naturally expected to relate to the response function. Now using the Wiener-Khintchine theorem, power spectral density is calculated as fourier transform of autocorrelation:

$$S_R(\omega) = \frac{2k_B T \gamma}{k^2 + (\omega\gamma)^2} \quad (1.30)$$

The frequency response can be found out by taking fourier transform of eq 1.29 and is given by $\chi(\omega) = \frac{1}{k(1+i\omega\tau)}$. It is then easy to see that there is a direct linear relationship between power spectral density and the imaginary part of frequency response function as :

$$S_R(\omega) = \frac{2k_B T}{\omega} \chi''(\omega) \quad (1.31)$$

This is fluctuation-dissipation theorem in frequency domain. It can be proven more rigorously without a model of overdamped harmonic oscillator. In time domain, it is then obvious that autocorrelation is just the time dependent response function $\Phi(t)$ in presence of external force. In other words, fluctuation-dissipation provides a relationship between spontaneous fluctuations in equilibrium to linear response in presence of small perturbation.

If one extracts the response of system directly by oscillating the system under small external force, it is generally termed as Active Rheology. Other technique in which the equilibrium fluctuations are measured and fluctuation-dissipation theorem is then used to relate it to the final response is called Passive Rheology. These two techniques will form central part of this thesis to specifically estimate the elastic response of single polymers.

1.7 Motivation and Objective

For a very long time, experimental investigation of elasticity of polymer chain have been indirect. With the advent of single molecule techniques, it was possible to manipulate single polymer chains and measure elasticity or force versus extension curves with high degree of precision. In initial development of force spectroscopy methods, molecules were stretched to high force with technique such as AFM (atomic force microscopy) and optical tweezers. Mode of constant velocity was used to generate force extension curves and became a standard in quantifying elasticity of polymer. When polymer is stretched to a force, it is important to accurately model the effect of this force on the statistical configurations of polymer and measure its entropic elasticity. Two main class of models i.e FJC (freely-jointed chain) or WLC (wormlike chain) have been used in describing entropic elastic response measured under force. A FJC model, already discussed briefly, is an ideal model that treats the polymer as being made up of discrete bonds connected freely with respect to each other. However, there is always a correlation between consecutive bonds due to some rotational hindrances along the bonds as pointed in eq (1.9). Contrast to this, WLC model has an exponential correlation in sequence of bonds and is a more realistic description of polymer elasticity. In 1990s, validity of FJC model was tested on biological polymer double stranded DNA and it failed to describe its entropic elasticity[14]. Indeed, as pointed out, there is no polymer which has satisfactorily shown a FJC behavior[15]. On the other hand, WLC model well describe elastic response of biological polymers like DNA and proteins with reasonable accuracy[14, 15]. Description is reasonable with respect to intrinsic parameter of Kuhn length b or persistence length $l_p = b/2$ which takes a physical value similar to other techniques that do not employ force. Surprisingly, using a WLC model to describe the synthetic flexible polymers has resulted in nonphysical values of b or l_p less than c-c bond length. In the last decade, experiments based on magnetic tweezer began to be used for measuring force-extension curves. The magnetic tweezer experiments operate force-extension profile in constant force mode. It became apparent that measurement on synthetic polymers is satisfactorily described by WLC with a physical value for persistence length[15]. It thus raises questions on the validity of WLC for simple synthetic polymers in AFM experiments. The major part of thesis aims to understand this discrepancy of persistence length in force spectroscopy based on AFM.

It is also observed in AFM force-extension curves that fluctuations about mean elastic behavior is very small. According to statistical physics of polymer, fluctuation depends sensitively on size or length of polymer chain. However, AFM experiments does not distinguish between different length polymers in regards to fluctuations. These questions need to be addressed as well.

It is to be noted that WLC and FJC are still average polymer backbone models which do not account for the presence of solvent and polymer side chains. They are

generally considered to be valid in good solvents and quality of solvent tend to alter the polymer configurations[26, 27]. However, it is still unknown in the literature as to how poor solvent effects will manifest in the high force AFM measurements. Water is a natural poor solvent for globular proteins which have hydrophobic side chains. It is assumed that persistence length obtained in AFM experiments is reasonable but molecular dynamic simulation suggest that it is still less than the expected value from considerations of rotational constraint[26]. We aim to also understand the effect of poor solvent on persistence length using simple hydrophobic homopolymer and more complex protein heteropolymer.

Elasticity of biopolymers is not just distinct from its synthetic counterparts in terms of quality of solvent. A globular protein like I27 domain of Titin is an important water soluble protein responsible for mechanical functions like muscle contraction. On the other hand, a membrane protein Bacteriorhodopsin is mainly concerned with transportation of ions and other nutrients across the cell membrane. There is no clear mechanical operation involved in functioning of this protein. Differences in functions is fundamentally linked to distinct mechanism of folding unstructured polypeptide chain into different secondary structures of globular and membrane proteins. The process of folding can be understood by identifying heterogeneity in structures or intermediates present in unfolded state. The comparison in elastic behavior of these protein is essential to understand heterogeneity and elucidate function-structure relationship.

1.8 Scope and Thesis outline

This thesis shed light on scope of different AFM based experiments while trying to measure the polymer elasticity. We use AFM based passive and active rheology to get estimates of elasticity, independent of conventional force-extension curves. We understand experimental differences between conventional AFM measurements and rheological estimates of elasticity using statistical mechanical analysis. In the processes, we address the discrepancy observed in force-extension curves.

In second chapter of thesis, I begin by introducing AFM (atomic force microscope) as a force measuring device. In this, I first discuss static force measurement in which cantilever is pulled away at a constant velocity from the sample to generate force-extension curves. After a brief discussion on interpretation of force-extension curves, I elaborate on various components of a AFM system and their principle of operation and design. Next, I introduce another force measurement technique called dynamic AFM in which cantilever is actively oscillated at some frequency. In this, I discuss modelling of cantilever dynamics in liquids that correctly relates amplitude and phase of oscillations to underlying elasticity or dissipation of the polymer. In effect, dynamic AFM allows us to perform Active Rheology measurements on polymers.

In third chapter, I describe main results on synthetic polymers using AFM based Active Rheology. I perform both conventional pulling and oscillatory rheology AFM measurement on PEG and Polystyrene in good and poor solvents. Both measurements of elasticity were analysed with entropic WLC model to extract persistence length. In particular, persistence length was compared for polymers in good and poor solvents. The differences in persistence length in two methods was explained with statistical mechanics of combined cantilever-polymer system. Also, polymer

fluctuations about the measured elasticity were compared for different length polymers. These results were explained using polymer physics.

In fourth chapter, I performed same measurements as done in chapter three but now with a home-built interferometer-based AFM. I discuss the basic principle of operation of optical fibre-based interferometer detection scheme employed to measure cantilever oscillations. This allowed for a simple verification of our past results. Commercial AFM used beam deflection scheme and not so straightforward analysis of beam vibrations to interpret the data. A simple and a clear-cut procedure with interferometer based active rheology firmly established our results.

In chapter five, I present my results of passive rheology measurements with biopolymers like I27 domain of protein Titin and membrane protein Bacteriorhodopsin. Compared to active oscillations, thermal fluctuation provides a non-invasive and time resolved tool to understand polymer elastic response. Time series analysis of thermal deflections of cantilever was performed to reveal elasticity of unfolded biopolymers. In particular, power spectral density was calculated at each extension of proteins and was analysed with Brownian simple harmonic oscillator (SHO) model to estimate elasticity. The limited sensitivity of fluctuation measurement to polymer response was revealed with statistical mechanical analysis of coupled cantilever-polymer system. This was different to active rheology measurements. The problem of non-stationary time series was also discussed.

In the end, we summarize all conclusions made from active and passive rheology on polymers and biopolymers and what it reveals about AFM force measurement.

Bibliography

- [1] Hermann Staudinger. Über polymerisation. *Berichte der deutschen chemischen Gesellschaft (A and B Series)*, 53(6):1073–1085, 1920.
- [2] P.J. Flory. Spatial configuration of macromolecular chains. nobel lecture, 1974.
- [3] Robert Pecora. Paul john flory. *Physics Today*, 39(11):116, 1986.
- [4] Kurt H Meyer, G v Susich, and E Valko. The elastic properties of organic high polymers and their kinetic interpretation. *colloid journal*, 59(2):208–216, 1932.
- [5] Werner Kuhn. über die gestalt fadenförmiger moleküle in lösungen. *Kolloid-Zeitschrift*, 68(1):2–15, 1934.
- [6] Eugen Guth and Hermann Mark. Zur innermolekularen, statistik, insbesondere bei kettenmolekiilen i. *Monatshefte für Chemie und verwandte Teile anderer Wissenschaften*, 65(1):93–121, 1934.
- [7] Peter Hinterdorfer and Antoine Van Oijen. *Handbook of single-molecule biophysics*. Springer Science & Business Media, 2009.
- [8] F Moreno-Herrero, J Colchero, J Gomez-Herrero, and AM Baró. Atomic force microscopy contact, tapping, and jumping modes for imaging biological samples in liquids. *Physical Review E*, 69(3):031915, 2004.
- [9] Alexei R Khokhlov, Alexander Yu Grosberg, and Vijay S Pande. *Statistical physics of macromolecules*, volume 1. Springer, 1994.
- [10] Michael Rubinstein, Ralph H Colby, et al. *Polymer physics*, volume 23. Oxford university press New York, 2003.
- [11] J Milton Harris. *Poly (ethylene glycol) chemistry: biotechnical and biomedical applications*. Springer Science & Business Media, 1992.
- [12] F Oesterhelt, M Rief, and HE Gaub. Single molecule force spectroscopy by afm indicates helical structure of poly (ethylene-glycol) in water. *New Journal of Physics*, 1(1):6, 1999.
- [13] Mariano Carrion-Vazquez, Andres F Oberhauser, Susan B Fowler, Piotr E Marszalek, Sheldon E Broedel, Jane Clarke, and Julio M Fernandez. Mechanical and chemical unfolding of a single protein: a comparison. *Proceedings of the National Academy of Sciences*, 96(7):3694–3699, 1999.
- [14] John F Marko and Eric D Siggia. Stretching dna. *Macromolecules*, 28(26):8759–8770, 1995.

- [15] Omar A Saleh. Perspective: Single polymer mechanics across the force regimes. *The Journal of chemical physics*, 142(19):194902, 2015.
- [16] David Keller and Carlos Bustamante. The mechanochemistry of molecular motors. *Biophysical journal*, 78(2):541–556, 2000.
- [17] Carlos Bustamante, Zev Bryant, and Steven B Smith. Ten years of tension: single-molecule dna mechanics. *Nature*, 421(6921):423–427, 2003.
- [18] Akiyoshi Kishino and Toshio Yanagida. Force measurements by micromanipulation of a single actin filament by glass needles. *Nature*, 334(6177):74–76, 1988.
- [19] Ernst-Ludwig Florin, Vincent T Moy, and Hermann E Gaub. Adhesion forces between individual ligand-receptor pairs. *Science*, 264(5157):415–417, 1994.
- [20] Gerd Binnig, Calvin F Quate, and Ch Gerber. Atomic force microscope. *Physical review letters*, 56(9):930, 1986.
- [21] Matthias Rief and Helmut Grubmüller. Force spectroscopy of single biomolecules. *ChemPhysChem*, 3(3):255–261, 2002.
- [22] Arthur Ashkin. Acceleration and trapping of particles by radiation pressure. *Physical review letters*, 24(4):156, 1970.
- [23] Arthur Ashkin, James M Dziedzic, John E Bjorkholm, and Steven Chu. Observation of a single-beam gradient force optical trap for dielectric particles. *Optics letters*, 11(5):288–290, 1986.
- [24] Arthur Ashkin. Optical trapping and manipulation of neutral particles using lasers. *Proceedings of the National Academy of Sciences*, 94(10):4853–4860, 1997.
- [25] Charlie Gosse and Vincent Croquette. Magnetic tweezers: micromanipulation and force measurement at the molecular level. *Biophysical journal*, 82(6):3314–3329, 2002.
- [26] Frauke Gräter, Pascal Heider, Ronen Zangi, and BJ Berne. Dissecting entropic coiling and poor solvent effects in protein collapse. *Journal of the American Chemical Society*, 130(35):11578–11579, 2008.
- [27] Greg Morrison, Changbong Hyeon, Ngo Minh Toan, Bae-Yeun Ha, and D Thirumalai. Stretching homopolymers. *Macromolecules*, 40(20):7343–7353, 2007.

Chapter 2

Force Spectroscopy using Atomic Force Microscope

2.1 General overview and chapter organisation

Atomic Force Microscope (AFM) is an indispensable and a versatile tool in the field of nanoscience and nanotechnology. It was discovered in 1986 by Gerd Binnig, Calvin Quate and Christoph Gerber, in the family of scanning probe microscopes that includes its predecessor Scanning Tunneling Microscope (STM)[1]. The general underlying principle involves positioning a sharp nanometer size probe close to the surface of interest. This led to generation of atomic resolution topography images and characterizing physio-chemical interactions at nanoscale. A unique feature of such microscopy techniques is that the resolution is not limited by diffraction limit as opposed to optical and electron microscopy. STM was first in the family of scanning probe microscope to be developed but it was limited to measurement on electrically conducting surfaces and mostly required UHV conditions for proper measurement. Therefore, soon after the discovery of STM, there was a need to understand a wide range of non-conducting materials ranging from material science to biology that eventually led to the development of AFM. It was AFM's capability to not only generate topographic images, but also to measure a host of local mechanical, electrical and physio-chemical properties that made it a very flexible and versatile tool[2]. In contrast to scanning probe techniques like STM, these measurements can be made in ambient or liquid medium without requiring vacuum conditions. This makes AFM easy to operate and made possible the imaging biological specimens in their native liquid environment[3]. AFM is a force measurement technique that operates by sensing forces of interactions between its sharp probe and the material. The tip-sample interactions are characteristic of the material properties of the sample and depends strongly on the relative separation between the tip and the sample. The sharp distance-dependent forces are precisely the reason why a good image contrast for a high resolution topographic imaging is obtained. The exact physical origin of this interaction then determines the local property of the substrate or the intervening medium that is mapped. These characteristic interaction forces between tip and the sample are recorded by the AFM as a function of their relative separation called force-distance curves[2]. Force-distance curves are very central to an AFM measurement which can now even be used to perform force mapping on the sample. Various kinds of short and long range interaction forces can act between the tip and

sample depending on the surrounding medium. The knowledge of interaction forces is important to interpret and analyze the measured force-distance curves and helps in choosing appropriate operation mode of AFM. In liquids for instance, it was realized that long-range forces are quenched between the tip and sample, which improved the resolution drastically.

In 1990s, force measurement technique, different from surface interactions, was added to the toolkit. This involves manipulating single polymer chains and stretching them under force[4]. This provided both equilibrium and kinetic information at single molecule level addressing fundamental problems in protein and cell biology under the realm of single molecule force spectroscopy. Early on, it shed light on mechanics of single polymer chains, which led to subsequent validation of basic principles in polymer physics and the physical mechanism of formation and breaking of bonds. AFM has contributed significantly in solving problems at interface of biology and physics such as single molecule biophysics along with techniques that include optical and magnetic tweezers. It has greatly enhanced our understanding of non-equilibrium statistical mechanics forming a perfect foreground to test relations like Jarzynski Equality. In last decade, these relations have been extensively used at single molecule level to construct free energy profiles of molecules.

2.1.1 Chapter Organisation

In this chapter, aim is to introduce AFM as a technique that can perform basic and advanced force measurements. The scope of this chapter includes physics and mathematical modelling required in various AFM operations along with fundamentals of AFM design and operation. The chapter can broadly be divided into two parts. First, we begin with a basic static AFM measurement of force-distance curve and how to interpret them. In this, we also explain components of AFM instrument and underlying principle involved. Second, dynamic AFM measurement is introduced in which the AFM probe is actively vibrated by an external source. Modelling of a vibrating cantilever in liquid is discussed, which is essential to extract important mechanical parameters.

In all, this will permit us to accurately measure, analyze and interpret force measurements using AFM.

2.2 Fundamentals of AFM

In this section we discuss basic principle of force measurement in AFM. This will include the technique of AFM including various requirements involved in its operation. A detailed interpretation of force-distance curve is discussed.

2.2.1 Principle of AFM- a force measurement device

It is fair to say that AFM has seen rapid growth in last two decades and expanded its scope to wide range of applications. The widespread use of AFM stems from its conceptual simplicity coupled with its ability to measure and apply piconewton forces and sub-nanometer vertical z resolution[5]. In practice, AFM is simple to understand with key to its operation requires a force sensing probe which consist of microcantilever with a sharp tip mounted vertically at its end. As shown in Fig.

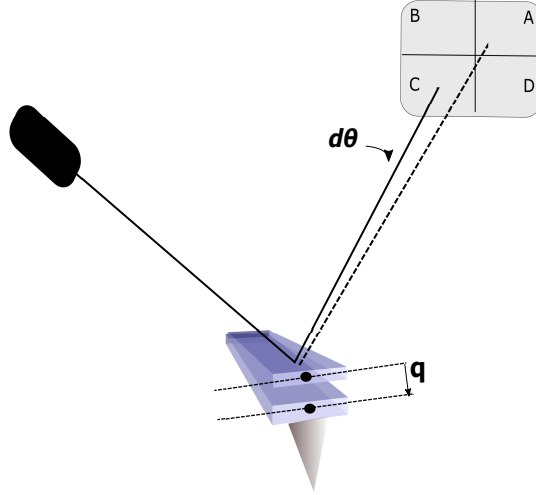


Figure 2.1: The principle of AFM operation

2.1 , cantilever-tip assembly is positioned at a distance Z from a substrate in the normal direction with a precision of 0.1 nm. The local force between the tip and the substrate deflects the cantilever by an amount q and this small deflection is recorded by a suitable detector. Under the assumption that the deflection is much smaller than length of the cantilever, we can approximate the cantilever like an ideal spring. In this case the force F due to deflection δ is given by Hooke's law:

$$F = kq \quad (2.1)$$

where k is the spring constant of the cantilever and q the cantilever deflection. The cantilever bends away from the substrate due to repulsive force and towards the substrate for an attractive force. In static equilibrium condition, force F experience by the cantilever is equal and opposite to the tip-substrate interaction force. As evident from eq. 1, sensitivity to a given force is critically determined by the choice of cantilever stiffness k and a sensitive way of detecting small deflections q of the cantilever. In order to measure interaction force which varies as a function of separation between the tip and the sample, it is required to move either the cantilever or the sample in the normal direction. Therefore, a precisely controlled motion of the cantilever with respect to the substrate is also required.

The aim of atomic force microscope is to be able to sense forces between the tip and the substrate that compares to atomic forces between two adjacent atoms in a solid. A simple calculation based on vibration frequency of atoms $\sim 10^{15}$ Hz together with atomic mass of 10^{-25} Kg gives interatomic stiffness as < 10 N/m. This implies that for interatomic separation of an angstrom, force less than nanonewton operates between atoms of a solid following Hooke's law. So the AFM cantilever required for sensing nanonewton forces should have stiffness equivalent to that between two atoms confined on a surface. Such cantilevers can be routinely micro-fabricated from silicon or silicon nitride using lithography technology used in semiconductor industry. It is usually of rectangular shape with typical length of $100 \mu m$ and thickness of the order of a $1 \mu m$. The stiffness of the lever critically depends on the thickness and the length of the lever. For the typical dimensions of the cantilever the stiffness range from 0.01 to 10 N/m. This stiffness range eventually dictates the minimum force that AFM can resolve while operating under thermal noise. This is because the ultimate

limit on detection of deflection q is set by thermal fluctuations in the environment. Under thermal noise, equipartition theorem states that $\frac{1}{2}k_c q^2 = \frac{1}{2}k_B T$, which means a vertical deflection sensitivity of 0.1 nm for typical stiffness of 0.1 N/m. Therefore, from eq 1, a minimum detectable force of 20 pN. In general, it follows from eq. 1 that for good force sensitivity a low stiffness cantilever and a sensitive detection scheme must be chosen. The design, optimal choice of a cantilever and the shape that cantilever takes under force will be discussed further in section 2.4.1.

Another critical component is a sensor that can detect small deflections of the cantilever. For a given force of nanonewton and typical stiffness of 10 N/m the deflection are as small as sub-nanometer. The most commonly used methods to detect cantilever deflections are the optical such as, optical lever or interferometric. The optical lever method is the most employed one, since it is simple to implement. It consists in focusing a laser beam at the end of the back side of cantilever and the reflected beam is detected by means of a position sensitive detector, that is usually a quadrant photodiode. The reflected beam changes its position on the photodiode due to changes in slope of the cantilever which is then recorded as a voltage change by the detector. The sensitivity of the photodiode used is such that it can easily detect sub-nanometer deflections with a bandwidth of around 10 KHz. The photodetector is able to achieve such high sensitivity due to large change in geometrical angle subtended at the photodiode for a small change in deflection. A further discussion of operational principle and design of optical lever and interferometric detection techniques is detailed in section 2.4.1.

In AFM force measurement, cantilever is required to move in normal Z direction relative to the substrate in a precisely controlled manner. In AFM imaging applications, it is moved in X-Y plane to map surface topography. This is achieved using piezoelectric scanners which can move with a precision of less than nanometer all the way upto tens of micrometer. Piezoelectric scanners can be used to either move the substrate or cantilever depending on the AFM setup. We will further discuss the functioning of piezoelectric scanners in next section.

Overall, these prominent components work in conjunction with intergrated control and electronics to make AFM a sensitive force measurement device.

2.2.2 Tip-sample interactions

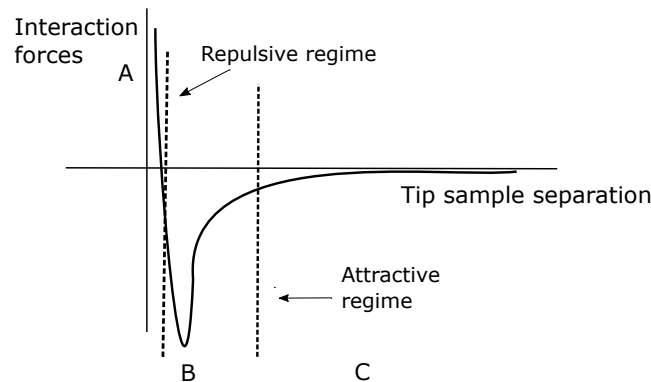


Figure 2.2: The graph shows distance variation of tip-sample interaction forces. The variation has both short range repulsive and long range attractive contributions.

As the name suggests, AFM is able to perform its operations due to ubiquitous presence of local forces between the tip of the cantilever and the substrate beneath it. An understanding of these forces is central to understanding how AFM functions[5]. AFM has demonstrated its ability to obtain high resolution topographic images. This breakthrough was possible due to the observation that AFM was able to study the interaction forces between the tip and sample which were responsible of those images. A precise information about tip-sample interaction forces helped in interpretation of high resolution images and choosing optimal modes of operation. Interaction force also contains important information about mechanical, chemical and surface properties of the sample. When AFM cantilever is located as close to 0.1-100 nm range of the sample, various intermolecular and surface forces act between the cantilever tip and the sample. In general, total interaction force can be approximated as a combination of different short range and long-range interaction forces. In ideal vacuum conditions, short range forces that decay rapidly within (< 0.3 nm) are composed of repulsive chemical forces whereas long range(1-100 nm)forces of Van der Waals, electrostatic and magnetic are attractive in nature. In ambient air, an additional meniscus or capillary forces due to absorbed layer of liquid on the tip or the sample contribute to long-range attractive interaction. These forces of atomic and molecular origin are summed over few atoms in the tip and local volume in the sample to yield a relation between force and tip-sample distance as shown in Fig 2.2. This shows repulsion force($F > 0$) that is present in short range close to the sample (region A). This sharp dependence at atomic scale(<0.3 nm) is reason for a good image contrast in AFM imaging and region is generally referred to as contact region. Region B and C comprise of attractive forces ($F < 0$) away from the sample that exist in a long range and referred as non-contact region. Few points about various forces that comprise the force-distance relation in Fig 2.2.

- Van der Waal force is always present between two objects due to induced dipoles in the atoms comprising the tip or the sample[2, 5]. Van der waal forces arise due to spontaneous formation of induced electric dipoles in neutral atoms under fluctuations. These fluctuating dipoles in the atoms of the tip and the sample tend to attract each other and result in a short range attraction that goes as $-\frac{1}{z^6}$. However when added up over atoms of macroscopic tip and the sample becomes a long range interaction going as $-\frac{1}{z^2}$.
- The chemical force can be attractive or repulsive but is always short range[2, 5]. Generally, there are forces including attractive forces due to overlap of outermost shells, which results in formation of chemical bond.
- If the tip and sample are made of conducting materials, electrostatic potential between them is nonzero. Therefore, attractive electrostatic force operative between the tip and sample that goes as $-\frac{1}{z}$.
- Capillary forces are important in ambient air because a layer of water may be adsorbed on tip or the sample[2]. When tip is brought close to the sample a bridge or meniscus between tip with sample is formed causing a net attraction. Capillary forces tend to dominate over all other attractive forces including van der waal forces in ambient environment.

The relation in Fig 2.2 is only qualitative because exact nature of interaction force and their dependence on tip-sample distance depends on the composition of

the tip or the sample and their sizes. Since summation of molecular forces need to be performed on well defined geometry of tip and sample, this relation also depends on shape of the tip and sample. A detailed discussion of these forces is not possible without the detailed knowledge of the system under study[5]. For present and subsequent discussion it is sufficient to say that their quantitative measurement in AFM is complicated due averaged out effect of various forces that act simultaneously as in Fig 2.2 and generally unknown composition or geometry of tip.

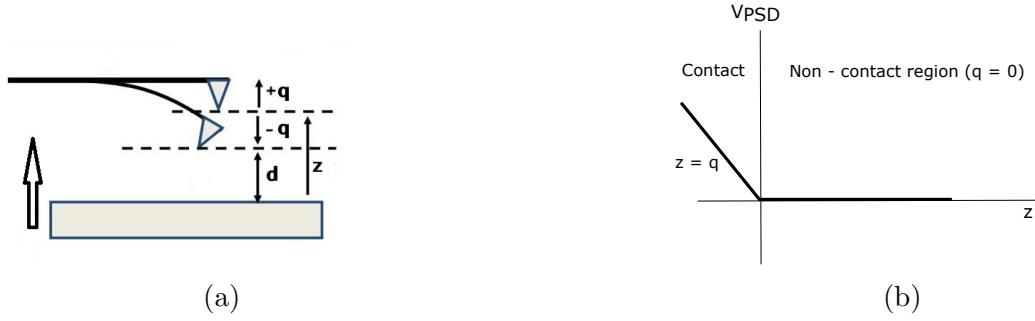
2.2.3 Force-distance curves

With AFM, goal is to measure the tip-sample force as a function of the tip-sample separation, d . In the process, useful information like adhesion, elasticity and other physical properties of interest can be extracted. Therefore, a fundamental output of AFM force measurement is a plot of the force experienced by the AFM cantilever versus the distance between the AFM tip and the sample surface[2, 5]. In order to acquire such a force-distance curve, tip and sample are approached towards each other until they make a well defined contact and then withdrawn. Depending on particular AFM setup, it is achieved by moving the tip or the sample in Z -direction, i.e. perpendicular to the sample, by means of a piezoelectric scanners. Once a predefined value of force is reached the approach is halted using a feedback control and sample is withdrawn away from the sample. According to the two directions of motion, a force-distance curve therefore encompasses two parts, the approach and retraction part. Now, at each position of the cantilever with respect to sample, two signals are recorded: 1) voltage change in the position sensitive photodiode V_{PSD} that is proportional to the deflection in the cantilever. Deflection signal is converted into force according to Hooke's law (eq. 1), if stiffness of the cantilever k is known. Under equilibrium condition, this force is equal and opposite to force due to tip sample interactions $F_{ts}(d)$ which is plotted on y-axis. 2) Another signal recorded is displacement z of the piezoelectric scanner which is plotted on the x-axis. Therefore, strictly speaking, a direct result of AFM force measurement is a plot of photodiode voltage V_{PSD} versus the displacement z of the piezoelectric scanner. A schematic of the tip-sample geometry when the sample is approached towards the cantilever tip is shown in Fig 2.3a. Here z is the distance between the surface of the sample and rest position of the cantilever. d is the actual distance between the cantilever tip and sample. Due to deflection these two are related as :

$$d = z + q \quad (2.2)$$

where q is positive when deflection is upward and negative when deflection is downward. Since quantity that is experimentally controlled in measurement is displacement z and not the actual tip-sample distance d , acquired curve are also called "force-displacement" curves. It is important note to the in Fig 2.3a displacement z measured is relative to an arbitrary and unknown initial offset $z = z_o$. Therefore location of zero distance, $z = 0$, when tip and sample are in contact is arbitrary in force displacement curve. It follows from eq. 2 that true distance d between tip and sample is also not a well defined quantity. Similarly, voltage V_{PSD} need to be divided with system sensitivity S in Volts/nm to get the deflection value $q = V_{PSD}/S$.

System sensitivity $S = \frac{\Delta V}{\Delta z}$ parameter and location of zero distance i.e $z = 0$ are inferred from the force curve itself and not through an independent method as explained below.



Force-displacement curve when $F_{ts}(d) = 0$

Typical force-displacement curve in absence of $F_{ts}(d) = 0$ is shown in Fig. 2.3b. This ideal scenario helps to understand how a basic force-displacement curve is measured from voltage from photodiode and arbitrary z position of piezoelectric scanner. Force-displacement curve consists of two distinct contact and noncontact regions. Contact region comprises of a linearly increasing line while noncontact region has a zero force line. These well defined parts are invariably present in the force curve even in presence of tip-sample interactions. The zero force line in noncontact region is recorded when the tip-sample distance is so large that no measurable force is acting between tip and sample. In absence of $F_{ts}(d)$ this is the only output in the noncontact region. For zero force line, voltage output from the position sensitive photodiode is some constant corresponding to zero deflection of the cantilever ($q = 0$). This voltage is therefore assigned a null value. Contact region consists of linearly increasing part which results from pressing on a hard solid sample such that cantilever deflects q as much as sample is displaced z . Thus for this line sample and cantilever move together such that $q = -z$ and distance between tip and sample d is zero. This line is referred to as contact line and slope of this line gives the sensitivity $S = \frac{\Delta V}{\Delta z}$ i.e. the voltage change in photodiode for a given change in deflection q or displacement z of the sample. Output from position sensitive photodiode V_{PSD} is divided with sensitivity S to get deflection q . Knowing the stiffness of the cantilever, deflection is ultimately converted into force using Hooke's relation. The zero distance of a force-displacement curve, and hence contact point between tip and sample, is the intersection between the zero force line and the contact line. In noncontact region, displacement of piezoelectric scanner z from the sample surface $z = 0$ and tip-sample distance d are equal since $q = 0$ in absence of tip-sample interactions. This procedure outputs a basic force-displacement curve.

Force-displacement curve when $F_{ts}(d) \neq 0$

The aim is to be able to measure tip-sample interaction as a function of distance d between the tip and sample. However, AFM measurement of force-displacement curve is not a representation of tip-sample interactions $F_{ts}(d)$ and can differ from force-distance curve considerably. To understand the connection between the two, it is necessary to consider force-displacement curve as a result of two contributions: the tip-sample interaction $F_{ts}(d)$ and the elastic force of the cantilever, $F = -kq = -k(d - z)$. The simultaneous action of these two contributions determines force-displacement curve and can be intuitively understood through a graphical construction[2]. Such a construction reveals a procedure to convert displacement

of the piezoelectric scanner, z , into the tip-sample distance d . It also explains the occurrence of the discontinuities in force-displacement curve. In Fig. 2.4, top panel shows the curve of F_{ts} the tip-sample interaction force as a function of d . This force curve has an attractive force ($F < 0$) and repulsive force ($F > 0$) as previously mentioned for fig. 2.2. The straight line 1-4 are the plot of line $F = -kq = -k(d - z)$ with slope equal to $-k$. The intersection of these lines with horizontal $F=0$ line correspond to rest position of the cantilever z from the sample. This is the distance we controlled and change systematically. So letting the straight lines shift from right to left by decreasing z starting with z_a till z_d produces the approach curve and from left to right produce retract curve. So all lines that goes from 1-3 produces the approach curve while 3 to 1 via 4 produces the retract curve. The resultant force-displacement curve is shown in the bottom panel with approach curve denoted with open circles and retract curve with grey points. Following important points need to be noted for such a process.

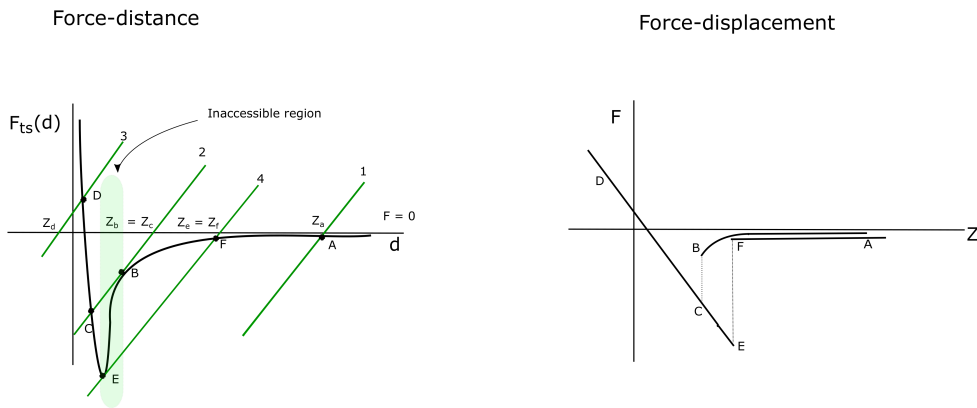


Figure 2.4: The conversion of a force distance profile to force-displacement profile.

1. While approaching the sample, at each separation z from the sample the tip experiences an attractive force due to the sample. As a result the cantilever bends by an amount q until the equilibrium position $d = z + q$ is reached. This equilibrium happens when tip-sample interaction force are counterbalanced by restoring elastic force due to cantilever $F_{ts}(d) = k(d - z)$. Graphically, this occurs at the intersection A-F of the straight line with the tip-sample force curve. The difference along the horizontal axis between these intersection points and z values gives the amount of deflection q . The equilibrium force values F_a till F_d are ordinates of these intersection points. These forces are assigned to z values z_a till z_d which we control experimentally, to obtain force-displacement relation for the approach part.
2. As the sample continues to approach the tip by shifting line 1 from right to left, the deflection of the cantilever increases due to the ever increasing magnitude of the tip-sample interaction force. Eventually, a situation will be reached at some new z_b value where the dashed line 2 with slope $-k$ will become tangent to the tip-sample force curve at point B. This point is unstable because any

small variation in distance will now make the tip deflection q to continuously deflect until the intersection point C is reached. All this occurs at the same z value and leads to jump-to-contact discontinuity BC in force displacement curve. Discontinuity indicates instability in the tip motion due to the ever increasing tip-sample gradient. The region between B and C is inaccessible due to instability and once point C is reached, the remainder of the force vs. z displacement curve can be obtained by decreasing z . The z is decreased upto a setpoint force predefined by user. This setpoint reverses the direction of z scanner so that a retract cycle is obtained.

3. The unstable regime (“jump-in contact”) is characterized by the point where the gradient of the attractive force is just about the spring constant k . Once the gradient of attractive force becomes larger than spring constant the cantilever jumps in. To explain this important condition one realize that stable equilibrium in a system must be insensitive to small changes in the position coordinates. Let us assume the tip moves a small distance towards the surface. Then the separation d decreases and the deflection increases: $\Delta d = -\Delta q$. This leads to a change of the total force of

$$\Delta F = k\Delta q + \frac{\Delta F_{ts}}{\Delta d}\Delta d = (k - \frac{\Delta F_{ts}}{\Delta d})\Delta q \quad (2.3)$$

If the spring constant is higher than the gradient of the attractive force ($k > \Delta F/\Delta d$) the total force F increases after a small, virtual movement of the tip. This leads to a restoring positive force, which drives the tip back to its previous position. However, when $\Delta F/\Delta d > k$ the net force is negative, the tip is driven further towards the sample surface and eventually jumps-in.

4. During the retract cycle, once again a tangent point is reached indicated by point E beyond which attractive forces exceeds the stiffness of the cantilever and cantilever jump to point F. This result in a jump-off-contact discontinuity EF in force-displacement curve and region of $F_{ts}(d)$ between E and F becomes inaccessible. Jump-off-contact happens at a different position z which is different from jump-in-contact leading to hysteresis in force-displacement curve.

Above construction provides a simple way to go from force-displacement curve to force-distance curve. However, such a analysis does not exactly reproduce the tip-sample interactions. Certain regions are inaccessible and in order to sample such regions the stiffness of the cantilever need to be increased. Large cantilever stiffness means that slope of line 1-4 in fig 2.4 is larger. This implies that straight lines 1-4 will now intersect the $F_{ts}(d)$ at only one point, thus reducing the inaccessible region. Therefore, a one-to-one construction of $F_{ts}(d)$ critically depends on stiffness of the cantilever and shape of tip-sample interaction forces.

2.2.4 Interpretation of force-distance curve

Both approach and retraction traces of force-displacement curve can be broadly divided into three regions: zero-line, contact region and non-contact region[2].

Zero force line, as already mentioned, are parts of force-displacement curves where tip and the sample surface are far separated from each other such that no

measurable force act between them. Despite no force in this portion of the curve, zero force lines have a great importance in that, it defines the cantilever rest position z . All important distances like deflection of cantilever or the tip-sample distance d are referenced with respect to the cantilever rest position. While working in a liquids, this line also gives information about viscosity of the liquid. Zero lines exhibit a hysteresis that results in a separation of approach and retraction traces. The hysteresis of zero lines is due to the viscosity of the liquid which pulls the cantilever upward when approaching and downward when the sample is retracted.

Contact region occurs when cantilever tip and the sample are pressed against each other. This results in contact lines seen represented by the lines CD and ED in bottom panel of Fig. 2.4 . From the contact lines of force-displacement curves it is possible to characterize elastic properties of sample and verify various elastic continuum theories as well. To see how contact region gives information about the elastic stiffness of the sample, one notes that in contact region distance between tip and sample is equal to small indentation δ of sample. In such a scenario, $k_s\delta$ is a harmonic force due to the deformation, where k_s is sample stiffness. Under static equilibrium, this force must be equal to elastic deflection force due to cantilever i.e $k_s\delta = kq$. Therefore, by replacing d with δ in eq. 2.2 and using the equilibrium condition, we have[2]

$$F = kq = \frac{k_s k}{k_s + k} z \quad (2.4)$$

When stiffness k of the cantilever is much larger than the sample stiffness k_s , then $F \approx k_s z$. Therefore, the slope of contact lines gives information about the sample stiffness k_s . When stiffness k of the cantilever is much smaller than the sample stiffness k_s , then deflection q is equal to displacement z of the sample. This yields a straight line with slope -1 as indicated in Fig. 2.3b which is further used to measure sensitivity so that voltage output of photo-diode gets converted to deflection q .

The other interesting regions of force-displacement curves are the two non-contact regions, containing the jump-to-contact and the jump-off-contact. Jump-to-contact region in approach trace gives information about attractive or repulsive force acting between the cantilever tip and sample just before contact with sample is made. In ambient air conditions, this force is mainly dominated by attractive force due to formation of meniscus between the tip and sample due to adsorbed layer of water on the tip. Jump-off-contact in the retract trace is a measure of strong attractive capillary or meniscus forces that tend to act against the pull-off. Although van der waal attractive forces are always present between the tip and sample, contribution made by them and other forces is masked by strong capillary forces indicated by maximum pull-off force F_e . This large force complicates the analysis of other smaller force contributions and possibly damage the sample. In order to reduce such forces, measurement in liquid environment were suggested which reduces maximum pull-off force due to removal of capillary forces in liquids[6]. Also, the amount of hysteresis between jump-off and jump-in contact is found to be much smaller in liquid than in air. This observation greatly favours AFM operation in liquids.

2.3 Cantilever mechanics

The cantilever is at the heart of AFM force sensing operation. It consist of a sharp tip mounted at the end on a flexible beam that interacts with a force at the surface of sample. The mechanics of the beam allows us to translate force on the tip into deflections that are subsequently detected to yield a high sensitive force. Two important quantities of the cantilever beam are critical in this regard , the stiffness and resonance frequency of the beam. Both of them characterize the mechanics of cantilever beam and determined by its geometrical and material properties. For a rectangular shape cantilever beam with dimensions width w , thickness t , and length L , the spring constant k_c is given by[7]

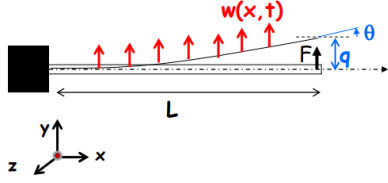
$$k_c = \frac{F}{q} = \frac{Ywt^3}{4L^3} \quad (2.5)$$

where Y is the young modulus of the material. and the resonance frequency is given by[7]

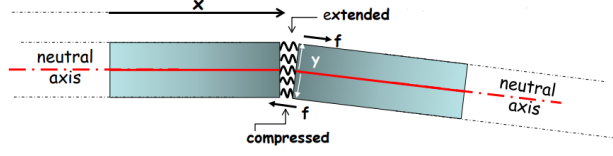
$$f = \frac{1}{4\pi} \frac{t}{2L^2} \sqrt{\frac{Y}{\rho}} \quad (2.6)$$

where ρ is mass density of the cantilever beam. It should be noted that eq 2.6 is only exact for a point mass particle, but as shown later, it is generally a good approximation for a continuum mass such as a cantilever. Ideally a low stiffness and high resonance frequency cantilevers are desired for operations. Low stiffness is required so that a large deflection sensitivity can be achieved for very small forces. For this, longer and thinner cantilevers need to be fabricated. Resonance frequency defines the time resolution of AFM $\tau = \gamma/f$. A high resonance frequency implies that the cantilever responds faster to changes in force. For larger resonance frequency the cantilever must be small according to eq 2. Therefore, in most cases choice of cantilever depends on the type of application and usually a compromise between speed and high force sensitivity. The first cantilevers were made from a gold foil with a small diamond tip attached to it[1]. Nowadays, cantilever are produced from microfabrication technology with well-defined mechanical properties. They are made of silicon or silicon nitride with tips intergrated with cantilever beam. The cantilever back side is generally coated with a metallic thin layer (often gold) in order to enhance reflectivity.

It is important to know the general shape of cantilever $w(x,t)$ under an applied force F at its end[5]. This quantity defines the cantilever mechanics by determining bending or inclination θ and deflection q due to applied force F as depicted in Fig 2.5a. The relation between deflection of the beam and force F calculates the bending stiffness k_c given by eq 2.5. The knowledge of how bending or inclination relates to deflection is important since most popular method of beam deflection measures a signal proportion to bending[2]. The geometry of cantilever with length L , width w_c and thickness t_c clamped at one end, with an external force F applied to its tip end is shown in Fig 2.5a. As a result of force, it bends by an angle θ and deflects by q from its unbent shape along the x-axis. The aim is to find the general shape described by function $w(x,t)$. In general, the shape will depend on the time and position. But assuming force F is in static equilibrium with the cantilever, time dependence is ignored so that $w(x,t)$ is just $y(x)$. We begin heuristically by noting



(a) Cantilever of length L , width w_c and thickness t_c lies unbent along x -axis. It is bent due to applied force with deflection q and bending θ .



(b) Internal stresses generated at position x inside the beam due to applied force F . It shows compression of hypothetical springs close to the bottom face (for $-y$) of beam and expansion along the top face (for $+y$). Along the neutral axis, there is no expansion or compression.

that at some position x along cantilever the torque because of applied force F is simply $\tau = (L - x) * F$. Position $r = L - x$ is assumed perpendicular to the force (Euler-Bernoulli assumption). Now, internal stresses will develop inside the beam as shown by hypothetical springs in fig. 2.5b. The springs close to top face ($+y$) expands and close to bottom ($-y$) are compressed. There exist an axis called neutral axis in the middle ($y = 0$) of cantilever which remains undeformed. These spring forces produces torque about the neutral axis such that they oppose applied torque and tend to restore the cantilever to its original unbent shape. From fig 2.6, it is seen that after the bent of segment dy at position y changes its length from l to $l + dl$. For any given y , it follows from the Hooke's law that spring force df acting on an area element $dA = w_c dy$ is proportional to strain dl/l . From the bent geometry, we have $d\theta = l/R = dl/y$ such that

$$\frac{df}{dA} = Y \frac{dl}{l} = Y \frac{y}{R} \quad (2.7)$$

In equilibrium, sum of all internal torques at x must balance the torque developed by the applied force F at x . Therefore,

$$(L - x)F = \int_{-t_c/2}^{t_c/2} df \cdot y = \int_{-t_c/2}^{t_c/2} Y w_c \frac{y^2}{R} dy = \frac{Y w_c t_c^3}{12} \frac{1}{R} \quad (2.8)$$

Now, by standard mathematical definition $1/R$ is just the curvature of the bent shape which is equal to d^2y/dx^2 . Substituting we have,

$$\frac{1}{R} = YI \frac{d^2y}{dx^2} = F(L - x) \quad (2.9)$$

The elastic response caused by compression of the cantilever at the top face and the expansion at the bottom face is given by $YI d^2y/dx^2$, where I is $I = w_c t_c^3/12$. Solving the above equation with boundary condition $y(x) = 0$ and $dy/dx = 0$ at clamped end $x = 0$, we get

$$y(x) = \frac{F}{YI} \left(\frac{Lx^2}{3} - \frac{x^3}{6} \right) \quad (2.10)$$

It follows from the the above shape of a bend cantilever that deflection $q = y(L) = \frac{1}{3} \frac{L^3}{YI} F$ and bending $\theta = \frac{dy}{dx} = \frac{L^2}{2YI} F$. Both deflection and bending that is generally measured are proportional to applied force. The bending stiffness of eq 2.5 given by $3YI/L^3$.

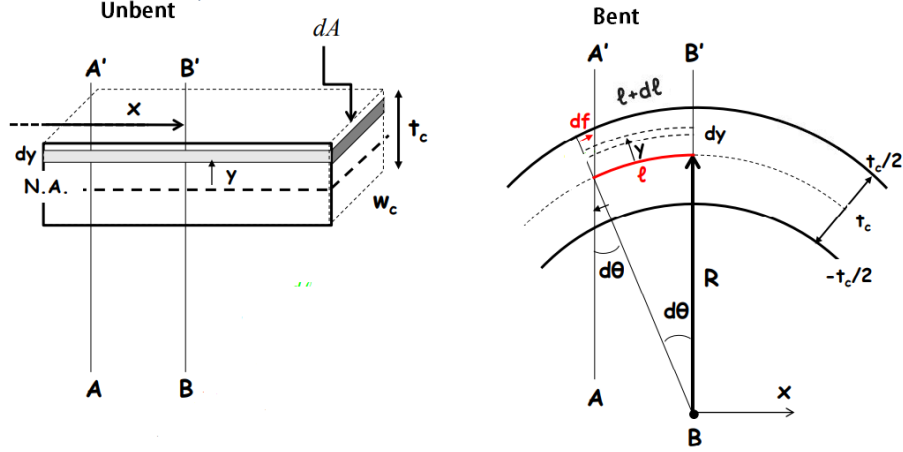


Figure 2.6: The enlarged view of a section of cantilever at position x before and after the bending due to force. A thin segment of the cantilever with thickness dy is located at a distance $+y$ from the neutral axis. After bending through an angle $d\theta$, the length of the segment changes from l to $l + dl$.

The above mathematical procedure can be generalised to obtain equation of motion that governs the dynamics of cantilever beam. In this case shape $w(x,t)$ depends on time and will be useful in modelling dynamic AFM discussed later.

2.4 AFM system components

A standard AFM consist of three essential components that integrate together to determine its operation to a large extent[8]. These components are 1) AFM head and sample stage 2) HV electronic control 3) and DSP(Digital Signal Processor) and computer software as laid out in fig 2.7. The AFM head consist the cantilever holder, the laser and photodiode. It also contains adjustable mirrors for focusing the laser on the cantilever and additional electronics made of operational amplifiers to pre-process the photodiode output. From this, vertical force (F_N), lateral force (F_L) together with sum intensity (Σ) of laser are detected due to deflections of cantilever. The AFM head is kept on a sample stage usually consisting of piezoelectric scanners that can precisely position the sample relative to cantilever tip in (Z) direction and scan sample surface in (XY) direction. Piezoelectric scanners can perform motion ranging from few nanometers to (~ 100) micrometers. In recent stand-alone AFM models where cantilever tip is scanned over the sample, piezoelectric scanners are itself part of AFM head. In such AFMs, head is equipped with stepper motors for coarse (> 100 micrometer) approach towards the sample. The HV electronics is responsible for amplifying the low (XYZ) voltage generated from DSP processor to about 100 V high (XYZ) voltage to be supplied for piezoelectric scanner(piezotube) motion in micrometer range. The HV amplifier are able to do this without generating electrical noises so that piezoelectric scanner is moved in vibrationless fashion. The electronics also transfers analog outputs(F_N, F_L, Σ) to DSP processor. As part of electronic control, an important feedback loop is implemented using DSP which ensures that a certain quantity (like force F_N) remains constant in time while trying

to map out sample properties. The DSP processor performs all calculations and signal processing required for operation. DSP microprocessor is located inside a dedicated computer which converts digital signals to analog using DAC(Digital-to-Analog converter) chip. These analog signals are passed onto HV electronics for further processing. Also, analog signals from photodiode are converted into digital using ADC(Analog-to-Digital converter). Finally, a customised computer software is required to acquire data, monitor outputs(F_N, F_L, Σ), input commands to DSP for piezoelectric scanners motion. The following sections will discuss the design and implementation of the various components required to make an AFM operative.

3. Computer software

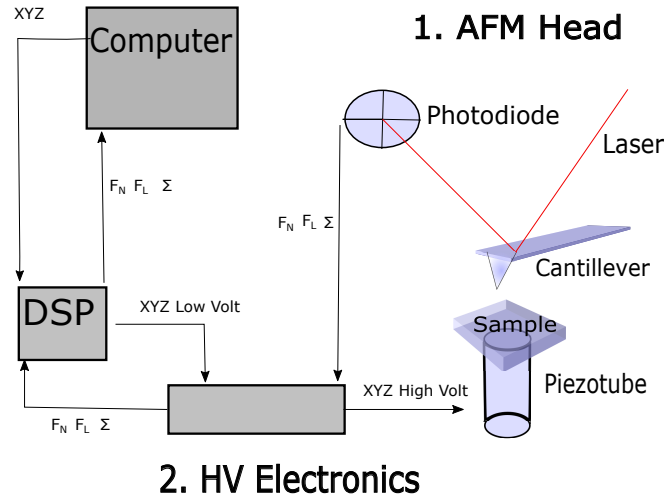


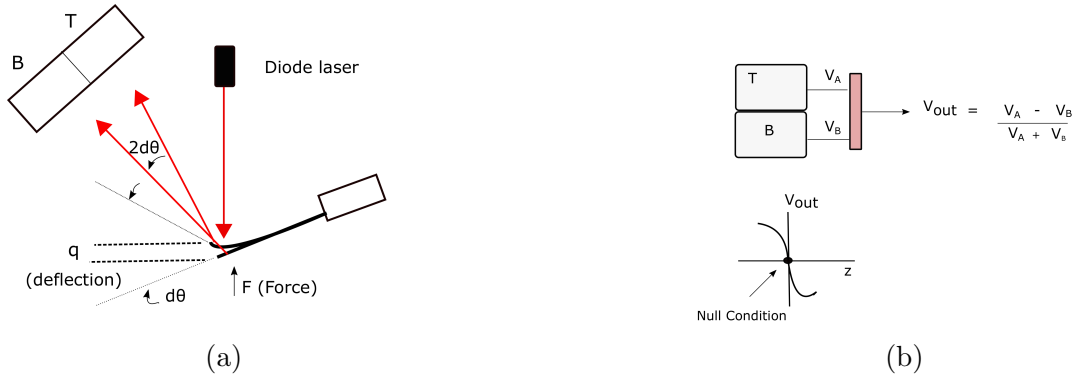
Figure 2.7: A schematic for components that form an AFM system. 1 AFM head and piezoelectoc stage. 2 HV electronics. 3 DSP and computer software.

2.4.1 Deflection Detection Methods

As discussed, AFM is to be able to sense forces acting between the cantilever tip and sample through the deflection of cantilever beam. Among various techniques employed to monitor this deflection, method of fiber-optic based interferometer and laser beam deflection have been developed to a higher degree of sophistication. We discuss these methods further in next two sections.

Beam deflection detection

In this method, a laser light from a laser diode is focused on the back side of cantilever using adjustable mirrors inside AFM head[8]. Typically, the laser requires $\sim 50\text{mA}$ current to produce a light beam with a power of $\sim 1\text{mW}$ and a diameter a few ten's of microns. As shown in fig 2.8a, laser reflects specularly from the cantilever and strikes the photodiode. When force F is applied to cantilever, it bends by an angle $d\theta$ and deflects by q . Due to this, the total change in angle subtended at the photodiode is twice the bending angle i.e $2d\theta$. This is because both angle of incidence and angle of reflection from the cantilever normal changes by $d\theta$. Therefore, total change in angle is $2d\theta$. As shown earlier in eq 2.10, bending angle $d\theta$ and deflection q are



related as $d\theta = \frac{3}{2} \frac{q}{L}$. Assuming the separation between cantilever and photodiode is S , change in position of laser spot on the photodiode would be

$$\Delta = 2d\theta S = 3 \frac{S}{L} q \quad (2.11)$$

Since $\frac{S}{L}$ is order of 100, there is significant amplification in laser spot on photodiode due to small deflection q . This makes beam deflection technique very sensitive in detecting deflection with resolution of upto 0.1 \AA . The vertical shift in laser spot position is shown clearly in fig 2.8b, measured using two segment photodiode. However, in general, a quadrant photodiode is employed to measure lateral deflections together with vertical deflections. The photodiode segments produce an electrical voltage output proportional to the intensity of laser light falling on them. By connecting the photodiodes to operational amplifiers an output signal that is difference in voltage from top T and bottom B segment is produced. This difference voltage is proportional to vertical deflection q but this signal is not used to measure deflections. An additional operational amplifier circuit produces sum of voltage from T and B . The output V_{out} formed from the ratio of difference and sum is finally measured. This is done to average out any intensity fluctuations in laser power so as to produce a robust output. A null condition in the output is achieved when intensity falling on both segments T and B is same. This is taken as a zero deflection or force on the cantilever when the cantilever is far from sample. It is noted that V_{out} from these diodes is linear only in limited range of deflections.

Interferometer-based detection

The beam deflection method is a popular choice in commercial AFM's because of ease of implementation. The deflection detection system based on optical fiber has become more accessible due to improved handling of optical-fiber technology[9]. As shown in fig 2.9, a diode laser with single mode fiber output is connected to a directional coupler input. At the output of the coupler, the laser power divides into half with one output connected to a reference photodiode and another attached to a single mode optical fiber that goes just on the top of cantilever. The end of optical fiber is partially reflecting and is cleaved precisely in a flat shape. The reflectivity of this cleaved end is just about 4 % and generally coated with a metal oxide(TiO_2) that increases reflectivity to 10 %. The reflected beam in the optic fiber interferes with 90 % of light that goes to cantilever gold surface and after reflecting from it comes back into the fiber. The final reflected signal in the fiber is split at the

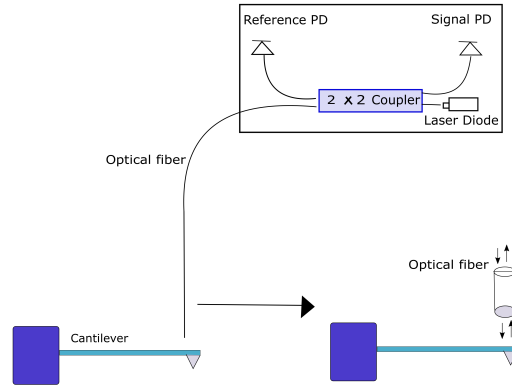


Figure 2.9: Optical-fiber based AFM deflection detection

coupler into half and then eventual fed to the signal photodiode. The output of signal photodiode is subtracted from reference photodiode to compensate for laser power fluctuations and yield the final interference pattern. When the fiber is placed close to cantilever surface in exactly perpendicular geometry, it results in multiple reflection from cantilever and fiber end whose ultimate interference in the fiber enhances the sensitivity. The fiber alignment is performed using 5-axis(x, y, z, θ, ϕ) nano-positioner based on inertial sliding principle. The fiber itself is mounted on a tube piezo(not shown) which perform upward and downward motion of fiber in z direction, to record interference pattern as a function of displacement between fiber and cantilever surface. As shown in figure 2.10, the interference pattern is extremely sensitive to relative displacement between optic-fiber end and cantilever surface. In this pattern, there are positions called quadrature points where slope or sensitivity is maximum. This is due to perfect constructive interference between light that is reflected from fiber and cantilever end. An algorithm is put in place to search for this maximum slope position and lock it there for further operation. This is done by connecting the tube piezo responsible for vertical motion of fiber to a PI feedback loop. We will further discuss discuss feedback loops in a later section. Fiber-interferometer, therefore, has a clear advantage in sensitivity and detects the cantilever deflection directly and not indirectly through change in inclination as in laser beam deflection detection[9].

2.4.2 Piezoelectric Positioners

The piezoelectric ceramics are used to move the cantilever tip with respect sample in an accurate manner. Piezoelectricity is a phenomenon where mechanical stresses applied across a crystalline solid results in generation of electrical voltage. In this processes, there is an alignment of atomic dipoles in crytallographic unit cell that results in a net electric polarization(voltage). This is due to asymmetric shift in atoms of a unit cell due to mechanical stress. The reverse phenomenon is also possible in which application of voltage to piezoelectric material leads to a mechanical motion. In context of AFM, this method is used to position tip with respect to sample with subnanometer precision. Fine piezoelectric powders usually based on Lead Zirconate Titanate (PZT) and Barium Titanate are calcined into a polycrystalline ceramic. These piezoceramic materials can then be easily moulded into a desirable shape(disc, tube etc..) for application. In most AFMs, tube shaped piezos

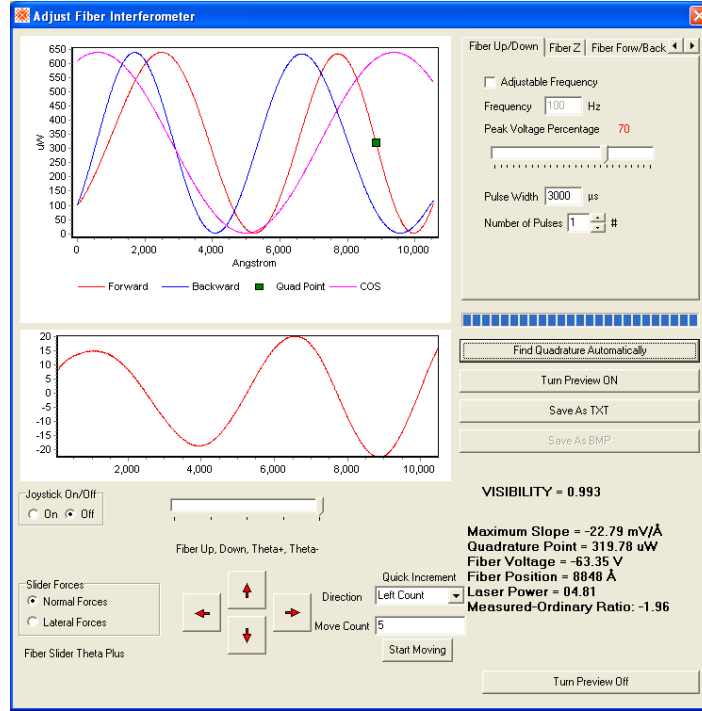


Figure 2.10: The top panel shows the interference pattern where X-axis is separation between fiber-tip and cantilever backside and Y-axis is intensity. In this, quadrature points are shown by a green square. The bottom panel is just the double derivative signal to intensity pattern in top panel, to locate the maximum slope position (quadrature points) on the interference pattern.

are used as depicted in fig 2.11. They are made like a thin-walled cylindrical tube

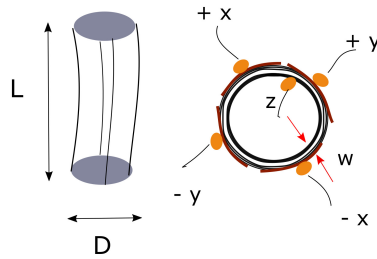


Figure 2.11

made from piezoceramic material whose exterior side is divided into four quadrant. A conducting electrode(+x,+y,-x,-y) is plated to each of these four segments and one electrode (z) to the entire inner side of the hollow tube. This tube can move in horizontal and radial direction by applying a voltage. A bias voltage $+V_0$ when applied between any one of the outer electrode and inner electrode produces x-y motion:

$$\Delta x = \Delta y = d_{31} \frac{L^2 V_0}{\pi D w} \quad (2.12)$$

where tube has length L , thickness w and diameter D . Note that d_{31} is strain coefficient that depends on type of piezoceramic. Similarly, bias voltage supplied

between all outer electrodes and z electrode (electrically neutral) produces z motion:

$$\Delta z = d_{31}L \frac{V_0}{w} \quad (2.13)$$

Typically, for tube piezos a motion of 20-25 nm is generated for per volt supplied voltage in x-y direction. Hence, a voltage of 100's of volt need to be supplied for micrometer range mapping. This task is performed by HV electronics which can generate and change this high voltage with submillivolt precision to achieve a systematic change of 0.05 nm.

2.4.3 Feedback loop

The aim of feedback loop in AFM operation is to keep certain quantity constant (for example force) in time as other other quantities are mapped out. This feedback loop, for instance, maintains the cantilever in contact with the surface by keeping the force between tip and surface constant in time. Any sharp changes in surface topography while mapping the surface makes the feedback instruct the z scanner to change its position such that force remains constant. Fig 2.12 shows a general

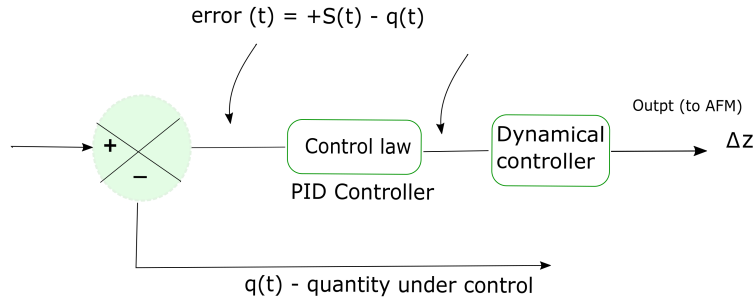


Figure 2.12: The feedback controller

feedback loop implementation. The quantity under control is usually the deflection $q(t)$ from the photo-diode, which is subtracted from set signal $S(t)$ preset by the user. In most cases $S(t)$ is just a constant set-point value that the user wants $q(t)$ to follow. This is achieved by feeding the error signal $S(t) - q(t)$ to a control law $K(t)$ which specifies an algorithm for minimizing the error signal. Algorithm consist of two correcting terms that are proportional(P) and integral(I) of the error signal with gain parameters K_P and K_I as:

$$K_P(S(t) - q(t)) \quad (2.14)$$

and

$$K_I \int_0^t (S - q(\tau)) d\tau \quad (2.15)$$

These two control signals are summed to finally give $K(t)$ that serves as an input to dynamical controller. The output of controller generates a voltage to adjust the z -scanner position Δz so that error signal is minimized. Based on this controlling algorithm, feedback is commonly known as a PI feedback loop. A proper choice of feedback parameters K_P and K_I must be made to produce a stable and reliable

feedback. Large values of parameters makes the feedback unstable to small changes in error signal making z-scanner oscillate and small values will make the feedback responds slowly. It is also important to note that both P proportional term alone is not sufficient for feedback. Although it being proportional to instantaneous error allows for fast changes compared to an integral but steady state error accumulated over time needs to be corrected using integral term.

2.5 Experimental calibrations

We recall that in measurement of force-distance curve a voltage is applied to z piezo scanner and output voltage from photodiode is primarily measured. The voltages to X,Y,Z piezos need to be appropriately calibrated to nanometer displacements of piezos. This task is easily carried out by running a AFM scan on commercially available gratings of known dimensions. Voltage output from the photodiode is proportional to bending angle or inclination $\theta = \frac{dy}{dx}$ which is ultimately proportional to cantilever deflection q . To measure deflections from this output, force-displacement curve on a hard substrate is performed with deflection measured in volts plotted against z-piezo displacement. As mentioned earlier, contact straight line in this curve correspond to condition where deflection in volts is equal to z displacement. In this way, slope of contact line gives sensitivity in volts/nm of beam deflection method. At this point deflection in nanometers needs to be converted to force following a Hooke's law. This requires calibration of spring constant k_c .

2.5.1 Spring constant calibration

To obtain quantitative AFM measurements spring constant need to be accurately calibrated. The calibration of spring constant k_c is important since value supplied by manufacturer based on formula from eq 2.5 are nearly approximate. This is usually because its value sensitively depends on the thickness (goes as t^3) but thickness is rarely known to high accuracy and spring constant could be off by a large factor. The methods based on geometric and thermal noise considerations are most commonly employed to directly measure the spring constant. The geometric method consist of using the dimensions of the cantilever such as width w and length L together with other parameters to determine spring constant. Estimate based on simple definition of spring constant of eq. 2.5 is one such geometric method. For rectangular cantilever, Sader etc. al[10] proposed using the resonance frequency ω_o and quality factor Q of the cantilever together with viscosity η and density ρ_f of medium in which the cantilever is immersed. According to hydrodynamic theory, following formula can be used to calculate spring constant

$$k_c = 0.1906\rho_f w^2 L Q \Gamma(Re) \omega_o^2 \quad (2.16)$$

where $\Gamma(Re)$ is so called "hydrodynamic function" that depends on Reynolds number $Re = \frac{\rho_f \omega_o w^2}{4\eta}$. Another elegant method most commonly employed in commercial AFM is based on the acquisition of spectrum of cantilever's thermal noise (square of the thermal fluctuations in amplitude as a function of frequency). According to thermodynamic equipartition theorem, there is a thermal energy of $\frac{1}{2}k_B T$ associated with each degree of freedom. By assuming cantilever a simple point mass with an

ideal spring k_c , Hutter and Bechhofer[11] proposed that thermal energy associated with this spring is $\frac{1}{2}k_B T$ according to equipartition theorem. Therefore, spring constant is:

$$\frac{1}{2}k_B T = \frac{1}{2}k_c \langle \Delta q^2 \rangle \rightarrow k_c = \frac{k_B T}{\langle \Delta q^2 \rangle} \quad (2.17)$$

The mean square thermal deflections $\langle \Delta q^2 \rangle$ are obtained by integrating the thermal spectrum over entire frequency range. This method seem to be independent of the shape the cantilever takes since point mass single degree of freedom scenario is assumed. However, this is a very convenient assumption and the shape of various vibration modes of cantilever must be accounted[12]. The calculation shows that for each vibration mode, mean square deflections is $\langle \Delta q_i^2 \rangle = \frac{k_B T}{k_c \alpha_i^4}$ where $\alpha_1 = 1.875, \alpha_2 = 4.694$ etc and summing this gives the result $\langle \Delta q^2 \rangle = \frac{k_B T}{k_c}$. In particular for first vibration mode we have,

$$k_c = \beta \frac{k_B T}{\langle \Delta q_1^2 \rangle} \quad (2.18)$$

where $\beta = 0.965$. This allows for accurate calibration of spring constant.

2.6 Dynamic-AFM

Until now we have been discussing the static situation in which no time variation of cantilever is discussed. A force applied at cantilever end and in static equilibrium cantilever deflection through cantilever mechanics is related to this force. In dynamic mode AFM, the cantilever is actively oscillated at a frequency and amplitude and phase response of system is used to interpret tip-sample forces. In its initial development dynamic mode was developed to overcome certain limitation of static AFM with regards to imaging application, however now it began to be used in making force measurements. In this section we discuss instruments and theory required in dynamic AFM mode. In particular, we focus on the case in which cantilever is excited at a fixed frequency but amplitude and phase is allowed to vary. This is generally termed as amplitude modulation AFM.

2.6.1 Cantilever Dynamics

With regards to dynamic AFM, it is useful to derive an differential equation that describes the dynamics of cantilever. Specifically, a differential equation describing transverse motion of cantilever $y(x, t)$ in both time t and spatial coordinate x along the cantilever is needed. It can be derived by generalising the discussions of section 2.3 regarding cantilever shape in static situation. Instead of applying a point force at the cantilever end, imagine applying a distributed force per unit length $P(x)$ acting along the length of cantilever. This force changes the shape of the cantilever until all internal forces generated from the cantilever balances this external force. Consider splitting the cantilever in two sections at some distance x from its base by an intersecting plane of small width Δx . As shown in fig 2.13, the left face of this element experiences force or torques from left section of cantilever and right face from remainder of the right section of cantilever. The internal forces and torques from cantilever act in such a way to produce no net acceleration of this tiny element.

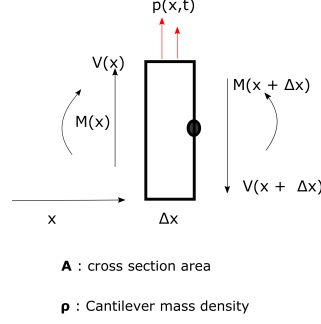


Figure 2.13

In this, two internal contributions are important 1) the internal torque or moment generated due to bend in the cantilever has the form $M(x) = YI d^2y/dx^2$ as noted in eq. 2.9. 2) internal shear force $V(x)$. In general for time dependent $p(x, t)$ a net force acting on element in fig 2.13 produces acceleration $\rho A(\Delta x)\ddot{y}(x, t)$ so that force balance condition is :

$$V(x) + p(x, t)\Delta x - V(x + \Delta x) = \rho A(\Delta x)\ddot{y}(x, t) \quad \text{as } \Delta x \rightarrow 0 \quad \text{we get}$$

$$\rho A\ddot{y}(x, t) = -\frac{dV(x)}{dx} + p(x, t) \quad (2.19)$$

Torque balance condition about the black dot on right face element is:

$$M(x + \Delta x) = M(x) + V(x)\Delta x + p(x, t)(\Delta x)(\Delta x/2) \quad \text{as } \Delta x \rightarrow 0 \quad \text{we get}$$

$$\frac{dM(x)}{dx} = V(x) \quad (2.20)$$

Combining the two equation together with the fact that $M(x) = YI d^2y/dx^2$, we get Euler-Bernoulli beam equation :

$$\rho A\ddot{y}(x, t) + YI \frac{d^4y(x, t)}{dx^4} = p(x, t) \quad (2.21)$$

This fourth-order equation describes the dynamics of cantilever for any point x along the cantilever and needs to be solved under four boundary conditions:

$$y(x, t)|_{x=0} = 0 \quad \frac{dy(x, t)}{dx}|_{x=0} = 0 \quad \frac{d^2y}{dx^2}|_{x=L} = 0 \quad \frac{d^3y}{dx^3}|_{x=L} = F \quad (2.22)$$

The boundary condition at a point where cantilever is pinned $x = 0$ are obvious. Second derivative boundary condition correspond to no bending torque $M(x)$ at cantilever end $x = L$, as there exist no element left to bend beyond this point. Third derivative boundary condition correspond to some external shear force F applied to cantilever end at $x = L$.

To gain simple insights from Euler- Bernoulli equation (2.21) let us assume that there is no distributed force $p(x, t)$ applied on cantilever. Then 1) In static case where acceleration $\ddot{y}(x, t)$ is zero, solving equation (2.21) with above boundary condition yields Hooke's relation (eq 2.5) between deflection and force F is applied at its end. Static case present the cantilever as a spring connected to a point mass with associated resonance frequency given by eq. 2.6. In this case, a simple picture of

cantilever emerges in which it is simply bent either up or down disregarding the continuous nature of cantilever beam. 2) In dynamic case where $\ddot{y}(x, t)$ cannot be neglected, the equation admits discrete eigenmodes when solved under force free ($F = 0$) boundary condition. The considerations of dynamics of cantilever via Euler Bernoulli equation assert that associated with each eigenmodes is a eigenmode frequency given by:

$$f_i = \frac{1}{2\pi} \left(\frac{\alpha_i}{L}\right)^2 \sqrt{\frac{YI}{\rho A}} \quad \text{where } \alpha_1 = 1.875 \quad \alpha_2 = 4.694 \text{ etc.}, \quad (2.23)$$

So, instead of a simple picture of static case, a cantilever can exist in all sort of shapes corresponding to different eigenmodes. In each of these eigenmodes cantilever can be oscillated when excited externally at eigenmode frequency. A cantilever's continuous nature is immediately evident in such a dynamic case.

When cantilever is oscillated by different means of excitation and tip-sample forces are present, boundary conditions will change and under appropriate boundary condition the Euler-Bernoulli equation need to be solved for analytical description of the system.

2.6.2 Hydrodynamics of cantilever

In liquid operation of AFM with dynamic mode, additional considerations are needed with regards to hydrodynamic force acting on the cantilever. An external hydrodynamic force acts on the cantilever because of its motion in viscous liquid significantly alters the cantilever dynamics compared to its operation in air or vacuum[3, 13]. The equation (2.21) valid for operation in air/vacuum needs to be modified to account for hydrodynamic force. This force is sum of two components: 1) viscous drag force acting per unit length on the cantilever proportional to its velocity i.e $\gamma_c \frac{dy(x,t)}{dt}$ and 2) added mass force due to additional mass of liquid that is effectively accelerated along with the cantilever i.e $M \frac{d^2y}{dt^2}$. Here γ_c is damping coefficient of lever and M is added mass which generally depends on frequency ω . The frequency dependence of these coefficients are given as[13]:

$$\gamma = -\frac{\pi}{4} \rho_l \omega t_c^2 \text{Im}[\Gamma(\omega)] \quad M = -\frac{\pi}{4} \rho_l t_c^2 \text{Re}[\Gamma(\omega)] \quad (2.24)$$

where $\text{Re}[\Gamma(\omega)]$ and $\text{Im}[\Gamma(\omega)]$ real and imaginary part of a complex hydrodynamic function $\Gamma(\omega)$ and ρ_l and t_c are liquid density and cantilever width respectively. Therefore, differential equation describing cantilever dynamics in liquids gets modified so that force per unit length $p(x, t)$ is substituted for hydrodynamic force :

$$m\ddot{y}(x, t) + YI \frac{d^4y(x, t)}{dx^4} + \gamma_c \frac{dy(x, t)}{dt} = 0 \quad (2.25)$$

where effective mass $m = M + \rho A$.

2.6.3 Cantilever excitation methods

An essential requirement of dynamic AFM is that cantilever is to be sinusoidal oscillated at a given frequency. There are different ways to achieve this and techniques

of excitation can be broadly divided into two parts: Indirect excitation and Direct excitation. An important and widely used indirect excitation scheme is described in fig 2.14a. Dither-piezo element is strongly attached to cantilever base to which a sinusoidal drive voltage is applied. The resulting change in shape of piezo drives the cantilever chip and in turn oscillates cantilever at frequency chosen for drive voltage. In direct excitation scheme, a cantilever is directly subjected to oscillating force and magnetic excitation is prominent way to achieve it. In this a thin film of ferromagnetic material is coated on cantilever probe and brought in close proximity to a solenoid coil. An alternating electric current to the coil produces an alternating magnetic field as shown in fig 2.14b. In presence of alternating magnetic field the cantilever experiences a direct oscillating force at frequency determined by alternating drive current.

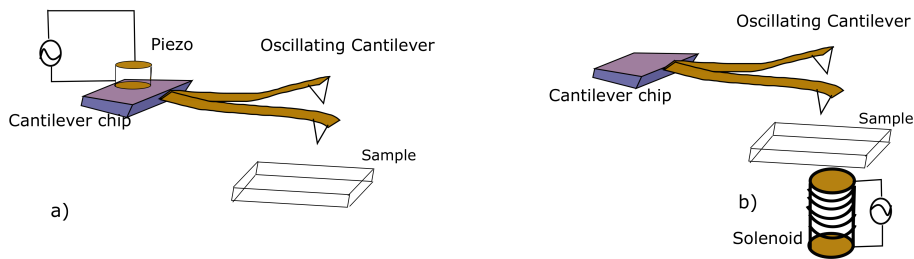


Figure 2.14: Piezo and Magnetic excitation modes of oscillating the cantilever

The base excitation which is of interest for the current thesis differs significantly in cantilever dynamical response $y(x, t)$ from direct magnetic excitation even in absence of tip-sample forces. This is mainly due to choice of detection methods. In beam deflection method commonly available in commercial AFMs the deflection is measured through change in bending angle $\theta = \frac{dy}{dx}$. This means that even if the cantilever tip is in hard contact with the surface, the cantilever beam will still keep on changing its slope θ even though there is no actual displacement of the tip. The change in slope will therefore be erroneously interpreted as a signal which is just equal to the base oscillatory motion. In other words it implies that beam deflection methods measures tip displacement with respect to the base and in order to correctly measure the response this base motion needs to be appropriately accounted for. However, no such problem arises in magnetic excitation scheme where base is never moved and remains fixed. In contrast to beam deflection detection, the direct displacement measurement based on interferometer detection does not distinguish between two excitation schemes.

2.6.4 Analytic theory of Dynamic AFM in liquids

The response of oscillating cantilever $y(x, t)$ in presence of tip-sample interactions is experimentally measured in terms of amplitude of cantilever oscillation and phase between drive voltage and actual cantilever oscillations. This amplitude and phase measured at a given frequency encodes the tip-sample interaction forces and an analytical expression relating them to tip-sample forces is needed. We next derive these expressions for beam deflection detection scheme using base excitation method.

In presence of tip-sample forces the boundary condition with base excitation

method are :

$$y(x, t)|_{x=0} = A_0 \sin(\omega t) \quad \frac{dy(x, t)}{dx}|_{x=0} = 0 \quad YI \frac{d^2 y}{dx^2}|_{x=L} = 0 \quad YI \frac{d^3 y}{dx^3}|_{x=L} = (k_i + i\gamma_i \omega)y(L) \quad (2.26)$$

The cantilever is hinged with the piezo-base at $x = 0$ which is excited sinusoidally at frequency ω so that $y(x, t)|_{x=0} = A_0 \sin(\omega t)$. At the cantilever end $x = L$ a linearized tip-sample force $(k_i + i\gamma_i \omega)y(L)$ is applied which is valid for small displacements $y(L)$. This force contains both elastic stiffness k_i and damping γ_i component so that boundary condition becomes $YI \frac{d^3 y}{dx^3}|_{x=L} = (k_i + i\gamma_i \omega)y(L)$. The rest of boundary condition remains the same. Now we seek a general solution $y(x, t)$ to partial differential equation (Euler-Bernoulli equation 2.21) under above boundary condition. The solution takes a separation of variable form $y(x, t) = \sin(\omega t)y(x)$ and substituting this in eq. 2.21 yields $y(x)$ as:

$$y(x) = a \sin \lambda x + b \cos \lambda x + c \sinh \lambda x + d \cosh \lambda x$$

$$\text{where } \lambda^4 = \frac{\rho A \omega^2 - i\omega \gamma_c}{YI} \quad \text{a, b, c and d are constants.} \quad (2.27)$$

This spatial part of the solution $y(x)$ when subjected to boundary conditions results in value of constants a, b, c, d. In beam deflection detection one measures slope change or inclination angle $\theta = \frac{dy(x)}{dx}|_{x=L}$. Although the exact calculation of these measured quantities is cumbersome but an analytical expression for can be written in terms of two dimensionless complex parameters:

$$g = 3 \frac{k_i + i\omega \gamma_i}{k_c} \quad \text{and} \quad z = \lambda L \quad (2.28)$$

apart from an overall factor of A_0 . If one assumes small values of complex parameter λ and $k_c = 3YI/L^3 \ll k_i$, parameters g and z takes very small values. The small value of λ implies choosing an excitation frequency ω which is atleast ten times less than first eigenmode frequency. The Taylor expansion about small parameters of g and z produces following simple analytical expressions :

$$\theta = \frac{dy(x)}{dx}|_{x=L} = -\frac{A_0 g}{2L} + \frac{A_0 z^4}{6L} \quad (2.29)$$

Since the above equation are complex valued, they also reveal phase information of the signal and not just amplitude magnitude. Both amplitude and phase are experimentally determined by lock-in amplifier.

Beam deflection detection

For beam deflection detection, in phase X and out-of phase Y component are:

$$X = \frac{A_0}{k_c} (-k_i + m\omega^2) \quad \text{and} \quad Y = -A_0 \omega \frac{\gamma_i + \gamma_c}{k_c} \quad (2.30)$$

The X and Y output of lock-in amplifier or its amplitude $A = \sqrt{X^2 + Y^2}$ and phase $\tan \phi = Y/X$ directly measures the stiffness k_i of tip-sample force.

2.6.5 Lock-in Technique

The lock-in amplifier is used to extract small AC signals from a noisy a signal. A lock-in is capable of measuring a signal whose amplitude is million times smaller than the noise. In a typical experiment, the system is excited from an external source (like function generators) at a fixed frequency reference ω_r and the response of the system at this frequency is say $V_{sig} \sin(\omega_r t + \theta_{sig})$. Lock-in operates by generating its own reference signal such that reference with a fixed phase shift θ_L with respect to θ_{sig} is produced. This task is generally accomplished using a phase lock-loop which generates a reference signal locked in phase to an external oscillation source for the experiment $V_L \sin(\omega_L t + \omega_L)$. Now a phase sensitive detector or multiplier simply multiplies the two signals together giving:

$$\begin{aligned} & V_L V_{sig} \sin(\omega_L t + \omega_L) \sin(\omega_r t + \theta_{sig}) \\ &= \frac{1}{2} V_L V_{sig} \cos((\omega_r - \omega_L)t + \theta_{sig} - \theta_L) + \frac{1}{2} V_L V_{sig} \cos((\omega_r + \omega_L)t + \theta_{sig} + \theta_L) \end{aligned} \quad (2.31)$$

If we choose the frequency from lock-in reference ω_L to be equal to signal frequency ω_r and perform time average or low pass filter we have a DC output $\frac{1}{2} V_{sig} V_L \cos(\theta_{sig} - \theta_L)$ proportional to signal amplitude. The importance of a fixed θ_L generated using phase lock-loop is evident since time variation of this angle would effectively produce zero output after time averaging. The dependence of final output on the phase difference between reference and signal $\theta = \theta_{sig} - \theta_L$ makes lock-in a phase sensitive detection. This phase difference θ and amplitude V_{sig} can be independently measured by using addition phase sensitive detector in which reference phase is pre-shifted by 90° . This yields an output Y or quadrature output as it is called, equal to $V_{sig} \sin(\theta)$ in addition to previously defined output X or in phase $V_{sig} \cos(\theta)$. The squaring and adding these terms gives signal amplitude and division gives phase θ .

2.7 Chapter Summary

In this chapter we began by summarizing basic principle behind operation of AFM which is essentially a force measurement device. We illustrated through measurement of force-distance curve how a force measurement is done with AFM. After a brief introduction to cantilever mechanics which is responsible for conversion of static deflections of cantilever into a measurable force, AFM system components were introduced. In this, we showed what are the various components involved and how they work in coordination to make AFM a highly sensitive force measuring instrument. After discussing instrumentation of AFM, dynamic AFM operation was discussed in which cantilever is actively oscillated at a given frequency. This required discussing cantilever dynamics along with excitation scheme used to oscillate the cantilever. The chapter was concluded by deriving analytical expressions for response of oscillating cantilever in presence of tip-sample forces. A clear distinction was made between different modes of detecting cantilever motion while arriving at the expressions for amplitude and phase response.

Bibliography

- [1] Gerd Binnig, Calvin F Quate, and Ch Gerber. Atomic force microscope. *Physical review letters*, 56(9):930, 1986.
- [2] Hans-Jürgen Butt, Brunero Cappella, and Michael Kappl. Force measurements with the atomic force microscope: Technique, interpretation and applications. *Surface science reports*, 59(1-6):1–152, 2005.
- [3] Arturo M Baró and Ronald G Reifenger. *Atomic force microscopy in liquid: biological applications*. John Wiley & Sons, 2012.
- [4] Andreas Janshoff, Marcus Neitzert, York Oberdörfer, and Harald Fuchs. Force spectroscopy of molecular systems—single molecule spectroscopy of polymers and biomolecules. *Angewandte Chemie International Edition*, 39(18):3212–3237, 2000.
- [5] Ronald Reifenger. *Fundamentals of Atomic Force Microscopy: Part I: Foundations*. World Scientific Publishing Company Pte. Limited, 2016.
- [6] AL Weisenhorn, PK Hansma, TR Albrecht, and CF Quate. Forces in atomic force microscopy in air and water. *Applied physics letters*, 54(26):2651–2653, 1989.
- [7] GY Chen, RJ Warmack, T Thundat, DP Allison, and A Huang. Resonance response of scanning force microscopy cantilevers. *Review of Scientific Instruments*, 65(8):2532–2537, 1994.
- [8] Bert Voigtländer. *Atomic Force Microscopy*. Springer, 2019.
- [9] D Rugar, HJ Mamin, and Peter Guethner. Improved fiber-optic interferometer for atomic force microscopy. *Applied Physics Letters*, 55(25):2588–2590, 1989.
- [10] John E Sader, James WM Chon, and Paul Mulvaney. Calibration of rectangular atomic force microscope cantilevers. *Review of scientific instruments*, 70(10):3967–3969, 1999.
- [11] Jeffrey L Hutter and John Bechhoefer. Calibration of atomic-force microscope tips. *Review of scientific instruments*, 64(7):1868–1873, 1993.
- [12] H-J Butt and Manfred Jaschke. Calculation of thermal noise in atomic force microscopy. *Nanotechnology*, 6(1):1, 1995.
- [13] John Elie Sader. Frequency response of cantilever beams immersed in viscous fluids with applications to the atomic force microscope. *Journal of applied physics*, 84(1):64–76, 1998.

Chapter 3

Active Rheology of Single Flexible Synthetic Polymer Chain in Different Solvents

3.1 Introduction

A single polymer elasticity is a fundamental problem in polymer physics[1]. A polymer stretched under force has been a widely studied problem in various context ranging from understanding mechanical properties of complex polymeric and biological systems[2] to mechanics of giant muscle protein titin which generates power for muscle contraction[3]. Apart from its technological importance in wound recovery, drug delivery and tissue engineering, it plays crucial role in protein collapse, protein folding[4] and fundamentals of microrheology[5]. Elasticity of polymer is mainly entropic in nature and it originates from huge changes in configuration space of polymer as external force applied to it is changed. This change is due to vast dihedral angles φ and ϕ that are possible for the whole length of polymer.

The technique of Single Molecule Force Spectroscopy (SMFS) is used to measure elasticity of polymer based on micro-manipulation tools like atomic force microscopy (AFM), optical Tweezers (OTs) and magnetic tweezers (MTs). Elasticity is measured by generating force versus extension curves with piconewton force resolution and nanometer spatial resolution[6]. In very low force regime (< 10 pN), extension of chain is linear with force ($x \sim f$) which is only true in ideal theta solvent but behaves as a swollen chain ($x \sim f^{2/3}$) in good solvent. As external force is further increased, extension of chain is nonlinear with force and approaches its maximum contour length. In the past, above nonlinear force-extension regime is described by mainly two model classes that include freely jointed chain(FJC)[1] and worm-like chain (WLC)[7] models. These models account for entropic nature of polymer elasticity. WLC model assumes polymer as a homogeneous continuum chain and a parameter called persistence length (l_p) describes the local bending flexibility of continuum chain. Persistence length is then usually estimated as model's adjustable fitting parameter. In the previous work with single molecule force spectroscopy, measurements have been performed on synthetic polymers and biopolymers[8, 9] that includes proteins[10], DNA[11] and polysaccharides[12]. Elasticity of DNA[13, 14], proteins[15, 16] and synthetic polymer chains [17, 18] in the force regime $f > k_B T/l_p$ was well described by WLC. Experiments such as these were typically performed

with magnetic tweezers(MTs) in the force range of 1-100 pN. However, AFM experiments that were carried out in relatively higher force regime of 20-500 pN estimated anomaly low and nonphysical values for persistence length [8, 19, 20, 21]. To possibly justify such nonphysical values, simplistic models like FJC or similar to FJC were chosen to describe force-extension curve [22, 9, 8]. As mentioned in chapter 1, FJC has completely rigid segments of effective statistical length b called kuhn length that span the length of polymer. These segments are also completely uncorrelated with each other compared to exponential correlation of tangent vectors in WLC. This is clearly not physical and choice of FJC remains ad-hoc.

For force spectroscopy experiments, one end of the polymer is fixed to a surface while the other end attached to macroscopic force probe like a bead or AFM cantilever. Then, force-extension curves are generated by either controlling the force externally and measuring end-to-end distance or vice versa. Based on choice of variable that is externally controlled, there correspond a statistical ensemble for the combined cantilever-polymer system. The choice of a statistical ensemble reflects the complexity of interpreting the experiment. In an AFM setup, end-to-end distance is changed at constant velocity and force on the polymer is indirectly measured from deflection of the cantilever. Such an experiment correspond to a coupled cantilever-polymer ensemble in which polymer and cantilever act simultaneously in an intricate way[23, 24, 25]. In this, basically, there exist a convolution of polymer elastic response with the cantilever probe that likely results in a biased force-extension curve. So, derivative of force-extension curve is not directly related to the intrinsic stiffness of the polymer. In contrast, MT experiments operates in constant force mode where force is kept constant and changed externally while position of the paramagnetic bead is recorded. Since no velocity is involved, polymer properties in true equilibrium sense are measured. Also, external control of force ensures that properties of an isolated polymer are measured, averaging out the effect of cantilever probe[24, 25]. In literature, different methods such as Weighted Histogram Analysis Method(WHAM)[23, 26],Jarzynski equality and others[27, 28] have been suggested to separate effects of cantilever probe and extract an intrinsic stiffness profile of the polymer.

Oscillatory rheology on composite mechanical system is an alternative way in which cantilever effects can be deconvoluted[28]. It is based on the fact that overall linear response of a composite cantilever-polymer system can be written as the additive sum of linear response of polymer and cantilever. This allows easy differentiation of individual component response from its coupling in overall system. This deconvolution can be carried out on composite cantilever-polymer system by adding oscillatory perturbation to cantilever probe. In this work, it is implemented this by adding oscillations to AFM cantilever while simultaneously pulling on the polymer at constant velocity. Measurements were done on Polyethylene Glycol(PEG) and Polystyrene(PS) in good solvents. By determining in-phase and out-of-phase linear response to these oscillations, a method is proposed to extract single polymer stiffness. It is shown that stiffness obtained from in-phase response deviates significantly from constant velocity experiments. When modelled with WLC, persistence length deviates about five time compared to pulling experiments and reconcile with equilibrium measurement done with MT. This is explained by deconvolution procedure implemented using oscillatory rheology.

Furthermore, the effect that quality of solvent has on dynamic oscillatory method

is studied. The poor solvent effects can drastically change the polymer elasticity [29, 22, 30, 31]. For poor solvents, such as Polystyrene(PS) in water, the deviation in stiffness measured using oscillatory and constant velocity method is not observed. This is explained by additional solvophobic effects of hydrophobic side chains of polystyrene.

Materials and Methods

Preparation of PEG sample : Poly(ethylene) glycol with molecular weight 10 kDa was bought from Sigma-Aldrich where one end was functionalized with a thiol group (-SH). For measurements of Poly(ethylene) glycol in water, PEG was dissolved in milli-Q water(>16 M Ω cm) with concentration of 20 μ M. A similar concentration for solution of PEG in 2-propanol was used. Gold coverslips were prepared using thermal evaporation method. Gold is chemically inert but accumulates organic contaminants over time. A UV ozone treatment was therefore used to remove any organic impurities from gold surfaces. An aliquot of 60 μ L solution of PEG was put on gold cover-slip. It was then incubated for 20 min for strong covalent bonding of thiol end of PEG onto gold surface. The coverslip mounted in a fluid cell was rinsed properly with solvents to remove unbounded PEG before filling in milli-Q water or 2-propanol for measurement.

Preparation of Polystyrene sample Polystyrene with molecular weight 192 kDa was bought from Sigma-Aldrich. A glass coverslip was cleaned with a hot piranha solution(4:1 mixture of concentrated sulphuric acid and hydrogen peroxide) and rinsed with ethanol before use. A solution with concentration of 0.1 μ M was prepared for polystyrene in THF(tetrahydrofuran). Thereafter, 50 μ l aliquot of the solution was incubated on glass coverslip for 10 min. To remove loosely adsorbed polymer, sample was rinsed with THF and dried. The sample mounted in fluid cell was filled with milli-Q water or 8M urea for measurement.

| | Concentration | Expected Kuhn Length | Contour length |
|-------------|---------------|----------------------|----------------|
| PEG | 0.5 mM | 1 nm | 100 nm |
| Polystyrene | 0.1 μ M | 1.5-2 nm | 1 μ m |

Force measurements

The force-extension measurements were carried out with Nanowizard II AFM from JPK, Berlin. The cantilever probes coated with gold were obtained from Mikro-Masch SPM probes. As explained in chapter 2, accurate measurements require a proper calibration of spring constant. To do this, cantilever was brought in hard contact with a clean coverslip in which case z-piezo motion (in nm) is equal to deflections of cantilever recorded in photodiode(in volts). Thus, sensitivity in units of nm/V was determined that converts deflection in nanometers. As explained in chapter 2, thermal deflections of cantilever are then used in thermal fluctuation method[32] to calculate spring constant. The spring constant for the measurement was 0.6 – 0.8 N/m with frequency of resonance \sim 13 KHz. Force-extension curves were obtained following a standard force spectroscopy procedure. A contact setpoint value of 2 nN

was chosen at which cantilever was kept for 2 seconds before cantilever tip with a polymer is retracted with constant velocity of 150 nm/s. The cantilever deflection that is recorded is converted into force using spring constant and plotted against the displacement of z-piezo. In experiments, it is important to record single molecule signature only since the attachment of polymer with cantilever tip is non-specific.

For this:(1) concentration of polymer solution was kept low and sample was rinsed many times before measurement. This was necessary to ensure that single binding events are most probable in total force profiles that were captured. (2) Chain extension was normalized with contour length obtained by fitting WLC model to force-extension curves(see results and discussion). This contour length is only the apparent contour length because polymer is picked at random points along its length. If the curves superimpose well after normalization, it ensured that single molecule signatures were captured.(3) Enough statistics of such normalizable and single event curves was obtained ($N \sim 50$) for each polymer-solvent condition. Curves were fitted to models in order to extract relevant parameters (data not shown). Throughout the chapter, ($N \sim 5$) curves are only shown for purpose of representation.

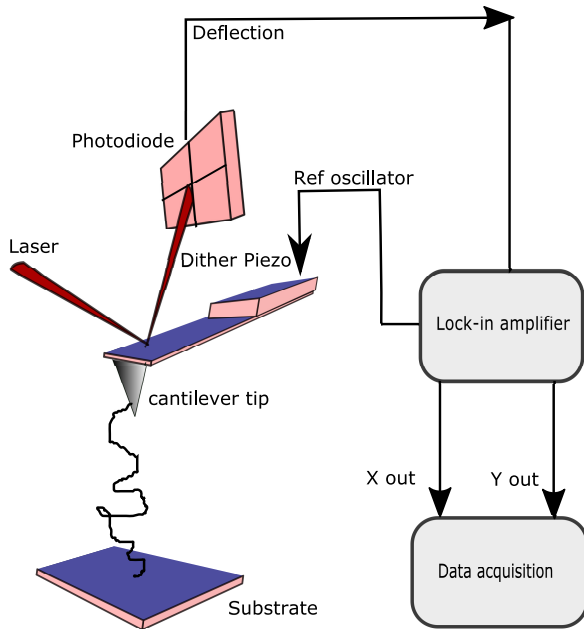


Figure 3.1: A schematic of experimental setup shows in-phase (X) and quadrature (Y) amplitude components of lock-in amplifier with a polymer attached between the tip and sample surface. A small piezo drive oscillates the cantilever with off resonance frequency ($\sim 1KHz$) and deflection amplitude from photodiode forms an input channel of lock-in amplifier.

Dynamic measurement

Dynamic oscillatory measurements were carried out with hyperdrive cantilever holder from Bruker. In this holder, base of cantilever was oscillated with a small dither piezo beneath it as shown in figure 1. A sinusoidal voltage with peak-to-peak amplitude of 1-2 nm was supplied to dither piezo using the lock-in amplifier SR830 from Stanford Research System. We chose off-resonance frequencies that were at least

one-tenth of resonance frequency of ~ 13 KHz. With reference signal same as sinusoidal oscillation, in phase X and quadrature Y component of amplitude from photodiode signal were recorded using lock-in. Small amplitudes of oscillations were chosen for a simultaneous comparison with constant velocity pulling experiment. In addition, low pulling velocity (40-70 nm/s) was required for narrow bandwidth of measurements (time constant 10 ms).

As discussed in chapter 2, the dynamics of vibrating cantilever beam is modelled with fourth-order partial differential equation called Euler-Bernoulli equation. This equation was solved under appropriate boundary condition. Under the assumption of small oscillation amplitudes for linearization of forces and off resonance frequency, it was shown that 'in phase' component $X = A \cos \delta$ and 'quadrature' component $Y = A \sin \delta$ of lock-in amplitude signal are linearly proportional to elastic k_i and dissipative γ_i response of polymer respectively. X and Y are given as:

$$X = \frac{A_b}{k_c}(-k_i + m^* \omega^2) \quad (3.1)$$

and

$$Y = \frac{-A_b \omega}{k_c}(\gamma_i + \gamma_c) \quad (3.2)$$

Here, m^* is added mass due to inertial loading of liquid that is accelerated along with the vibrating lever plus the cantilever tip mass, γ_c is viscous damping of the cantilever in the liquid and k_c is cantilever spring constant.

A_b is the amplitude with which base of cantilever is dithered and its accurate estimate is essential for a proper quantification of stiffness.

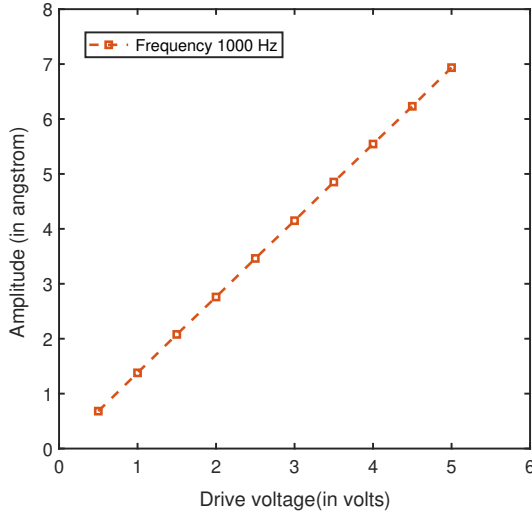


Figure 3.2: Drive amplitude A_b calibration against an externally applied drive voltage using home-built fiber-interferometer detection. A drive frequency of 1 KHz was chosen for calibration.

An indirect way of measuring A_b is by bringing cantilever in hard contact with glass wherein coverslip lock-in amplitude signal $\tilde{A} = \frac{2}{3}L \frac{dz}{dx} = A_b$ follows the motion of dithering base. Although this relation is a valid estimate but it may still involve error contribution due to liquid borne excitation's as suggested by Raman et. al[33]. It is therefore required that A_b be measured directly and we do this using home

built optical fibre based interferometer method shown in fig 3.2. This method of detecting cantilever deflection was discussed at length in chapter 2. The calibration gives a value that is within 10 % of value given by establishing a hard contact with surface.

Error analysis of stiffness measurement was also done. It is revealed from such analysis that primary contribution to error in stiffness stems from systematic error in A_b . Error in stiffness from eq(3.1) is $\delta k/k = \sqrt{(\delta A_b/A_b)^2 + (\delta k_c/k_c)^2 + (\delta X/X)^2}$. Error in stiffness k_c and amplitude X are negligible (<5 %) and a maximum error of 20% in A_b will not alter our final observations in any significant manner. In our estimate of stiffness from X , it is shown that the stiffness deviates from constant velocity pulling experiments only for the intermediate extensions. This means that contributions from error in A_b is insignificant. The simultaneous dynamic measurements corresponding to single molecule force events were analyzed. The number of curves analysed for PEG and Polystyrene were :50 curves in water and 40 curves in 2-propanol for PEG and 40 in water and 20 curves in 8M urea for Polystyrene. Only single curves for representation are shown in results and discussion.

Results and Discussion

3.1.1 Poly(ethylene)glycol

Force-extension measurement

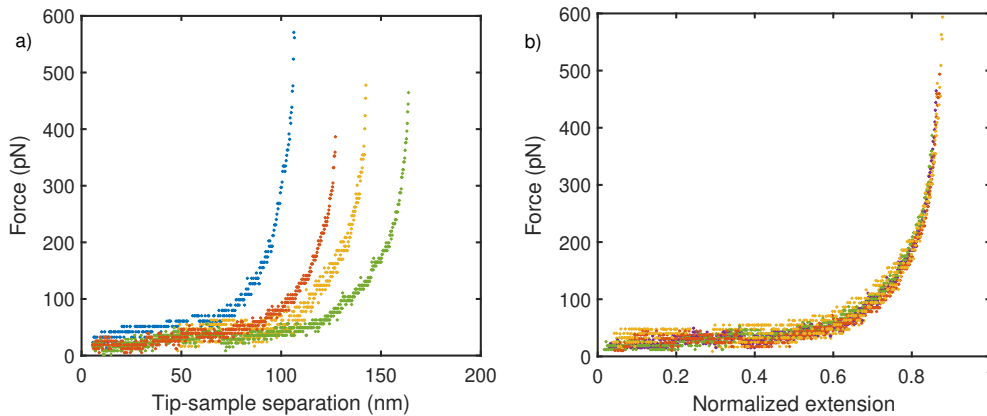


Figure 3.3: a) Force-extension curves for PEG in 2-propanol and b) its rescaling with apparent contour lengths.

The non-linear force-extension curves for poly(ethylene)glycol (PEG) in 2-propanol are shown in Figure 3.3a. Depending on the point of anchoring with cantilever tip, PEG is pulled to different contour lengths ranging from 80 to 150 nm as seen in Figure 3.3a. The polydispersity index for PEG was 1.8. In Figure 3.3b is shown the normalized force-extension curves obtained by rescaling each chain extension by their different contour lengths L . The apparent contour length is obtained by fitting

WC model of eq 3.3. As explained in chapter 1, statistical WLC model assumes the polymer as a continuous homogeneous string and describes the entropic nature of polymer elasticity. It characterizes the chain with a parameter called persistence length l_p and contour length L . Persistence length defines a local length scale for bending of chain beyond which thermal energy $k_B T$ is able to bend the polymer. Therefore, it is a measure of local flexibility of the polymer. As discussed in chapter 1, equation 3.3 is an WLC interpolation formula between force F and extension x valid for low $F < k_B T/l_p$ as well as high force $F > k_B T/l_p$ regime

$$F = \frac{k_B T}{l_p} \left(\frac{1}{4(1 - \frac{x}{L})^2} - \frac{1}{4} + \frac{x}{L} \right) \quad (3.3)$$

After normalization of force-extension curves in Figure 3.3b, it is observed that curves superimpose well over one another. This analysis procedure indicated that single molecule events with a fixed value of persistence length were obtained. The normalized curves are then fitted with WLC in Figure 3.4a.

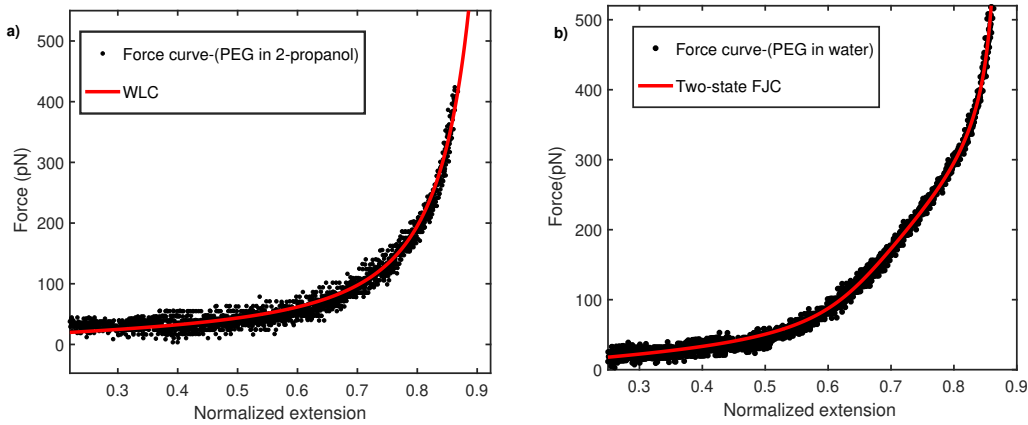


Figure 3.4: a) Normalized force-extension curves in 2-propanol fitted to WLC. Persistence length estimated is $l_p = 0.13$ nm. b) Normalized force-extension curves in water fitted with Two-state FJC model. The estimated Kuhn Length is 0.24 nm.

The persistence length estimated from model fitting is $l_p = 0.13 \pm 0.02$ nm. WLC fits the entire extension range very well but persistence length is even lower than the C-C bond length (0.16nm). Models with additional parameters (such as extended-WLC) were tested but they did not yield any change in the value of persistence length. Force-extension were also obtained for PEG in water as shown in 3.4b.

When PEG is stretched in water, it is known to show a transition from trans-trans-gauche conformation of monomers to all-trans conformations as force is increased. These conformers of PEG were described in chapter 1 and well documented in both experiments[34, 35] and simulation[36]. The manifestation of this transition is a linear-regime seen between 100 and 300 pN force in 3.4b. This signature clearly does not exist for PEG in 2-propanol. To account for such transition, force-extension curves are described with two-state FJC model[34, 37].

In this model[34, 37], trans-trans-gauche is a shorter conformer with length L_{gauche} and all-trans is a longer conformer of length L_{trans} . As force F increases there is a probability of transition from shorter to longer conformer proportional

to Boltzmann weighted free energy barrier ΔG between them. The model then combines length transition probabilities with entropic elasticity of FJC model and overall relative extension z is given by:

$$z = \left[\frac{L_{gauche}}{e^{\frac{-\Delta G}{k_B T}} + 1} + \frac{L_{trans}}{e^{\frac{\Delta G}{k_B T}} + 1} \right] * z_{fjc} / L_{trans} \quad (3.4)$$

where $\Delta G = (G_{trans} - G_{gauche}) - F(L_{trans} - L_{gauche})$ and $z_{fjc} = \coth\left(\frac{Fb_k}{k_B T}\right) - \left(\frac{k_B T}{Fb_k}\right)$

Here L_{trans} is fixed at 0.256 nm, corresponding to length of two consecutive C-C bond length. When normalized force-extension curves are fitted with two-state FJC model as shown in Figure 3.4b, it resulted in best fit estimate of $\Delta G = 3.1k_B T$ and $L_{gauche} = 0.23$ nm. The Kuhn length b_k estimated was 0.24 nm. This value of Kuhn length is consistent with value obtained in 2-propanol ($2l_p \sim 0.25$ nm) and other organic solvents[38]. However, its estimate of 1.2 nm (or persistence length 0.6 nm) in magnetic tweezers is at least five times more compared to AFM experiments[17, 39].

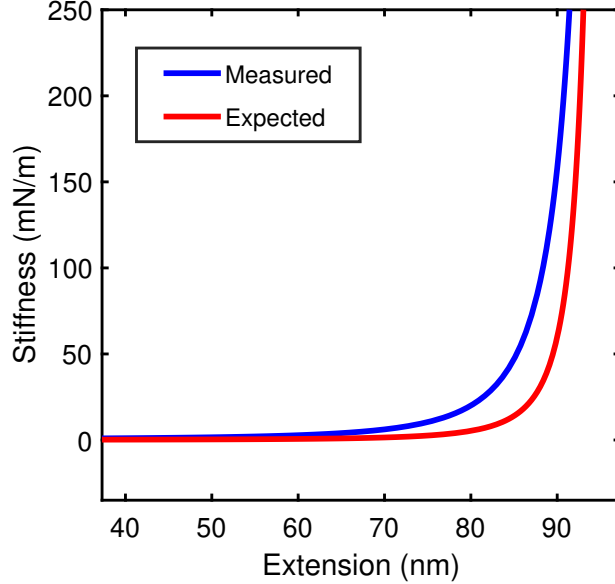


Figure 3.5: Expected versus Measured stiffness-extension behavior in good solvent.

One possibility that explains this discrepancy is that WLC or FJC model are not a sufficient description in relatively higher force range 20 – 500 pN of AFM experiments. This is large compared to force range 1 – 100 pN in magnetic tweezer setups. It has been suggested[40, 41] that choice between two main class of models i.e FJC and WLC depends on the range of applied forces and determined by length scales of persistence length l_p and effective monomer separation/bond length b . Beyond a threshold force, the nonlinear force-extension regime will go over from continuum WLC to a discrete behavior of (FJC) polymer chain[40, 41]. Therefore, a WLC-FJC interpolation model was proposed which interpolates between WLC and FJC like behavior[41]. WLC-FJC formula was used to analyze AFM pulling data on different polymers(see Appendix C, ref.[41]). But the value of persistence length did not improve from its low and unphysical value and are similar to original fitting with WLC model.

A value for transition force can also be calculated. At high forces $F \gg k_B T/l_p$, nonlinear WLC force relation (eq 3.3) is given by $1 - x/L \sim (4Fl_p/k_B T)^{-1/2}$. However, beyond a critical force, intrinsic bending stiffness between consecutive bonds (l_p) becomes irrelevant and discrete nature of polymer backbone (b) comes into play. Thus, chain should be viewed as being made up of freely jointed bonds with force relation given by FJC chain $1 - x/L \sim (Fb/k_B T)^{-1}$. Comparing the above high force scaling relations gives the WLC to FJC transition force as $F_c \sim 4k_B T l_p/b^2$. For synthetic polymers, typical value of persistence length as measured in low-force magnetic tweezer manipulation (or force free condition) is $l_p = 0.6$ nm [1, 17, 39] and C-C bond length $a = 0.15$ nm, this transition force is about 500 pN. This force is beyond the range of forces covered in typical AFM experiments and below this force WLC should be a valid description. Although WLC model fits the force-extension data with persistence length l_p as adjustable parameter, the nonphysical estimate of l_p suggest that WLC model is still inadequate.

Other possibility is that conventional AFM pulling experiments itself produce a biased polymer response. It has been pointed out that polymer response may couple intricately with AFM cantilever in constant velocity pulling experiments [23, 24]. This may not allow the polymer to sample its intrinsic equilibrium conformations. Constant velocity pulling experiments are in contrast to constant force measurement with magnetic tweezers, that measure response of an isolated polymer [24]. In the next section, we address this discrepancy using oscillatory rheology measurements on polymer chains.

Dynamic measurement

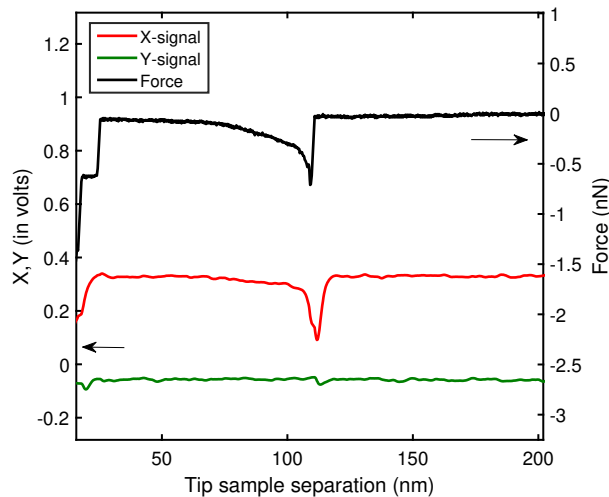


Figure 3.6: The raw profiles for PEG in water which include force-extension curve in constant velocity (~ 60 nm/sec) experiment (black) and lock-in amplifier's in-phase X-signal amplitude (red) and quadrature Y signal amplitude (green).

We perform direct measurement of PEG elastic response chain using oscillatory rheology to address the concerns raised in previous section. These measurements are performed simultaneously with force-extension curve of constant velocity pulling experiments. To do this, the cantilever with PEG polymer anchored to it is pulled

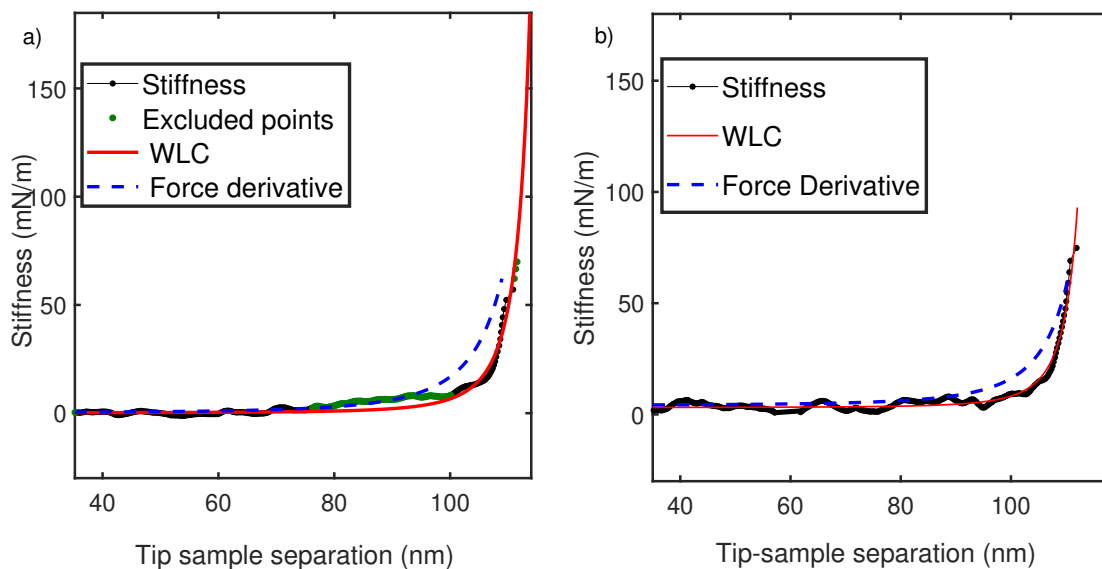


Figure 3.7: The figure shows comparisons between stiffness-extension data for PEG obtained by oscillatory response and simultaneously measured force-extension curve a) For PEG in water, derivative of WLC which was fitted to force-extension data in pulling experiments (blue dash) with $l_p = 0.13$ nm and stiffness-extension data from oscillatory response (black) when fitted with WLC (red) gives $l_p = 0.65$ nm. The green data regime between 100 and 300 pN (or between 80 and 100 nm) was excluded when fitting to WLC with both methods. b) For PEG in 2-propanol, WLC derivative (blue dash) with $l_p = 0.13$ nm again obtained from fitting the force-extension data and stiffness-extension data by oscillatory response (black) when fitted with WLC (red) gives $l_p = 0.64$ nm.

at nominal velocity of ~ 60 nm/s and simultaneously oscillated at an off resonance frequency of 1 KHz. Using lock-in amplifier we record deflection amplitudes which reports a dynamic linear response at the chosen frequency. In Figure 4.4 is shown the raw X and Y signal amplitudes of lock-in amplifier for PEG and also the simultaneously measured force-extension curve. As evident from equation 3, in-phase X signal is linearly proportional to stiffness k_i and thus has similar features as that of force-extension curve. After subtracting a constant contribution $m * \omega^2$ from hydrodynamic loading of cantilever one extracts the stiffness response of PEG. Quadrature Y signal is the effective friction $\gamma_i + \gamma_c$ of the coupled polymer-cantilever assembly. It is observed from fig 4.4 that Y signal show no variation whatsoever and remains flat and featureless in the entire extension range. This is due to much faster timescales for polymer's intramolecular diffusion ($\sim ns$) than the experimental timescales ($\sim ms$) [42]. This implies that polymer γ_i is immeasurably low compared to γ_c and polymer linear response is dictated by elasticity alone. In our previous work [43], we also showed similar behavior for unfolded I27 domains of protein titin. Figure 3.7a shows the stiffness of PEG in water obtained from in-phase X signal (in black) and WLC derivative extracted from force-extension data (in blue dash).

Derivative of WLC fit to force-extension curve was used since direct derivative of data is always noisy and thus not suitable for any comparisons. The WLC derivative from force-extension curve reveals a marked deviation from stiffness obtained directly using oscillatory response. Least square fitting of stiffness data with WLC (red) yields a persistence length l_p of 0.65 ± 0.19 nm. In comparison, the WLC derivative of force-extensions has l_p of 0.13 ± 0.02 nm. In this fitting of data with WLC, we excluded part of the data in range of 80 to 100 nm (green) that did not fit to both force-extension and stiffness-extension data. This is done because of PEG undergoing a conformational transition from trans-trans-gauche state to all-trans state under stretching force in water[34, 35, 36]. The effect shows up characteristically as linear force versus extension change in forces between 100 and 300 pN (or 80 and 100 nm)[35]. The observed deviation in similar force regime(or 80 and 100 nm) for stiffness-extension data confirms that oscillatory method is sensitive to such conformational transition. However, this effect is also not encapsulated in simple WLC model and thus no meaningful extraction of persistence length is possible with WLC. But such analysis is sufficient to reveal a overall deviation between oscillatory and pulling experiments.

Next, we made direct stiffness-extension measurements on PEG in organic solvent 2-propanol. A good solvent for PEG, experiments with 2-propanol were performed in many sets of few hours due to volatility of organic solvent. Stiffness-extension data (in black) in figure 3.7b) together with force-extension curve from pulling experiments in figure (figure 3.4a) do not show any signatures of conformational change. The direct stiffness-extension measurements via oscillatory response reports a persistence length l_p value of 0.64 ± 0.19 nm. In contrast to Figure 3.7a, WLC is well fitted to entire extension range (in red) in figure 3.7b) without any exclusion of data regime because of effects of hydration. The force-extension curve from pulling experiments yield a persistence length l_p value of 0.13 ± 0.02 nm. The derivative of WLC is shown as blue dash in figure 3.7b. The estimated persistence length of 0.64 ± 0.19 nm is in agreement with equilibrium measurements made using low force magnetic tweezers[17, 39] and other bulk methods[1, 44]. Innes-gold et. al[39] and Dittmore et. al[17] reported the persistence length value of ~ 0.6 nm. Smith et. al[44] measured persistence length for PEG as 0.6 nm from neutron scattering experiments.

For the purpose of extracting viscoelasticity, oscillatory response have been extracted for single biological and synthetic polymers[45, 46, 47]. These studies have measured dissipation for single polymer by oscillating the cantilever with frequencies near to cantilever resonance. With appropriate modelling the dynamics of oscillating cantilever in liquid recent study suggest issues in interpreting dissipation of single-molecule[48, 43]. It points out to an impossibility of separating elastic and dissipated signals which are in reality coupled to each other for frequencies close to cantilever resonance. Only a true off resonance analysis as done in our case provides an unambiguous way of distinguishing the elastic response from dissipated response.

3.1.2 Polystyrene

Water is an important physiological medium for proteins and other biomolecules. For instance, an unfolded polypeptide due to hydrophobic side chains collapse in water to form a globule. This step is thought to be critical in driving self-assembly

of globular proteins in protein folding. Polystyrene, due of its homogeneous and simple chemical structure, is used as a model hydrophobic polymer to study collapse in globular proteins. The aromatic side chains of polystyrene are hydrophobic and polystyrene collapse in poor solvent like water[49].

In this section measurements on polystyrene(PS) in good and poor solvents are shown. This helps in understanding the influence of solvent condition on entropic elasticity of polymer.

Force-extension measurement

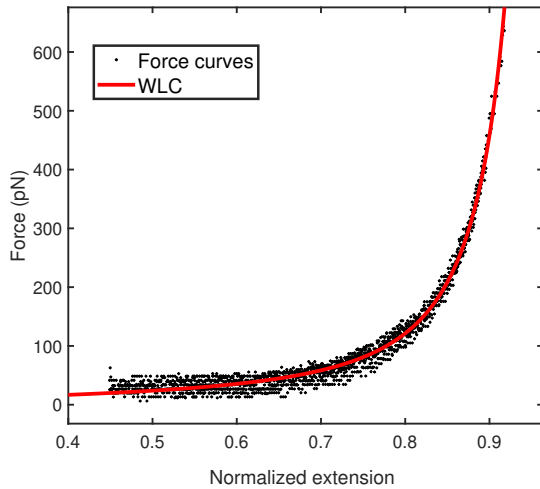


Figure 3.8: Polystyrene force-extension curves in water modelled with WLC having persistence length $l_p = 0.23$ nm.

Normalized force-extension curves for polystyrene in water are shown in Fig 3.8. They are modelled and fitted with WLC model in force regime greater than 20 pN. The flat plateau region exist for forces < 20 pN due to coil-globule transition for polystyrene in poor solvent like water[50]. Beyond this force regime polymer entropic elasticity is thought to dominate the force extension curve. Persistence length estimated from fitting is $l_p = 0.23 \pm 0.02$ nm, which is same as earlier observation[19]. The value of 0.25 nm is also quoted for good solvents like toluene[22, 50]. However, these values are low considering the aromatic side chain of benzene is 0.72 nm long. Persistence length is determined by steric hindrances of side chains and expected to be greater than 1 nm. Hence, there is a debate about value of persistence length[22].

Dynamic measurement

To address this concern, we carried out oscillatory measurement on polystyrene simultaneous with conventional pulling force-extension curves. Figure 3.9a shows measurements made in water. The stiffness measured by dynamic oscillatory method and its fit to WLC are shown in black and red respectively. Persistence length estimated is $l_p = 0.21 \pm 0.02$ nm. The derivative of WLC which was fitted to force-extension curve is shown with blue dash. Interestingly, all curves superimpose well with one another without any deviation. This is in contrast to observation made on PEG in good solvents like water or 2-propanol(3.7). It is also observed that proteins

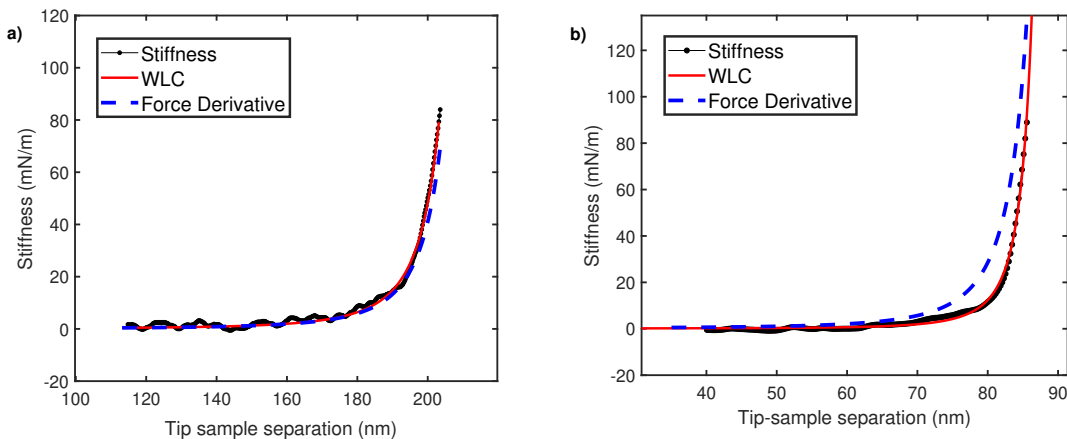


Figure 3.9: a) Measurements with polystyrene in water. It shows stiffness measured using dynamic oscillatory method in black which is then fitted with WLC in red. For comparison, derivative of WLC obtained from fitting to force-extension curve is shown with blue dash. b) The same measurements with Polystyrene in 8M urea.

with hydrophobic amino acids have similar persistence length in AFM pulling[10], oscillatory[48, 43] and constant force MTs[15] experiments. We believe that in such hydrophobic (poor solvent) cases persistence length is not an intrinsic parameter of polymer. It just acts as a heuristic parameter that makes up for the poor solvent conditions. Simulations[30] and experiments[16] have suggested a need to include poor solvent effects along with backbone entropic contribution.

To further understand poor solvent effects, we carried out measurements for polystyrene in good solvent condition. It has been demonstrated recently that high concentration aqueous solution of urea acts as good solvent for PS [51, 52, 53]. Hydrophobic interactions which are majorly responsible for polymer collapse to a globule are diminished in presence of urea. Figure 3.9b shows the results for oscillatory measurements in 8M urea.

It shows stiffness measured using oscillatory method in black and is fitted with WLC in red. The value of persistence length estimated from fit is $l_p = 0.8$ nm. The derivative of WLC obtained from previously fitting constant velocity force-extension curve is shown in blue dash with a persistence length $l_p = 0.25$ nm. It is interesting to note that deviation in persistence length observed is quite similar to what was seen for PEG in good solvents. This l_p obtained from oscillatory measurements is acceptable since it is greater than monomer size 0.72 nm. We discuss the statistical physics behind these observations further in the next section.

3.1.3 Deconvolution Principle

The observed deviation between dynamic oscillatory measurements and constant velocity force-extension measurements needs a quantitative explanation. We argue in the following section that it is because of a deconvolution procedure implemented on biased force-extension. The implementation is due to oscillatory rheology measurements. We first began by explaining the bias in force-extension curves and then the deconvolution procedure.

In good solvent

For proper interpretation of force-extension measurement, it is necessary to consider a full statistical mechanical treatment of combined cantilever-polymer system. This is because the entropic elasticity of polymer has a description in statistical mechanics and thus its resulting measurement with cantilever need statistical considerations of coupled cantilever-polymer system. This ultimately determines force-extension relation. In constant velocity pulling experiments we neither control the extension x nor the force (or deflection δ) on the polymer. The displacement $D = \delta + x$ of cantilever is the only quantity that is controlled and is changed at a constant velocity. In this constant displacement D ensemble both extension of molecule and force on it are determined indirectly through deflections of cantilever. This statistical ensemble, therefore, represent a coupled cantilever-molecule system.

Since the cantilever and polymer molecule are connected in series, the canonical partition function for coupled cantilever-molecule system in equilibrium would be [23, 24] :

$$Z_{system}(D) = \int dx Z_m(x) * Z_c(D - x) \quad (3.5)$$

where Z_m and Z_c are partition function for isolated or uncoupled polymer molecule and cantilever respectively. There is no external force acting on system under equilibrium. Hence, the average force on the polymer by the cantilever or vice-versa is

$$\bar{F} = -\frac{1}{Z_{system}} \frac{\partial Z_{system}}{\partial D} = \frac{k_c}{Z_{system}} \int dx (D - x) Z_m(x) Z_c(D - x) = k_c(D - \bar{x}) \quad (3.6)$$

As noted from eq 3.6, coupling term $Z_m * Z_c$ which is present in both numerator and denominator of eq 3.6 determines the force on the molecule. Because overall response of a chain is additive in its the monomer subunits, molecule partition function Z_m can be written as $e^{-\beta F(x)}$ where $F(x)$ is molecular free energy per monomer. Similarly, cantilever partition function Z_c can be approximated in terms of its stiffness k_c and deflection $\delta = D - x$ that determines harmonic biasing potential $k_c(D - x)^2/2$. Therefore, the coupling term is

$$Z_{system}(D) \sim Z_m * Z_c = e^{-\beta F(x)} * e^{-\beta k_c \delta^2/2} \quad (3.7)$$

A closer look at the coupling term indicates that it is just a mathematical convolution of isolated polymer response in Z_m and cantilever bias in Z_c . Therefore, simultaneous action of cantilever and polymer determine the average force. So, the question is how do we extract isolated polymer response determined by Z_m only.

- One way is to work at high forces where deflection is large so that contribution from cantilever biasing potential is minimized and in the limit of large deflection Z_c approaches delta function i.e, $Z_c \rightarrow \delta(D-x)$. As a result, derivative of force-extension curve and stiffness from the oscillatory measurement coincide at high forces in fig 3.6a, 3.6b and fig 3.8b.
- Another possibility is to do experiments in low force using magnetic tweezers. The tweezer experiments operate by keeping the force constant. This means that effective stiffness of probe is low or close to zero. In this case, it can be shown that coupled partition function Z_{system} reduces to that for isolated molecule[24].

In conclusion, it is safe to say that effect of convolution would be maximum at typical intermediate forces ~ 250 pN explored in AFM. To elaborate on this, we see that thermodynamic free energy(F) in equation 3.7 is entropy dominated with ($F = -TS_{WLC}$). At a typical force of say ~ 250 pN cantilever biasing potential of ~ 12 kT dominates over entropic contribution of about 2 kT. This gives high weightage to cantilever in determining Z_{system} , resulting in a biased force-extension curve.

For external oscillations of cantilever, the overall measured response of the coupled system is simple addition of individual cantilever and polymer response. This is explicit in equation (3.1) and (3.2) and implies a parallel coupling between individual components. This parallel pathway allow easy separation of polymer inherent response from its coupling to cantilever probe.

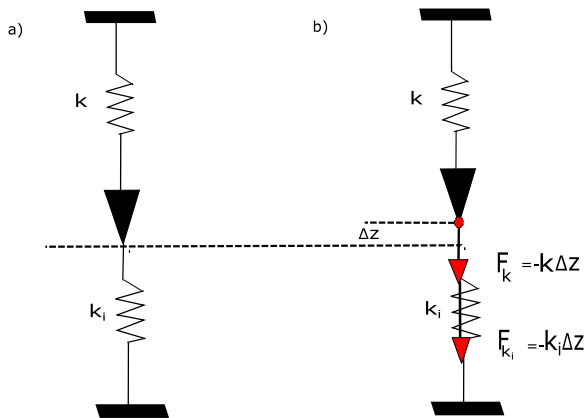


Figure 3.10: Parallel coupling between spring constant of cantilever(k) and polymer(k_i).

To explain this consider representing polymer and cantilever as a point mass with some spring constant k and damping k_i respectively[54, 55]. They are connected as depicted in figure 3.9. Under equilibrium condition represented in fig 3.9(a), point of attachment is at equilibrium position $z= 0$. When system is oscillated with a small amplitude Δz , the shift in equilibrium point results in net harmonic force due to cantilever and polymer spring in same direction. As a result, there is net force of $\Delta F=-(k+k_i)\Delta z$. This analysis implies that two springs add in parallel for oscillatory AFM. This observation is directly responsible for in parallel pathway in equation 3.1, valid for off-resonance frequency operation. It can be explicitly shown through analysis of cantilever dynamics with a point mass simple harmonic oscillator model[55].

In poor solvent

The poor solvent interacting with a polymer can significantly effect its elasticity. Water is a poor solvent for polystyrene because of presence of hydrophobic side chains. In here, energetic contribution from hydrophobic polymer-solvent interactions together with entropy of polymer backbone determine elasticity. [30, 31, 22, 56]. As a result polymer softens and its persistence length is effectively reduced[30, 31]. Thermodynamically, the strength of hydrophobic interactions is described with hydration free energy that is additional required to expose the hydrophobic side chains of polymer as it is extended . This free energy turns out to positive and larger than

$k_B T$ [56]. This means that an extra amount work is required to stretch the polymer and area under force-extension curve is increased. However this only happens at expense of decrease in curvature of force-extension curve. Hence persistence length that is a measure of curvature, is reduced substantially.

Experiments with stretching a hydrophobic polymer to large extension suggest that hydration free energy to be atleast six times the entropy of chain[30]. The hydration free energy per monomer of polystyrene aromatic side chain is about ~ 20 kT[57]. We see from equation (3.7) that total free energy that combines polymer backbone entropy and hydration energy due to hydrophobic interaction $F(F_{hydration} + F_{WLC})$ just dominates over cantilever bias in the overall Z_{system} . Hence, oscillatory and the constant velocity experiments results in similar elasticity in poor solvent.

Chapter Summary

We performed AFM based oscillatory rheology technique to get a local and direct estimate of elastic response simultaneously with constant velocity pulling experiments. We showed through a proper quantification of such elastic response that it deviates significantly from conventional pulling force-extension curves. This was true for good solvent condition in which case elastic response could be modelled with WLC entropic model of elasticity. The persistence length estimated by fitting the stiffness-extension data with WLC result in a large and physically acceptable value for persistence length and matches well with equilibrium magnetic tweezer experiments. This result suggest that oscillatory rheology provides a deconvolution between polymer intrinsic response and microscopic AFM cantilever probe and therefore correctly estimates elastic response.

In addition, for a polymer in poor solvent no such deviation in elastic response was observed between oscillatory technique and constant velocity pulling experiments. We explained this result by accounting for additional contribution made by hydrophobic free energy and further effect it would have on sampling the equilibrium configuration. Such a analysis procedure yielded same elastic response for polymer chain in poor solvent.

The present study is the first to suggest a bias in constant velocity pulling experiments using oscillatory rheology. Although WLC model is currently used at a phenomenological level, a consistency in values of persistence length using AFM experiments in high force regime and magnetic tweezers experiments in low force regime underlines WLC success in describing polymer elasticity measured with AFM. It also suggest that WLC is successful across all force regime provided the good solvent conditions, but hint at avoiding its use in describing AFM data on elasticity of polymers in poor solvents.

Bibliography

- [1] Michael Rubinstein, Ralph H Colby, et al. *Polymer physics*, volume 23. Oxford university press New York, 2003.
- [2] Jan-Michael Y Carrillo, Fred C MacKintosh, and Andrey V Dobrynin. Nonlinear elasticity: from single chain to networks and gels. *Macromolecules*, 46(9): 3679–3692, 2013.
- [3] Edward C Eckels, Rafael Tapia-Rojo, Jamie Andrés Rivas-Pardo, and Julio M Fernández. The work of titin protein folding as a major driver in muscle contraction. *Annual review of physiology*, 80:327–351, 2018.
- [4] Gabriel Žoldák and Matthias Rief. Force as a single molecule probe of multidimensional protein energy landscapes. *Current opinion in structural biology*, 23(1):48–57, 2013.
- [5] Charles M Schroeder. Single polymer dynamics for molecular rheology. *Journal of Rheology*, 62(1):371–403, 2018.
- [6] Keir C Neuman and Attila Nagy. Single-molecule force spectroscopy: optical tweezers, magnetic tweezers and atomic force microscopy. *Nature methods*, 5(6):491–505, 2008.
- [7] John F Marko and Eric D Siggia. Stretching dna. *Macromolecules*, 28(26): 8759–8770, 1995.
- [8] Marina I Giannotti and G Julius Vancso. Interrogation of single synthetic polymer chains and polysaccharides by afm-based force spectroscopy. *ChemPhysChem*, 8(16):2290–2307, 2007.
- [9] Yu Bao, Zhonglong Luo, and Shuxun Cui. Environment-dependent single-chain mechanics of synthetic polymers and biomacromolecules by atomic force microscopy-based single-molecule force spectroscopy and the implications for advanced polymer materials. *Chemical Society Reviews*, 49(9):2799–2827, 2020.
- [10] Toni Hoffmann and Lorna Dougan. Single molecule force spectroscopy using polyproteins. *Chemical Society Reviews*, 41(14):4781–4796, 2012.
- [11] Carlos Bustamante, Zev Bryant, and Steven B Smith. Ten years of tension: single-molecule dna mechanics. *Nature*, 421(6921):423–427, 2003.
- [12] Piotr E Marszalek and Yves F Dufrêne. Stretching single polysaccharides and proteins using atomic force microscopy. *Chemical Society Reviews*, 41(9):3523–3534, 2012.

- [13] Carlos Bustamante, John F Marko, Eric D Siggia, and S Smith. Entropic elasticity of λ -phage dna. *Science*, 265(5178):1599–1600, 1994.
- [14] Omar A Saleh, DB McIntosh, P Pincus, and N Ribeck. Nonlinear low-force elasticity of single-stranded dna molecules. *Physical review letters*, 102(6):068301, 2009.
- [15] Jessica Valle-Orero, Jaime Andrés Rivas-Pardo, and Ionel Popa. Multidomain proteins under force. *Nanotechnology*, 28(17):174003, 2017.
- [16] Guillaume Stirnemann, David Giganti, Julio M Fernandez, and BJ Berne. Elasticity, structure, and relaxation of extended proteins under force. *Proceedings of the National Academy of Sciences*, 110(10):3847–3852, 2013.
- [17] Andrew Dittmore, Dustin B McIntosh, Sam Halliday, and Omar A Saleh. Single-molecule elasticity measurements of the onset of excluded volume in poly (ethylene glycol). *Physical Review Letters*, 107(14):148301, 2011.
- [18] Omar A Saleh. Perspective: Single polymer mechanics across the force regimes. *The Journal of chemical physics*, 142(19):194902, 2015.
- [19] Sabah Al-Maawali, Jason E Bemis, Boris B Akhremitchev, Haiying Liu, and Gilbert C Walker. Single-molecule afm study of polystyrene grafted at gold surfaces. *The Journal of Adhesion*, 81(10-11):999–1016, 2005.
- [20] Hongbin Li, Wenke Zhang, Weiqing Xu, and Xi Zhang. Hydrogen bonding governs the elastic properties of poly (vinyl alcohol) in water: single-molecule force spectroscopic studies of pva by afm. *Macromolecules*, 33(2):465–469, 2000.
- [21] M-N Dessinges, Berenike Maier, Y Zhang, M Peliti, David Bensimon, and Vincent Croquette. Stretching single stranded dna, a model polyelectrolyte. *Physical review letters*, 89(24):248102, 2002.
- [22] Milad Radiom, Plinio Maroni, and Michal Borkovec. Influence of solvent quality on the force response of individual poly (styrene) polymer chains. *ACS Macro Letters*, 6(10):1052–1055, 2017.
- [23] Ignacio Franco, Mark A Ratner, and George C Schatz. Single-molecule pulling: phenomenology and interpretation. *arXiv preprint arXiv:1205.5068*, 2012.
- [24] HJ Kreuzer, SH Payne, and L Livadaru. Stretching a macromolecule in an atomic force microscope: statistical mechanical analysis. *Biophysical journal*, 80(6):2505–2514, 2001.
- [25] Douglas B Staple, Felix Hanke, and Hans Jürgen Kreuzer. Comment on “sub-angstrom conformational changes of a single molecule captured by afm variance analysis”. *Biophysical journal*, 95(2):1001, 2008.
- [26] Shankar Kumar, John M Rosenberg, Djamal Bouzida, Robert H Swendsen, and Peter A Kollman. The weighted histogram analysis method for free-energy calculations on biomolecules. i. the method. *Journal of computational chemistry*, 13(8):1011–1021, 1992.

- [27] Michael Hinczewski, J Christof M Gebhardt, Matthias Rief, and D Thirumalai. From mechanical folding trajectories to intrinsic energy landscapes of biopolymers. *Proceedings of the National Academy of Sciences*, 110(12):4500–4505, 2013.
- [28] Michael Hinczewski, Yann von Hansen, and Roland R Netz. Deconvolution of dynamic mechanical networks. *Proceedings of the National Academy of Sciences*, 107(50):21493–21498, 2010.
- [29] A Halperin and Paul M Goldbart. Early stages of homopolymer collapse. *Physical Review E*, 61(1):565, 2000.
- [30] Kirstin A Walther, Frauke Gräter, Lorna Dougan, Carmen L Badilla, Bruce J Berne, and Julio M Fernandez. Signatures of hydrophobic collapse in extended proteins captured with force spectroscopy. *Proceedings of the National Academy of Sciences*, 104(19):7916–7921, 2007.
- [31] Frauke Gräter, Pascal Heider, Ronen Zangi, and BJ Berne. Dissecting entropic coiling and poor solvent effects in protein collapse. *Journal of the American Chemical Society*, 130(35):11578–11579, 2008.
- [32] H-J Butt and Manfred Jaschke. Calculation of thermal noise in atomic force microscopy. *Nanotechnology*, 6(1):1, 1995.
- [33] Daniel Kiracofe and Arvind Raman. Quantitative force and dissipation measurements in liquids using piezo-excited atomic force microscopy: a unifying theory. *Nanotechnology*, 22(48):485502, 2011.
- [34] F Oesterhelt, M Rief, and HE Gaub. Single molecule force spectroscopy by afm indicates helical structure of poly (ethylene-glycol) in water. *New Journal of Physics*, 1(1):6, 1999.
- [35] Wolfgang Ott, Markus A Jobst, Magnus S Bauer, Ellis Durner, Lukas F Milles, Michael A Nash, and Hermann E Gaub. Elastin-like polypeptide linkers for single-molecule force spectroscopy. *ACS nano*, 11(6):6346–6354, 2017.
- [36] Berthold Heymann and Helmut Grubmüller. Elastic properties of poly (ethylene-glycol) studied by molecular dynamics stretching simulations. *Chemical Physics Letters*, 307(5-6):425–432, 1999.
- [37] Wanhao Cai, Song Lu, Junhao Wei, and Shuxun Cui. Single-chain polymer models incorporating the effects of side groups: an approach to general polymer models. *Macromolecules*, 52(19):7324–7330, 2019.
- [38] Zhonglong Luo, Bo Zhang, Hu-jun Qian, Zhong-yuan Lu, and Shuxun Cui. Effect of the size of solvent molecules on the single-chain mechanics of poly (ethylene glycol): implications on a novel design of a molecular motor. *Nanoscale*, 8(41):17820–17827, 2016.
- [39] Sarah N Innes-Gold, Ian L Morgan, and Omar A Saleh. Surface-induced effects in fluctuation-based measurements of single-polymer elasticity: A direct probe of the radius of gyration. *The Journal of chemical physics*, 148(12):123314, 2018.

- [40] Angelo Rosa, TX Hoang, D Marenduzzo, and A Maritan. Elasticity of semi-flexible polymers with and without self-interactions. *Macromolecules*, 36(26):10095–10102, 2003.
- [41] Andrey V Dobrynin, Jan-Michael Y Carrillo, and Michael Rubinstein. Chains are more flexible under tension. *Macromolecules*, 43(21):9181–9190, 2010.
- [42] Andreas Möglich, Karin Joder, and Thomas Kiefhaber. End-to-end distance distributions and intrachain diffusion constants in unfolded polypeptide chains indicate intramolecular hydrogen bond formation. *Proceedings of the National Academy of Sciences*, 103(33):12394–12399, 2006.
- [43] Shatruhan Singh Rajput, Surya Pratap S Deopa, Jyoti Yadav, Vikhyaat Ahlawat, Saurabh Talele, and Shivprasad Patil. The nano-scale viscoelasticity using atomic force microscopy in liquid environment. *Nanotechnology*, 32(8):085103, 2020.
- [44] Grant D Smith, Do Y Yoon, Richard L Jaffe, Ralph H Colby, Ramanan Krishnamoorti, and Lewis J Fetters. Conformations and structures of poly (oxyethylene) melts from molecular dynamics simulations and small-angle neutron scattering experiments. *Macromolecules*, 29(10):3462–3469, 1996.
- [45] Masaru Kawakami, Katherine Byrne, Bhavin S Khatri, Tom CB McLeish, and D Alastair Smith. Viscoelastic properties of single poly (ethylene glycol) molecules. *ChemPhysChem*, 7(8):1710–1716, 2006.
- [46] Masaru Kawakami, Katherine Byrne, Bhavin S Khatri, Tom CB Mcleish, Sheena E Radford, and D Alastair Smith. Viscoelastic measurements of single molecules on a millisecond time scale by magnetically driven oscillation of an atomic force microscope cantilever. *Langmuir*, 21(10):4765–4772, 2005.
- [47] Xiaobin Liang and Ken Nakajima. Investigating the dynamic viscoelasticity of single polymer chains using atomic force microscopy. *Journal of Polymer Science Part B: Polymer Physics*, 57(24):1736–1743, 2019.
- [48] Fabrizio Benedetti, Yulia Gazizova, Andrzej J Kulik, Piotr E Marszalek, Dmitry V Klinov, Giovanni Dietler, and Sergey K Sekatskii. Can dissipative properties of single molecules be extracted from a force spectroscopy experiment? *Biophysical journal*, 111(6):1163–1172, 2016.
- [49] Isaac TS Li and Gilbert C Walker. Interfacial free energy governs single polystyrene chain collapse in water and aqueous solutions. *Journal of the American Chemical Society*, 132(18):6530–6540, 2010.
- [50] Nikhil Gunari, Anna C Balazs, and Gilbert C Walker. Force-induced globule-coil transition in single polystyrene chains in water. *Journal of the American Chemical Society*, 129(33):10046–10047, 2007.
- [51] Ronen Zangi, Ruhong Zhou, and BJ Berne. Urea’s action on hydrophobic interactions. *Journal of the American Chemical Society*, 131(4):1535–1541, 2009.

- [52] Jagannath Mondal, Duncan Halverson, Isaac TS Li, Guillaume Stirnemann, Gilbert C Walker, and Bruce J Berne. How osmolytes influence hydrophobic polymer conformations: A unified view from experiment and theory. *Proceedings of the National Academy of Sciences*, 112(30):9270–9275, 2015.
- [53] Jeremy L England and Gilad Haran. Role of solvation effects in protein denaturation: from thermodynamics to single molecules and back. *Annual review of physical chemistry*, 62:257–277, 2011.
- [54] JB Pethica and WC Oliver. Tip surface interactions in stm and afm. *Physica Scripta*, 1987(T19A):61, 1987.
- [55] NA Burnham, G Gremaud, AJ Kulik, P-J Gallo, and F Oulevey. Materials’ properties measurements: choosing the optimal scanning probe microscope configuration. *Journal of Vacuum Science & Technology B: Microelectronics and Nanometer Structures Processing, Measurement, and Phenomena*, 14(2):1308–1312, 1996.
- [56] John M Gosline. Hydrophobic interaction and a model for the elasticity of elastin. *Biopolymers: Original Research on Biomolecules*, 17(3):677–695, 1978.
- [57] Michael H Abraham, Gary S Whiting, Richard Fuchs, and Eric J Chambers. Thermodynamics of solute transfer from water to hexadecane. *Journal of the Chemical Society, Perkin Transactions 2*, (2):291–300, 1990.

Chapter 4

Active Rheology Measurements on Flexible Polymers using Interferometer based AFM

4.1 Introduction

The force spectroscopy on single molecule has become an indispensable tool to study both intermolecular and intramolecular interaction of biomolecules and soft matter complexes [1]. The manipulation of single molecules with high force sensitivity and spatial resolution has allowed for better understanding of nanoscale mechanics of proteins and simple polymers. Generally, it is of interest to know conformational landscape of molecules and how molecules achieve equilibrium under an applied force by following a diffusive dynamics. In this regard, measurement of force-extension signal provides great insights in exploring various region of conformational landscape. Both thermodynamic free energy of landscape[2] and dynamical information[3, 4] can be extracted with these experiments.

However, single molecule force-extension measurements are also sensitive to artifacts and can lead to misinterpreting data as valid representation of single molecule trajectory. In the recent past, a great number of experiments[5, 6, 7, 8, 9] and simulations[10, 11] have focused on extracting intrinsic thermodynamic and kinetic signatures of molecule from effects of instrument. These studies address the instruments effects like finite response time of AFM cantilever probe and its stiffness on limiting the accuracy of force-extension measurements. A simple and most common way of generating force-extension curve is to perform AFM pulling experiments in constant velocity mode. As we saw in the previous chapter, AFM force extension curve in this mode may not represent a valid single molecule trajectory. Importantly, the estimates of persistence length are unphysical when modelling force-extension curve using wormlike-chain[12, 13, 14, 15]. Instead of global pulling protocol, a local oscillatory protocol is better suited for intrinsic sampling of conformational landscape. This is mainly due to two reasons : 1) the oscillatory techniques is bidirectional in nature and hence is accurate in sampling the conformational space[16] 2) As shown in previous chapter, extracting an oscillatory response allows for a simple interpretation of intrinsic elasticity from the convolution of instrument effects[17].

However, when oscillating the cantilever base end with a piezo drive and than using the optical beam deflection scheme to detect oscillations, naturally necessitates

viewing the cantilever as continuum beam. This is primarily because the optical beam deflection detection measures changes in cantilever endslope with respect to the base. A beam theory approach described in chapter 2 is typically used to describe the cantilever oscillating dynamics using a fourth-order partial differential equation. Under various Euler-Bernoulli assumption and strict boundary conditions, this equation need to be solved. The strict assumptions about boundary condition may not necessarily be satisfied while nonspecific tethering the polymer of interest to cantilever-tip and oscillations in liquid environment. Importantly, explicit solving of fourth order differential equation involves various approximation that limits its universal description. This include approximations about the geometrical shape of beam[18] together with parameters that satisfy Taylor series expansions[19]. In practice these assumptions may not be satisfied and can lead to misinterpretation. In addition, our recent work showed that beam deflection scheme can lead to artefacts due to various sources like initial hydrodynamic phase uncertainty[20]. To avoid the complexity of interpretation, fiber-based interferometer detection scheme is employed in this work. Because of direct and local detection of cantilever displacement at a point, it allows for a simple point - mass description of the cantilever[21]. The equation of motion for dynamics of point mass is the classical damped simple harmonic oscillator(SHO). Hence, a straightforward and universal hydrodynamics based on SHO is suitable for accurate measurement of elastic response.

In this chapter, we employ home-built fiber-interferometer based AFM to measure elastic response of flexible polymers. Measurements were made on PEG and Polystyrene in good and poor solvents. Along with pulling on the polymer with constant velocity, sub-nanometer oscillatory perturbations were applied to extract the elastic response. The measured response was interpreted with WLC model of entropic elasticity and persistence length was extracted. It turns out that, similar to results in chapter 3, persistence length show significant deviation from conventional pulling experiments for PEG and Polystyrene in good solvents but no such deviation are observed for Polystyrene in poor solvent. In addition to this, the fluctuations about a mean elastic response also showed large variance for shorter length polymer like PEG compared to larger length Polystyrene. The results were rationalised with statistical mechanics of combined cantilever-polymer system and suggest that deconvolution of instruments effects due to oscillatory protocol produces intrinsic response for polymers.

4.2 Materials and Methods

4.2.1 Sample preparation

Polystyrene of molecular weight 192 KDa was purchased from Merk and rigorously dissolved in THF(Tetrahydrofuran) to μM concentration. Thereafter, a drop of $60 \mu\text{l}$ was incubated on a clean glass coverslip and later cleaned excessively with THF solvent. After drying the coverslip, it was loaded into the fluid cell and filled with water and 8M Urea for experiments in respective solvents. For experiments with PEG, a 10 KDa molecular weight was purchased in powder form and dissolved in Milli-Q water ($18 \text{ M}\Omega \text{ cm}$) to 1 mM concentration. A sample of about $80 \mu\text{l}$ was then incubated for half an hour on freshly prepared gold coverslip. The coverslips were prepared from thermal evaporation deposition and first treated with UV ozone

to remove organic impurities before use. The thiol terminated PEG is then able to form a covalent bond with gold surface. This procedure not only results in strong attachment but also gives off large rupture force when polymer detaches from AFM tip. The sample was rinsed clean with Milli-Q before mounting it in a fluid cell for further measurements in water.

4.2.2 Fiber-Interferometer AFM

In AFM which is based on fiber-based interferometer[22, 23, 24], three major assemblies work in conjunction to determine its overall operations. 1) One assembly is that of optic-fiber based interferometer detector which was clearly explained in chapter 2. This detector uses a single mode fiber to detect an interference pattern formed from combination of light reflected at fiber end and cantilever end which are placed very close to each other. Interference pattern is very sensitive to separation between the cantilever and fiber and points of maximum sensitivity are chosen for operation. To form the interference pattern, cantilever surface and fiber end are made parallel to each other which is ultimately ensured by a perpendicularly aligning the fiber on the back side of cantilever. This precise alignment is made possible by another component of the assembly called 5-axis fiber slider or nanopositioner[23]. 2) As shown in figure 4.1, it consists of two mutually perpendicular slider plates (shown in light red) each capable of moving in its plane and rotate about an axis perpendicular to plane. The plates are driven by stack of shear piezos, in set of three, glued onto them and are connected to each other by magnetic screws for optimal sliding force. The $yz\phi$ slider has polished sapphire plates glued to it which slide against the sapphire balls attached on top of piezostacks for $xz\theta$ slider. By providing logical voltage pulses to piezo stacks, inertial sliding motion is initiated and sliders move in $xz\theta$ and $yz\phi$ directions giving rise to motion along five independent axis (x,y,z,θ,ϕ) . The optical fiber is attached to a steel plate holder which also holds a tube piezo (yellow part in fig 4.1) for vertical motion of fiber. This plated holder is moved by piezostacks of $yz\phi$ slider as depicted in figure 4.1. Thus, 5-axis slider can precisely position the fiber very close and perpendicular to cantilever backside for a good interference pattern. 3) For force spectroscopy experiments, the sample stage assembly is required to be approached or retracted from the cantilever-tip. as shown in figure 4.1, it is done using scanner and hammer tube piezo for finer and coarser motion respectively. The sample holder is mounted on a scanner piezo tube which is enclosed in a glass tube. The end of this glass tube is attached onto a hammer tube piezo and glass tube itself is held at place by leaf spring. The bottom end of hammer piezo tube supports a steel disk (hammer disk) and provides the necessary inertia for coarser motion along vertical z direction. The hammer piezo when given large voltage pulses with slow rise and rapid fall give rise to coarser motion along z direction. During the slow rising part hammer piezo contacts but this does not disturb the the glass tube attached at its top end and held by leaf spring. However, with sharp fall, piezo suddenly try to expand and this is opposed by inertia of hammer disk which forces glass tube overcome leaf spring and slide against it. Similarly, external electrode of scanner piezo tube is segmented into four quadrants and application of suitable pulses produces finer x,y,z motion as explained in chapter 2.

For measurements, a gold coated cantilever purchased from micromash were used. The cantilever stiffness and resonance frequency were $0.8N/m$ and $13KHz$. The

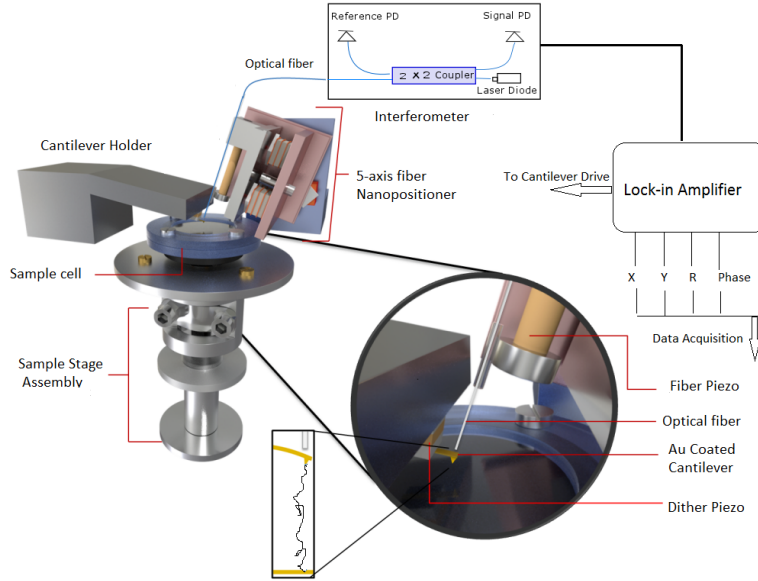


Figure 4.1: A schematic diagram of AFM used in experiment. It consist of three major components 1) fiber-interferometer 2) 5-axis nanopositioner and 3) sample-stage assembly. A lock-in amplifier is used to detect amplitude and phase changes from signal photodiode(PD) output.

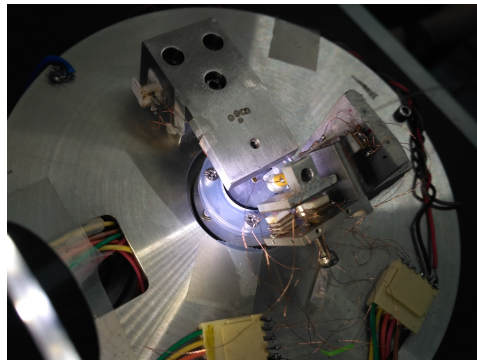


Figure 4.2: A photograph of interferometer based AFM setup.

cantilever was mounted on a holder with stacks of dither piezo beneath it. Cantilever was oscillated at an off-resonance frequency of 500 KHz using internal oscillator from lock-in. The fiber was accurately aligned on the back of cantilever using 5-axis nanopositioner. The interference pattern so produced was looked for point of maximum sensitivity and locked at this position using a feedback loop for further operations. Thereafter, the sample was approached towards the cantilever-tip using cantilever oscillating amplitude as setpoint value. Once approached, the sample was retracted at constant velocity of $80\text{nm}/\text{sec}$ and output of signal photodiode was fed as input to lock-in amplifier to record amplitude R phase θ , X and Y output of lock-in amplifier. The stiffness-extension curves measured for PEG in water were 25 and for polystyrene in water and 8M Urea were 26 and 17 respectively. The concentration of polymers stock solution was low so that mostly single binding events with cantilever tip were detected. The stiffness-extension profiles which could be normalized by their apparent contour length (obtained by fitting to WLC) were finally chosen for analysis.

4.2.3 Modelling cantilever-polymer dynamics

The beam deflection method that is commonly used to detect cantilever deflections, measures them as changes in slope of cantilever beam with respect to the clamped base. In contrast, fiber-interferometer detection scheme described above measures deflections directly and locally at a point on the cantilever beam. This has important implication for modelling cantilever dynamics when it is oscillated at its clamped base. For beam deflection method, it becomes necessary to view the cantilever as a continuum beam. Its modelling is then based on fourth-order partial differential equation which is valid under various Euler-Bernoulli assumptions[18]. In addition to these assumptions being not true in practice, the analysis is also complicated by hydrodynamics of cantilever in liquid operation. This can further lead to artifacts[20].

However, for fiber-interferometer method, a simple point-mass description becomes valid due to local detection at a point. The dynamics of oscillating cantilever is therefore that of damped simple harmonic oscillator(SHO). If we model polymer as dumbbell with spring k_i and dashpot γ_i than the combined response of cantilever plus polymer is described by following equation of motion :

$$m * \ddot{z} + \gamma \dot{z} + kz = A_0 k_c \cos \omega t \quad (4.1)$$

The cantilever and polymer contribution simply add in parallel with $k = k_i + k_c$ and $\gamma = \gamma_i + \gamma_c$. Here, A_0 is free amplitude of cantilever in absence of polymer.

For off-resonance condition $\omega \ll \omega_0$, where $\omega_0^2 = k_c/m*$, the dissipative $\gamma \dot{z}$ and inertial term $m * \ddot{z}$ are negligible compared to kz term[25]. In this condition, if we seek a steady state solution $z = A \cos \omega t + \delta$ with amplitude response A and phase difference δ between cantilever drive and cantilever oscillations, we get, for interferometer based detection:

$$A = A_0 \left(1 - \frac{k_i}{k_c}\right) \quad \text{and} \quad \delta \sim 0 \quad (4.2)$$

The phase difference is introduced due to dissipation γ but in off-resonance condition this quantity does not dominate and hence we should have almost zero phase difference. The amplitude and phase are measured with lock-in amplifier outputs.

4.3 Results and Discussion

4.3.1 Polyethylene Glycol (PEG)

Force-extension curve of a polymer measures the entropic elasticity arising due to large changes in accessible configurations of polymer. As explained in chapter 3, these curves are modelled with two classes of entropic models of WLC (WormLike Chain) and FJC (Freely Jointed Chain) and their modifications. The intrinsic parameter of polymer chain i.e persistence length l_p or its equivalent Kuhn length $b = 2l_p$ are estimated from respective models of WLC and FJC. Figure 4.3 shows the force-extension curves of polyethylene glycol (PEG) modelled with WLC and modified FJC. In figure 4.3a) WLC model is fitted to PEG force-extension curve while excluding the region between 100 and 300 pN. As already explained in chapter 3, this is due to conformational transition of PEG monomer in water as the polymer

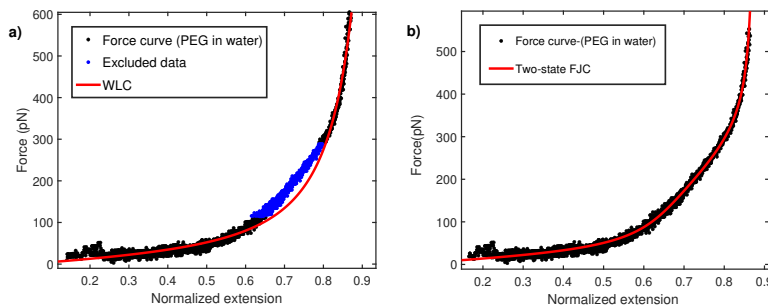


Figure 4.3: **(a)** Force-extension curve for PEG in water fitted with WLC with a persistence length $l_p = 0.12 \pm 0.02$ nm. A region between 100 and 300 pN does not fit and is also excluded. **(b)** Force-extension curve fitted with two-state FJC model with Kuhn segment length 0.24 ± 0.02 nm.

is stretched. However, the overall value of persistence length estimated from the fit is 0.12 ± 0.02 nm. To make the fitting procedure more realistic, a two-state FJC model[26, 27, 28] defined in chapter 3 (eq 3.4) is fitted to the same force-extension data as shown in figure 4.3b). Fitting yields a Kuhn segment length of 0.24 ± 0.02 nm or a persistence length of 0.12 nm. The persistence length of 0.12 nm is even lower than c-c bond length (0.16 nm) as well as about five times lower than its measurement with magnetic tweezers[29, 30]. It is noted that a wide variety of polymers show anomaly low value of persistence length estimated in AFM constant velocity pulling measurements and raise question on validity of WLC model[12, 13, 14, 15, 31].

To understand this, local oscillatory rheology measurements were performed on polymer while it is pulled at a constant velocity ~ 70 nm/s. The cantilever was oscillated by sinusoidal driving at it's base using dither piezos. Amplitude of cantilever oscillations and phase difference of cantilever oscillations with respect to drive are measured using fiber-interferometer and recorded using lock-in amplifier. Figure 4.4 shows that phase difference is close to zero and featureless due to an almost negligible contribution from viscous dissipation in off-resonance frequency[20, 32, 21]. Contrary to this, amplitude signal shows a non-linear feature coinciding with pulling of polymer. From equation 2, amplitude signal changes are linearly proportional to elastic response of polymer k_i and equation is therefore used to convert the amplitude-extension relation to stiffness-extension relation. The stiffness-extension curve (in black) is shown in Figure 4.4. As evident, there is a substantial deviation of stiffness-extension curve from force-extension derivative (blue) obtained in global pulling experiments. The model of WLC is then fitted to stiffness-extension curve but the regime between 50 and 70 nm is not fitted well. This regime corresponds to linear regime between 100 and 300 pN observed for force-extension curves and likely a result of length conformational transition for PEG monomer in aqueous medium. The above result affirms that our measurement is sensitive to conformational transition and measures a persistence length of 0.5 ± 0.1 nm. The persistence length of 0.5 nm, obtained using oscillatory rheology, matches well with equilibrium magnetic tweezer measurements in low force regime[29, 30, 33]. Specifically, Innes-gold et. al[30] and Dittmore et. al[29] measured persistence length of 0.55 and 0.5 nm respectively. In addition, ensemble measurements using neutron scattering and other bulk techniques [34, 35] report persistence length l_p of 0.6 nm.

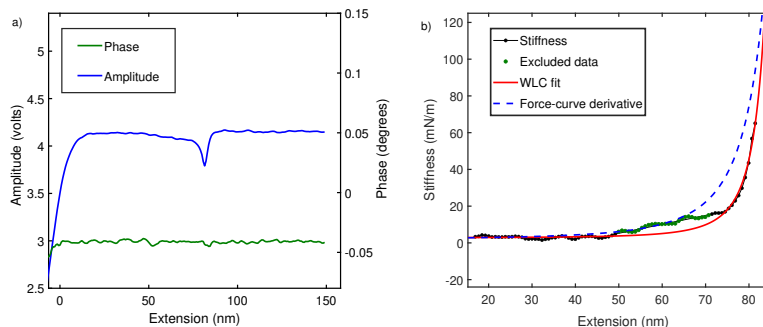


Figure 4.4: **(a)** The raw amplitude A and phase δ profiles measured using fiber based interferometer for PEG in water. **(b)** Comparison of stiffness-extension curve measured from amplitude signal (black) with derivative of force-extension curve (blue-dash). It also shows fitting of stiffness-extension curve with WLC (red) while excluding region between 50 and 70 nm is shown in green. A similar behavior is seen in fig. 2a for force-extension curves. Persistence length estimated is 0.5 ± 0.1 nm.

Due to variety of sources[20, 19], the beam deflection scheme of measuring cantilever deflections is prone to artefacts. This is mainly because it measures slope of cantilever rather than direct deflection detection as done above. It therefore puts our result on a stronger footing compared to previous oscillatory measurements on polymers[36, 37, 38]. Moreover, direct deflection detection using optical fiber allowed us to interpret the measurement within a universal point mass description, independent of assumptions used in describing hydrodynamics of cantilever beam.

4.3.2 Polystyrene

Polystyrene is treated as an ideal homopolymer to study complex self-assembly of proteins like globular proteins[39]. This is due to its homogeneous structure and hydrophobic side chain of polystyrene which results in hydrophobic collapse similar to what is observed for globular proteins.

A protein molecule tend to denature in high concentration of aqueous urea and dominant mechanism responsible for denaturation is the weakening of hydrophobic region of proteins by urea. Therefore, urea is generally considered a good solvent for hydrophobic homopolymers and water a poor solvent[40, 41, 42]. In this part, we describe our local oscillatory rheology measurement on Polystyrene in water and 8M urea.

A force-extension curve of polystyrene in constant velocity pulling experiments report a persistence length (l_p) of 0.23 nm in poor solvent of water[13] and 0.25 nm in good solvent like toluene[31, 43]. They are at odds with the fact that there is 0.72 nm long side group that can offer significant steric hindrances. Therefore, these values of persistence length are debated [31, 35]. To address this, we measured the oscillatory response of polystyrene while it is pulled at a constant velocity. The results for polystyrene in water (milli-Q) are depicted in Figure 4.5a. It shows that stiffness-extension curve (black) generated from amplitude signal of lock-in using equation 2. This curve shows no noticeable deviation from derivative of force-extension curve (in blue-dash) with l_p 0.23 nm. The WLC fit (in red) to stiffness-extension data gives a

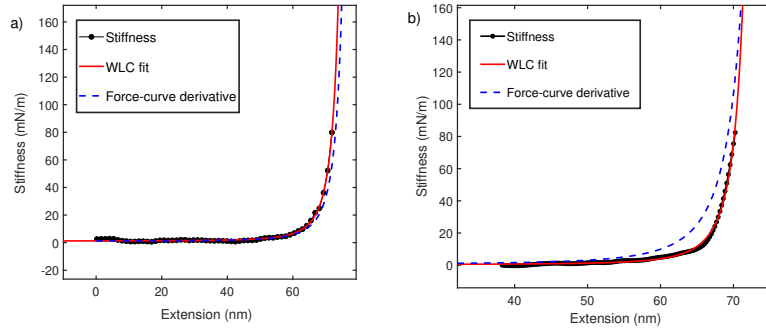


Figure 4.5: (a) Polystyrene stiffness-extension curve in water (black) measured using interferometer based AFM and fitted with WLC model (red). It is compared with derivative of force-extension curve with l_p 0.23 nm (blue-dash). (b) Polystyrene stiffness-extension curve taken in 8M Urea (black) fitted with WLC (red) of $l_p = 0.88 \pm 0.02$ nm and compared with force-extension derivative (blue-dash) of l_p 0.23 nm.

persistence length of 0.26 ± 0.02 nm. It is interesting to note that globular protein domains alike I27 have been studied with both oscillatory and pulling experiments and similarly show no deviation[44, 19, 20]. The persistence length is also similar to that measured with magnetic tweezers[45]. We already explained this in chapter 3, where we noted an additional contribution from hydrophobic free energy, which makes fitting with WLC alone an ad-hoc process. WLC only accounts for entropic elasticity of polymer backbone and no side chain effects are considered. In case of poor solvents like water, persistence length is a heuristic parameter which may take a lower value to accommodate hydrophobic interaction and makes up for inadequacy of model describing the polymer elasticity[46, 47].

We next carried out similar experiments in 8M Urea. Figure 4.5b shows stiffness-extension curve (black) from oscillatory measurement which deviates significantly from derivative of force-extension curve (blue-dash). When stiffness-extension data is fitted with WLC model. This yields a persistence length of 0.88 ± 0.02 nm.

The data in Figure 4.5b, is consistent with our observation in Figure 4.4. It can be concluded that for polymer chain in good solvents, the stiffness measurement using oscillatory rheology deviates from derivative of force-extension curves (Figure 4.5b and 4.4b). The direct measurement of stiffness using oscillatory measurements yields reasonable values of persistence length, which are consistent with other techniques. We explained this observed deviation in chapter 3 using a deconvolution of cantilever from polymer intrinsic response. For sake of completeness, we again put up a section at the end to explain deviation and non-observation of deviation in good and poor solvent respectively.

4.4 Fluctuations about mean

So far, we have focused on average thermodynamic behavior of force-extension curve. However, fluctuations about mean behavior also reveal an important information about deconvolution of cantilever from intrinsic polymer response. Figure 4.6 shows the force-extension curve for PEG and polystyrene taken with commercial AFM in a) and b) respectively. The force-extension curve shows no distinction in

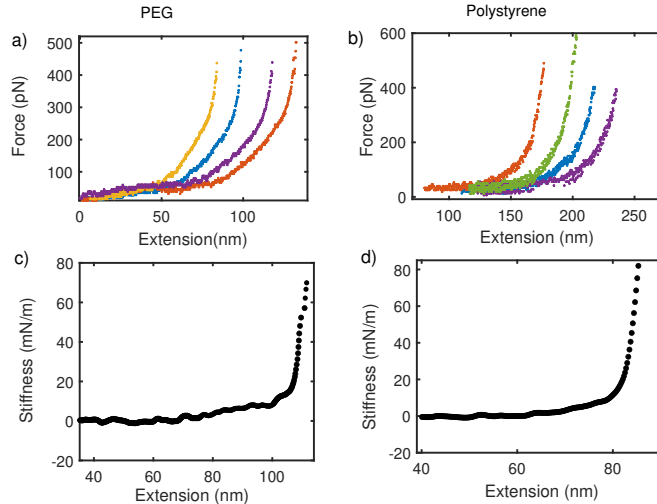


Figure 4.6: (a) and (c) shows force-extension and stiffness-extension curves for PEG in water. Similarly, (b) and (d) are force-extension and stiffness-extension curve for Polystyrene in water respectively. Fluctuations about mean stiffness are strong in PEG with molecular weight 10 kDa than a longer polymer of Polystyrene with molecular weight 200 kDa. No size dependent variation in fluctuation is observed for force-extension curve.

terms of fluctuation about the mean behavior between two polymers of different size or molecular weight. PEG has a molecular weight of 10 kDa while Polystyrene is a 200 kDa polymer. It is expected on basis of statistical mechanics of polymers that fluctuation about mean would go as $1/\sqrt{N}$ where N is monomer units, following a Poisson statistics. Fluctuations in force for a finite size system like polymer are expected to be large but force-extension curve in pulling experiments show no large fluctuation and no variation with size of polymer. This is because of overall fluctuation in the coupled cantilever-polymer system are dominated by cantilever[48, 49]. On the other hand, the stiffness-extension curve from oscillatory measurement show a clear distinction in terms of fluctuations about the mean in two polymers. Fluctuations in low size polymer of PEG are large compared to large size Polystyrene. This support the argument that an intrinsic polymer response is captured by local oscillatory response than from global pulling experiments.

2

4.5 Explanation of Deviation

The observed deviation between force-extension and stiffness-extension curve is explained using deconvolution principle elaborated in chapter 3. Briefly, entropic elasticity of polymer in good solvent condition is statistical in character, arising from a probability distribution over various accessible configurations. For its correct interpretation, it is important therefore to consider combined statistical mechanics of polymer- cantilever system. If canonical partition function of polymer and cantilever are Z_m and Z_c respectively, then overall partition function Z_{system} is[50, 48, 49]:

$$Z_{system} \sim Z_m * Z_c = e^{-\beta F(x)} * e^{-\beta k_c \delta_c^2 / 2} \quad (4.3)$$

Here β is $1/k_B T$ and $F(x)$ is free energy as a function of end-to-end length coordinate x . As explained in chapter 3, $Z_m * Z_c$ is a mathematical convolution if we substitute deflection δ_c as $D - x$ in cantilever's harmonic biasing potential $k_c \delta_c^2 / 2$. Here, D is the displacement of cantilever with sample surface at constant velocity and x is end-to-end length of polymer. It means that both cantilever and polymer are acting simultaneously to determine the overall force-extension profile. However, this effect of convolution can be diminished by either working in high deflection (force) regime or performing experiments with low force magnetic tweezer setup. Constant-force measurement performed with magnetic tweezers are effectively zero stiffness measurement, which integrates out the effect of cantilever and an isolated response from Z_m only[48, 49] is sampled. It also explains our match of persistence length with magnetic tweezer measurements and suggest that oscillatory measurements are sampling an intrinsic polymer response. The likely reason for intrinsic measurement in stiffness-extension curve is the parallel coupling of oscillating measurements. For the total amplitude response A in equation 2, the stiffness of cantilever k_c and stiffness of polymer k_i effectively adds up. Compared to an intricate convolution, this allows for a much clearer separation of polymer intrinsic response from cantilever contribution.

For polymer in poor solvent such as polystyrene in water, we observed no deviation between force-extension and stiffness-extension curve. As explained in chapter 3, reason for this is the large and positive hydrophobic free energy required to stretch a hydrophobic polymer in water[51, 47, 46]. The bulky aromatic side group of polystyrene contributes significantly to hydrophobic free energy in addition to conformational entropy of polymer backbone described by WLC[52]. This results in perceived softening of polymer and a lower value of persistence length[46, 47]. Hence, stiffness-extension curve show no systematic deviation with respect to force extension curve. Importantly, WLC fitting only produces persistence length as an effective parameter to account for inadequacy of WLC model in poor solvent.

4.6 Chapter Summary

In conclusion, we performed elasticity measurement on PEG and Polystyrene with a home-built fiber-interferometer based AFM. Our work confirms the previous measurement with commercial AFM setup based on beam deflection detection scheme and highlights the importance of a simplified and universal simple harmonic oscillator (SHO) for describing cantilever dynamics. Elastic response was measured by oscillating the cantilever base and recording the amplitude and phase response using lock-in amplifier. The amplitude signal, in particular, was quantified to obtain stiffness-extension profiles and analysed with WLC entropic model. For both polymers, stiffness-extension curve deviates significantly from conventional force-extension curve in good solvent condition. When modelled with phenomenological WLC model, it's fitting of stiffness-extension curve produce a reasonable estimate of persistence length (0.55 nm for PEG and 0.8 nm for Polystyrene), which is about five times more compared with conventional pulling experiments (0.1 nm for PEG and 0.2 nm for Polystyrene). The value is also consistent with equilibrium measurements with magnetic tweezers and other force-free techniques. Although fluctuations about mean elastic behavior are known not to dominate pulling force-extension curve, local oscillatory measurement of stiffness-extension curve does reveal a clear

size dependence of fluctuations. This underlines the importance of convolutional coupling between AFM probe and intrinsic polymer elasticity. In addition, stiffness-extension curve shows no deviation from force-extension curve in poor solvent case of Polystyrene in water. As earlier, we attribute this to additional hydrophobic contribution that effectively lowers the persistence length and suggest that WLC entropic model is ad-hoc in poor solvents.

Bibliography

- [1] Wolfgang Ott, Markus A Jobst, Constantin Schoeler, Hermann E Gaub, and Michael A Nash. Single-molecule force spectroscopy on polyproteins and receptor–ligand complexes: The current toolbox. *Journal of structural biology*, 197(1):3–12, 2017.
- [2] Michael T Woodside and Steven M Block. Reconstructing folding energy landscapes by single-molecule force spectroscopy. *Annual review of biophysics*, 43: 19–39, 2014.
- [3] Olga K Dudko, Jérôme Mathé, Attila Szabo, Amit Meller, and Gerhard Hummer. Extracting kinetics from single-molecule force spectroscopy: nanopore unzipping of dna hairpins. *Biophysical journal*, 92(12):4188–4195, 2007.
- [4] Ignacio Tinoco, Pan TX Li, and Carlos Bustamante. Determination of thermodynamics and kinetics of rna reactions by force. *Quarterly reviews of biophysics*, 39(4):325–360, 2006.
- [5] Hao Yu, Matthew GW Siewny, Devin T Edwards, Aric W Sanders, and Thomas T Perkins. Hidden dynamics in the unfolding of individual bacteriorhodopsin proteins. *Science*, 355(6328):945–950, 2017.
- [6] Michael Hinczewski, J Christof M Gebhardt, Matthias Rief, and D Thirumalai. From mechanical folding trajectories to intrinsic energy landscapes of biopolymers. *Proceedings of the National Academy of Sciences*, 110(12):4500–4505, 2013.
- [7] Ronen Berkovich, Rodolfo I Hermans, Ionel Popa, Guillaume Stirnemann, Sergi Garcia-Manyes, Bruce J Berne, and Julio M Fernandez. Rate limit of protein elastic response is tether dependent. *Proceedings of the National Academy of Sciences*, 109(36):14416–14421, 2012.
- [8] Michael Hinczewski, Yann von Hansen, and Roland R Netz. Deconvolution of dynamic mechanical networks. *Proceedings of the National Academy of Sciences*, 107(50):21493–21498, 2010.
- [9] Krishna Neupane and Michael T Woodside. Quantifying instrumental artifacts in folding kinetics measured by single-molecule force spectroscopy. *Biophysical journal*, 111(2):283–286, 2016.
- [10] Michael T Woodside, John Lambert, and Kevin SD Beach. Determining intrachain diffusion coefficients for biopolymer dynamics from single-molecule force spectroscopy measurements. *Biophysical journal*, 107(7):1647–1653, 2014.

- [11] Changbong Hyeon, Greg Morrison, and D Thirumalai. Force-dependent hopping rates of rna hairpins can be estimated from accurate measurement of the folding landscapes. *Proceedings of the National Academy of Sciences*, 105(28):9604–9609, 2008.
- [12] Marina I Giannotti and G Julius Vancso. Interrogation of single synthetic polymer chains and polysaccharides by afm-based force spectroscopy. *ChemPhysChem*, 8(16):2290–2307, 2007.
- [13] Sabah Al-Maawali, Jason E Bemis, Boris B Akhremitchev, Haiying Liu, and Gilbert C Walker. Single-molecule afm study of polystyrene grafted at gold surfaces. *The Journal of Adhesion*, 81(10-11):999–1016, 2005.
- [14] Hongbin Li, Wenke Zhang, Weiqing Xu, and Xi Zhang. Hydrogen bonding governs the elastic properties of poly (vinyl alcohol) in water: single-molecule force spectroscopic studies of pva by afm. *Macromolecules*, 33(2):465–469, 2000.
- [15] M-N Dessinges, Berenike Maier, Y Zhang, M Peliti, David Bensimon, and Vincent Croquette. Stretching single stranded dna, a model polyelectrolyte. *Physical review letters*, 89(24):248102, 2002.
- [16] Oliver Braun, Andreas Hanke, and Udo Seifert. Probing molecular free energy landscapes by periodic loading. *Physical review letters*, 93(15):158105, 2004.
- [17] Vikhyaat Ahlawat, Shatruhan Singh Rajput, and Shivprasad Patil. Elasticity of single flexible polymer chains in good and poor solvents. *Polymer*, 230:124031, 2021.
- [18] Gary K Fedder, Christofer Hierold, Jan G Korvink, and Osamu Tabata. *Resonant MEMS: fundamentals, implementation, and application*, volume 22. John Wiley & Sons, 2015.
- [19] Fabrizio Benedetti, Yulia Gazizova, Andrzej J Kulik, Piotr E Marszalek, Dmitry V Klinov, Giovanni Dietler, and Sergey K Sekatskii. Can dissipative properties of single molecules be extracted from a force spectroscopy experiment? *Biophysical journal*, 111(6):1163–1172, 2016.
- [20] Shatruhan Singh Rajput, Surya Pratap S Deopa, Jyoti Yadav, Vikhyaat Ahlawat, Saurabh Talele, and Shivprasad Patil. The nano-scale viscoelasticity using atomic force microscopy in liquid environment. *Nanotechnology*, 32(8):085103, 2020.
- [21] Shatruhan Singh Rajput, Surya Pratap S Deopa, VJ Ajith, Sukrut C Kamerkar, and Shivprasad Vitthal Patil. Validity of point-mass model in off-resonance dynamic atomic force microscopy. *Nanotechnology*, 2021.
- [22] D Rugar, HJ Mamin, and Peter Guethner. Improved fiber-optic interferometer for atomic force microscopy. *Applied Physics Letters*, 55(25):2588–2590, 1989.
- [23] Shivprasad Patil, George Matei, Hang Dong, Peter M Hoffmann, Mustafa Karaköse, and Ahmet Oral. A highly sensitive atomic force microscope for linear measurements of molecular forces in liquids. *Review of Scientific Instruments*, 76(10):103705, 2005.

- [24] AHMET Oral, RA Grimble, HAKAN ÖZGÜR Özer, and JB Pethica. High-sensitivity noncontact atomic force microscope/scanning tunneling microscope (nc afm/stm) operating at subangstrom oscillation amplitudes for atomic resolution imaging and force spectroscopy. *Review of Scientific Instruments*, 74(8):3656–3663, 2003.
- [25] Dror Sarid, Roland Coratger, François Ajustron, and Jacques Beauvillain. Scanning force microscopy-with applications to electric, magnetic and atomic forces. *Microscopy Microanalysis Microstructures*, 2(6):649–649, 1991.
- [26] F Oesterhelt, M Rief, and HE Gaub. Single molecule force spectroscopy by afm indicates helical structure of poly(ethylene-glycol) in water. *New Journal of Physics*, 1(1):6, 1999.
- [27] Wolfgang Ott, Markus A Jobst, Magnus S Bauer, Ellis Durner, Lukas F Milles, Michael A Nash, and Hermann E Gaub. Elastin-like polypeptide linkers for single-molecule force spectroscopy. *ACS nano*, 11(6):6346–6354, 2017.
- [28] Berthold Heymann and Helmut Grubmüller. Elastic properties of poly(ethylene-glycol) studied by molecular dynamics stretching simulations. *Chemical Physics Letters*, 307(5-6):425–432, 1999.
- [29] Andrew Dittmore, Dustin B McIntosh, Sam Halliday, and Omar A Saleh. Single-molecule elasticity measurements of the onset of excluded volume in poly(ethylene glycol). *Physical Review Letters*, 107(14):148301, 2011.
- [30] Sarah N Innes-Gold, Ian L Morgan, and Omar A Saleh. Surface-induced effects in fluctuation-based measurements of single-polymer elasticity: A direct probe of the radius of gyration. *The Journal of chemical physics*, 148(12):123314, 2018.
- [31] Milad Radiom, Plinio Maroni, and Michal Borkovec. Influence of solvent quality on the force response of individual poly(styrene) polymer chains. *ACS Macro Letters*, 6(10):1052–1055, 2017.
- [32] Andreas Möglich, Karin Joder, and Thomas Kiefhaber. End-to-end distance distributions and intrachain diffusion constants in unfolded polypeptide chains indicate intramolecular hydrogen bond formation. *Proceedings of the National Academy of Sciences*, 103(33):12394–12399, 2006.
- [33] Omar A Saleh. Perspective: Single polymer mechanics across the force regimes. *The Journal of chemical physics*, 142(19):194902, 2015.
- [34] Grant D Smith, Do Y Yoon, Richard L Jaffe, Ralph H Colby, Ramanan Krishnamoorti, and Lewis J Fetters. Conformations and structures of poly(oxyethylene) melts from molecular dynamics simulations and small-angle neutron scattering experiments. *Macromolecules*, 29(10):3462–3469, 1996.
- [35] Michael Rubinstein, Ralph H Colby, et al. *Polymer physics*, volume 23. Oxford university press New York, 2003.

- [36] Masaru Kawakami, Katherine Byrne, Bhavin S Khatri, Tom CB McLeish, and D Alastair Smith. Viscoelastic properties of single poly (ethylene glycol) molecules. *ChemPhysChem*, 7(8):1710–1716, 2006.
- [37] Masaru Kawakami, Katherine Byrne, Bhavin S Khatri, Tom CB Mcleish, Sheena E Radford, and D Alastair Smith. Viscoelastic measurements of single molecules on a millisecond time scale by magnetically driven oscillation of an atomic force microscope cantilever. *Langmuir*, 21(10):4765–4772, 2005.
- [38] Xiaobin Liang and Ken Nakajima. Investigating the dynamic viscoelasticity of single polymer chains using atomic force microscopy. *Journal of Polymer Science Part B: Polymer Physics*, 57(24):1736–1743, 2019.
- [39] Isaac TS Li and Gilbert C Walker. Single polymer studies of hydrophobic hydration. *Accounts of chemical research*, 45(11):2011–2021, 2012.
- [40] Ronen Zangi, Ruhong Zhou, and BJ Berne. Urea’s action on hydrophobic interactions. *Journal of the American Chemical Society*, 131(4):1535–1541, 2009.
- [41] Jeremy L England and Gilad Haran. Role of solvation effects in protein denaturation: from thermodynamics to single molecules and back. *Annual review of physical chemistry*, 62:257–277, 2011.
- [42] Jagannath Mondal, Duncan Halverson, Isaac TS Li, Guillaume Stirnemann, Gilbert C Walker, and Bruce J Berne. How osmolytes influence hydrophobic polymer conformations: A unified view from experiment and theory. *Proceedings of the National Academy of Sciences*, 112(30):9270–9275, 2015.
- [43] Nikhil Gunari, Anna C Balazs, and Gilbert C Walker. Force-induced globule-coil transition in single polystyrene chains in water. *Journal of the American Chemical Society*, 129(33):10046–10047, 2007.
- [44] Toni Hoffmann and Lorna Dougan. Single molecule force spectroscopy using polyproteins. *Chemical Society Reviews*, 41(14):4781–4796, 2012.
- [45] Jessica Valle-Orero, Jaime Andrés Rivas-Pardo, and Ionel Popa. Multidomain proteins under force. *Nanotechnology*, 28(17):174003, 2017.
- [46] Kirstin A Walther, Frauke Gräter, Lorna Dougan, Carmen L Badilla, Bruce J Berne, and Julio M Fernandez. Signatures of hydrophobic collapse in extended proteins captured with force spectroscopy. *Proceedings of the National Academy of Sciences*, 104(19):7916–7921, 2007.
- [47] Frauke Grater, Pascal Heider, Ronen Zangi, and BJ Berne. Dissecting entropic coiling and poor solvent effects in protein collapse. *Journal of the American Chemical Society*, 130(35):11578–11579, 2008.
- [48] HJ Kreuzer, SH Payne, and L Livadaru. Stretching a macromolecule in an atomic force microscope: statistical mechanical analysis. *Biophysical journal*, 80(6):2505–2514, 2001.

- [49] Douglas B Staple, Felix Hanke, and Hans Jürgen Kreuzer. Comment on “sub-angstrom conformational changes of a single molecule captured by afm variance analysis”. *Biophysical journal*, 95(2):1001, 2008.
- [50] Ignacio Franco, Mark A Ratner, and George C Schatz. Single-molecule pulling: phenomenology and interpretation. *arXiv preprint arXiv:1205.5068*, 2012.
- [51] John M Gosline. Hydrophobic interaction and a model for the elasticity of elastin. *Biopolymers: Original Research on Biomolecules*, 17(3):677–695, 1978.
- [52] Michael H Abraham, Gary S Whiting, Richard Fuchs, and Eric J Chambers. Thermodynamics of solute transfer from water to hexadecane. *Journal of the Chemical Society, Perkin Transactions 2*, (2):291–300, 1990.

Chapter 5

Passive Rheology measurements on Protein Molecules

5.1 Introduction

The influence of mechanical forces is ubiquitous in all of biology and life. It is a common perturbation encountered in many natural phenomenon of biology ranging from flipping of wings by hummingbird, shooting of tongue by salamanders to bending of plant in response to light. At a cellular level, mechanical forces come into play in different processes like DNA replication, DNA transcription, to cellular differentiation, adhesion and muscle elasticity[1, 2]. Thus, force is an essential parameter relevant in physiology of all living organisms down to cellular level.

The mechanism by which cells sense, generate and transduce forces is microscopically linked to mechanical role played by protein molecules. A protein, as a part of cell is not just freely diffusing but in fair amount also tethered to cell membrane, cell cytoskeleton, organelles and extracellular matrix[3]. Therefore, proteins are naturally subjected to mechanical forces. In response to force selection, they have evolved into diverse mechanical functions that includes giant titin protein present in cardiac and skeletal muscles sacromere responsible for its passive elasticity, tenascin and fibronectin in cell's extracellular matrix that have force-dependent affinity towards its partners to regulate cell adhesion and motor proteins like kinesin that move along microtubules tract to transport chromosomes[1]. These proteins with well defined mechanical function are usually present as tandemly arranged repeats of folded domains and characterized by their ability to withstand or exert forces between 1-200 pN *in vivo*[4]. In addition, domains undergo mechanical unfolding and refolding cycles in performing various cellular activities such as contraction of muscles and regulating cell-adhesion[4, 5]. The folded domains mostly has hydrogen bonded beta-sheet topology that has high resilience to unfolding and when arranged in series they possibly provide a good solution to resist mechanical forces. This design seem to have risen through evolution[4]. For instance, the immunoglobulin (Ig) domain that is most abundant in nature and present in variety of proteins including muscle and cell-adhesion proteins have such a mechanical design. Hence, study of mechanical response of these proteins would provide a great deal of information about how proteins transduce and sense mechanical forces to perform its designated functions.

During the last decades, single molecule force spectroscopy (SMFS) techniques

of optical-tweezers (OTs) and atomic force microscope (AFM) has enhanced our understanding of protein mechanics[6]. It is now possible to mimic biological conditions of folding and unfolding of proteins and measure mechanical response in a controlled manner. Beside studying proteins with mechanical function, SMFS technique have been extensively used to probe free energy landscape of protein folding[6, 7]. All important functions inside a cell are carried out by proteins irrespective of their mechanical or non-mechanical nature. To do so, a protein molecule has to fold into its native three-dimensional conformation from a linear sequence of amino acids encoded by DNA. This processes of protein folding is usually described in terms of a funnel shaped free energy landscape over which protein folds downhill to free energy minima of the native 3-d conformation[8]. The unique 3-d conformation is reached by a diffusive search over innumerate possible conformation of a unfolded polypeptide polymer that makes up the free energy landscape. However, for this search to be effective there should exist predefined folding pathways that guides the protein in its search[9]. The main motive of protein folding studies is to search for independent folding pathways by making the protein unfold, refold, collapse and extend. However, once a protein is unfolded, say by, temperature or chemical denaturation, it is just a polymer with entropic elasticity described by worm-like chain model. The complexity of protein folding can thus be qualitatively described in terms of polymer entropic elasticity plus some non-covalent interactions like electrostatic, hydrophobic and hydrogen bonds. These interaction eventually stabilize protein to its unique 3-d conformation . Hence, single molecule force spectroscopy becomes a natural candidate to not just probe protein mechanics but to understand protein folding pathway even for non-mechanical proteins.

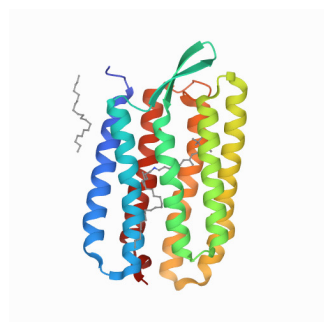
In this chapter, we investigate tandem repeats of immunoglobulin domain I27 of protein titin and protein bacteriorhodopsin found in cell membrane. The first protein titin has a clear mechanical function in elasticity of striated muscle tissue[10, 11]. It acts as a molecular spring that ensures the return of basic contractile unit of tissue called sacromere to its original configuration after a muscle has relaxed[11]. It also actively participates in generating mechanical power for contracting muscle by undergoing continuous unfolding and refolding under force[12]. The second membrane protein bacteriorhodopsin is responsible for the transport of proton ion across the cell membrane by responding to light stimuli[13, 14, 15]. It converts light energy into a proton gradient against which a proton is pumped across the membrane and ultimately used for ATP production(chemical energy) inside the cell. It therefore act as an effective channel for communicating with cell microenvironment. The unfolding behavior of above proteins have been studied with SMFS techniques like AFM constant velocity pulling experiments. The force-extension curve are recorded which depicts the entire unfolding process of proteins in series of force peaks or steps each representing an unfolding intermediate. The sequence of unfolding intermediates in the curve constitute an unfolding pathway. It was shown that protein with a clear mechanical function like titin and seemingly non-mechanical membrane protein have fundamentally distinct unfolding pathways[15].

In this work, we investigate the unfolding pathways using Passive Rheology. For this, local elastic response of protein is probed from thermal fluctuations. We measure the elastic response by recording fluctuations of AFM cantilever probe as the protein is pulled away at constant velocity. In this regard, we make use of results from fluctuation-dissipation theorem described in chapter 1. It tells us the fluctua-

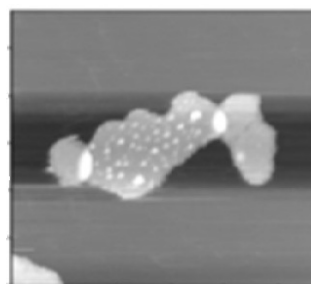
tions in a system encodes its mechanical response and allows us to measure response from calculation of frequency power spectrum of the fluctuation. At each extension of pulled protein, power spectral density (PSD) is calculated from time-series fluctuation to reveal the local elastic response. The study of thermal fluctuation is important because it could provide non-invasive and time-resolved way to distinguish various unfolding peaks associated with unfolding pathway. It gives access to finer-scale information about unfolding process. For AFM setup to measure the response of the single protein molecule only, it is crucial to understand the response due to cantilever probe and decouple its effect from intrinsic protein molecule response. This discussion forms a major part of the chapter where we discuss limited resolution to protein response from fluctuation measurement. We compare and contrast this to direct measurement of protein response discussed in chapter 3 and chapter 4 using active rheology.

5.2 Materials and Methods

Bacteriorhodopsin(BR) purple membrane preparation: To probe Bacteriorhodopsin(BR), the native purple membrane isolated from *Halobacterium salinarum* was adsorbed onto a freshly cleaved mica surface. The purple membrane patch forms a flat two-dimensional surface in which BR molecules are embedded in a trimer assembly. Each BR molecule is folded into seven closely packed transmembrane α -helices with short polypeptide loops connecting them as seen in figure 5.1a. The helices are labelled from A to G with G helix having C-terminus of polypeptide chain. The surface of purple membrane top forms the cytoplasmic side of membrane that exposes the C-terminal end and N-terminal end is in the extracellular side of membrane. To carry out AFM pulling experiments, a stock solution of $10\mu\text{g}/\text{ml}$ in buffer (300 mM KCl, 10 mM tris-HCl, pH 7.8) was prepared and drop of $30\ \mu\text{l}$ was incubated for 15 min. Thereafter, solution was first rinsed with buffer to remove loose membrane patches and AFM imaging of the patch was done in buffer as shown in figure 5.1b. The patch area was zoomed in to position AFM cantilever tip at the location for force map measurements.



(a) 3-D structure of Bacteriorhodopsin (BR) with seven trans-membrane helices connected by polypeptide loops.



(b) AFM image of patch of purple membrane taken using tapping mode and zoomed in to extract BR molecule.

Figure 5.1

I27 domain repeats preparation: The recombinant DNA technology is used

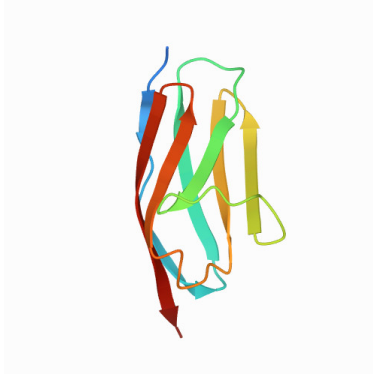


Figure 5.2: The I27 domain from protein Titin consisting of beta-sheet secondary structure connected with hydrogen bonds (not shown).

in the past to engineer polyproteins that consist domains of I27 (shown in fig 5.2) arranged in tandem. The polyprotein used here is 8 tandem repeats of Immunoglobulin (I27) domain from muscle protein Titin. To measure AFM force-extension curves, a $10 \mu\text{l}$ stock solution polyprotein in PBS buffer was prepared after purification procedure. Thereafter, gold coverslips were manufactured from thermal vapor deposition system and $60 \mu\text{l}$ of solution was incubated on clean gold coverslip. The polyprotein forms a thiol bond between the cysteine group of protein and gold surface for strong attachment. Before force measurement, the sample was rinsed several times to remove loosely bound molecules.

AFM Force measurements

For Bacteriorhodopsin force measurements, tip of the AFM cantilever was brought in contact with the membrane for 1 s with a contact force of 1 nN. This allows a random and non-specific adsorption of some site on the protein to AFM tip. The cantilever was then pulled away from protein surface with a constant velocity of 200 nm/s . The force-extension curves with different extensions ranging from 20 to 75 nm were generated. At this point, a data selection criteria was adopted in which curves with maximum extension close to 70 nm were only analyzed. This length of 70 nm corroborate well with total length of 248 amino acids of unfolded protein and ensures that AFM tip attached to C-terminal end is extracted and fully unfolded. The AFM pulling experiments on BR were performed using silicon nitride (Si_3N_4) cantilevers from Micromash with a spring constant value $k \sim 0.03 \text{ N/m}$. The calibration of spring constant of a cantilever is critical for accurate force measurements and is determined using the thermal noise method [16] described in chapter 2. All pulling experiments were carried out in Tris-buffer solution (300 mM KCl, 10 mM tris-HCl, pH 7.8).

The AFM pulling experiments on I27 were performed similar to BR molecules. The cantilever was approached in contact with a force of 1 nN for 1 s. The choice of cantilever spring constant was $k \sim 0.03 \text{ N/m}$. Through nonspecific attachment, the polyprotein molecule is pulled away at constant velocity of 200 nm/s . This generated a characteristic force-extension profile for polyprotein as discussed later. In contrast to BR molecule, selection of one force curve over another need not be made due to unfolding signatures comes from the same domain type. It is true that not all the time all 8 domains are unfolded due to nonspecific attachment but information about domain at a single molecule level can still be easily extracted. In

our analysis, we selected force curves where more than 4 domains were unfolded. In addition, time series data collection and analysis was similar to BR molecule.

Deflection Time series

The high frequency time series of deflection signal was additionally recorded using dedicated computer fitted with Data Acquisition card (14 bit PCI-9820 Adlink Technology) . With this analog signal from photodiode was digitized and sampled with rate of 500 KHz. Before sampling at this rate the deflection signal was low pass filtered at 250 KHz(Nyquist frequency) by feeding the photodiode signal to hardware filter. This is done to avoid aliasing problem in digitization with DAQ card. The total time series data of few seconds was divided into time windows of 1.6 ms and in each window power spectral density was calculated on time series $X(t)$ as:

$$S_X(\omega) = \lim_{T \rightarrow \infty} \frac{|\int_0^T dt X(t) e^{i\omega t}|^2}{T} \quad (5.1)$$

where intergral on $X(t)$ is the finite time discrete fourier transform. By resampling the data in the time window, 10 power spectral density(PSD) estimate $S_X(\omega)$ were calculated using Welch method with hanning window. These 10 PSD estimate were averaged to obtain a final PSD assigned to 1.6 ms time window. This process is expected to reduce the noise in Power Spectral density. Therefore, at each extension or time step of 1.6 ms power spectral density was calculated.

5.3 Results and Discussion

5.3.1 Bacteriorhodopsin

The force extension curve in figure 5.3 records a typical extraction and unfolding process of Bacteriorhodopsin from purple membrane. The observed series of force peaks represent unfolding of structural element as mechanical force lowers the energy barrier stabilizing the structural elements. The unfolding proceeds in sequence of structural elements beginning with C-terminal and ending at N-terminal end where all elements are unfolded for extension upto 70 nm. After stretching the free C-terminal, the helix G and F unfolds in pair first, followed by E and F and finally B and C. The pair unfolding is observed as three main peaks at force of ~ 140 pN in figure 5.3. The peak unfolding force decreases as chain is extended and more elements in sequence are unfolded. This is due to destabilization caused by already unfolded segment's to the overall structure. In between the peaks is WLC stretching of unfolded segments that behave as polymer with entropic spring. The intermediate unfolding events could also be seen that correspond to partially stable loops interconnecting the helices. For a detailed assignment of force peaks to structural elements please see [13]. When the force extension curves are repeated, the three main peaks are observed with almost 90% probability while intermediates are observed with a lesser probability. This indicates that sequence of unfolding intermediates represents a rare unfolding pathway and infact indicates that there exist multiple pathway of protein unfolding.

Power spectral density analysis of thermal deflection time series

Next step in the analysis was to collect the time series data for thermal deflection of cantilever as protein is extended. From this time series, Power Spectral Density was computed at each extension using equation 5.1. As explained in chapter 1,

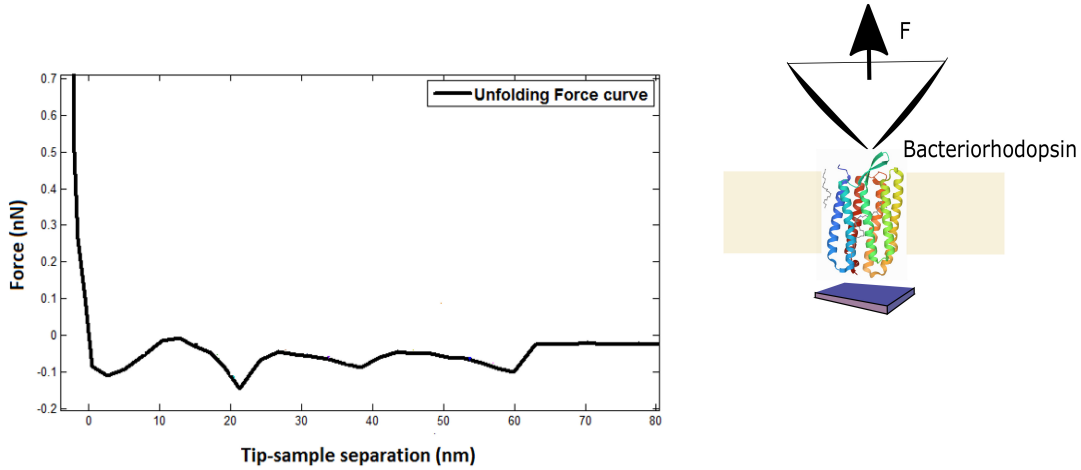


Figure 5.3: The unfolding force profile of Bacteriorhodopsin (BR) as a function of extension. The protein is pulled from C-terminal end and seven helices of secondary structure unfolds in pair as depicted with three main force peaks.

equilibrium fluctuations are intimately related to linear response of system to time dependent external perturbation. We already extracted the linear response for simple polymers in chapter 2, by directly oscillatory the AFM cantilever. Here, we use thermal fluctuation to indirectly compute linear response, in particular the elastic response. According to fluctuation dissipation theorem, power spectral density $S_X(\omega)$ of dynamical variable $X(t)$ describing the time series of thermal fluctuations is proportional to frequency response function $\chi(\omega)$ and given as:

$$S_X(\omega) = \frac{2k_B T}{\omega} \chi''(\omega) \quad (5.2)$$

Importantly, the measured PSD in experiments will be determined by the combined response of cantilever and protein. To model combined response, we need to consider the response of cantilever and protein separately and eventually couple them suitably. In absence of protein, dynamics of cantilever displacement $X(t)$ can be simply described by simple harmonic oscillator (SHO) model $m\ddot{X} + \gamma_c\dot{X} + k_cX = f_b(t)$, subjected to stochastic brownian forces $f_b(t)$. A protein attached to cantilever, on other hand, can be represented by a dumbbell model consisting of spring k_p and dashpot γ_p of protein. At all times, the displacement of protein will be equal and opposite to cantilever but force exerted by dumbbell $-\gamma_p\dot{X} - k_pX$ must be balanced by SHO cantilever for internal equilibrium. The equation of motion for the system becomes

$$m\ddot{X} + \gamma\dot{X} + kX = f_b(t) \quad (5.3)$$

Therefore, combined protein and cantilever response again correspond to SHO model where protein stiffness and damping effectively adds to cantilever such that $k = k_p + k_c$ and $\gamma = \gamma_p + \gamma_c$. This addition signifies a parallel coupling mechanism where response of dominant component in system determines the overall response. This is in contrast to series coupling mechanism where least dominant component determines the overall response. We will see the implication of such coupling pathway

later. Now, on taking fourier transform of eq 5.3 we get frequency response $\chi(\omega)$. Plugging $\chi(\omega)$ into equation 5.2 yields the following form of PSD :

$$S_X(\omega) = \frac{2k_B T \gamma}{(k - m\omega^2)^2 + (\omega\gamma)^2} \quad (5.4)$$

The modelling of experimentally measured PSD with above analytical form of PSD reveals the elastic k and dissipative γ information about the protein. Our previous study has shown that dissipative response from protein molecule γ_p is immeasurably low and therefore can be neglected[17]. Hence, we focus our attention on stiffness k_p extraction from measured PSD with $\gamma = \gamma_c$.

Figure 5.4a shows the various location points (arrows) along the unfolding force curve of Bacteriorhodopsin where time series data was sampled. The time series for thermal deflections of cantilever at blue arrow and red arrow point are explicitly shown in figure 5.4a and subsequently converted to PSD in figure 5.4b. The bright green arrow timeseries which represents a free cantilever without protein was also converted to PSD and depicted in fig 5.4b. The PSD peak observed close to resonance frequency (~ 4 KHz) are well defined but there exist various other peaks for frequency less than 2 KHz and greater than 8 KHz. The origin of peak in red PSD at frequencies less than 2 KHz lies in noisy time series that is sampled. The red time series is clearly non-stationary in time due to presence of multiscale noise sources and this gets reflected as noise peaks in frequency domain. Similarly, the timeseries in blue that appear stationary compared to red still has peaks in PSD at frequencies larger than 8 KHz. The noise sources responsible are not only instrument measurement noise and drift but also associated with finite discrete sampling of continuous cantilever fluctuations. Finite sampling noise causes the PSD to vary and fluctuate from one sampled series to another and therefore a larger time window close to 10 ms was chosen for sampling to reduce variation in observed PSD. However, there always exist a trade-off between time resolution required and noise in measured PSD. The well defined PSD peaks were fitted with eq 5.4 and stiffness k_p was extracted by subtracting the cantilever contribution k_c .

| Stiffness event 1 Stiffness (mN/m) | Stiffness event 2(mN/m) | Stiffness event 3(mN/m) |
|------------------------------------|-------------------------|-------------------------|
| 19 | 12 | 13 |
| 42 | 14 | 14 |
| 22 | 22 | 12 |
| | 17 | 19 |

Table 5.1

Table 5.1 shows the stiffness extracted for three main unfolding events. For event 1, stiffness was calculated for three locations marked with arrow in figure 5.4a. Similarly, 4 locations each for unfolding event 2 and 3 were calculated for stiffness. The force-extension curve shows that unfolding event 1 has a steep change in stiffness compared to unfolding event 2 and event 3. However stiffness k_p measured for this event tabulated at three locations in table 5.1 does not change significantly from free cantilever. It is clear from the table that stiffness although does change slightly at increasing force but is not in accord with sharp changes seen in force extension curve.

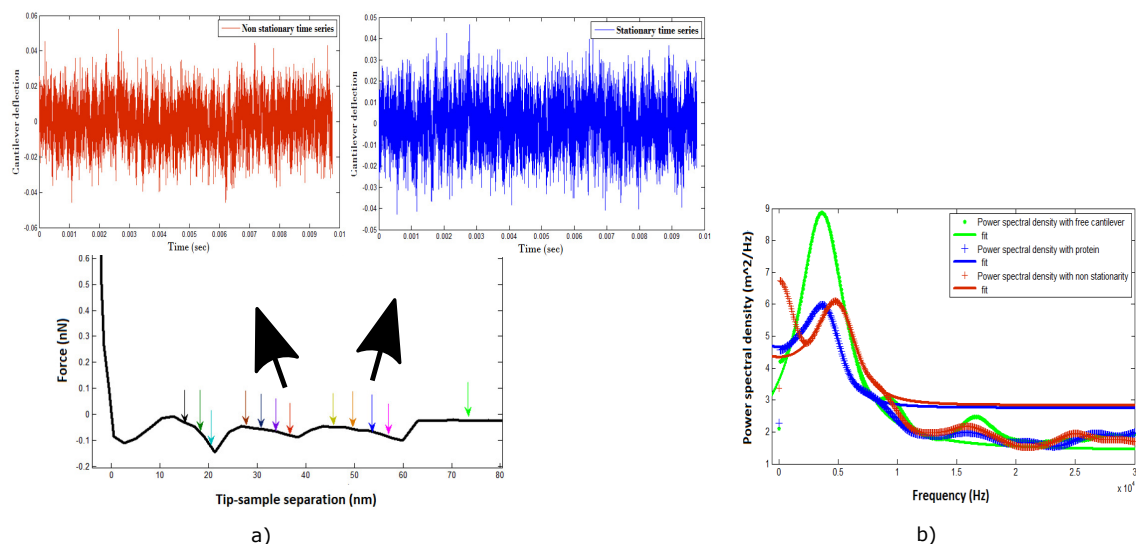


Figure 5.4: a) Time series data collected as various locations along the unfolding protein marked by arrows. The time series corresponding to blue and red arrow point are shown in an enlarged view. b) The Power Spectral Density (PSD) estimate for free cantilever (green arrow) and cantilever plus protein (blue and red arrow)

5.3.2 I27 repeats

The AFM pulling experiment on eight tandem repeats of immunoglobulin domains from protein titin are shown in figure 5.5. It shows a characteristic sawtooth pattern with discontinuities at periodic intervals of length 25 to 28 nm. Each discontinuity represents the cooperative unfolding of a I27 domain in all or none fashion and force peak observed in the pattern close to 200 pN measures the unfolding force. A protein once unfolded behaves like a polymer coil described by WLC entropic elasticity and its further stretching contributes an increased length or extension of chain by 25-28 nm. Since the protein is picked at random, anywhere between 0 to 8 unfolding events could mostly be observed before protein detaches from the AFM tip. The unfolding of repeats proceeds by mechanical force lowering a kinetic barrier and thermal kicks randomly guides any one of domain to unfold first and some other domain next and so on. So the unfolding is not sequentially but probabilistic in which any domain in tandem arrangement could unfold [18, 19]. This is different from BR unfolding where first structural element in the sequence and close to AFM tip unfolds first and then subsequent elements comes out from the membrane. As observed, the unfolding pathway for this protein is straightforward with no intermediate unfolding events. This means that protein simply folds in a two-state manner, choosing one single pathway instead of multiple pathway on protein energy landscape. This is expected for proteins with singular mechanical function that involved simple stretching and contraction of muscle.

Next, we grabbed the thermal deflection of AFM cantilever as a function of extension as shown in figure 5.6. From the time series we selected location with domain unfolding (red arrow) and a free cantilever without protein (green arrow). Corresponding to these time series power spectral density (PSD) was calculated as shown in figure 5.6b. This allows straight comparison of changes in stiffness of protein by looking at the peak of PSD. As observed, the peak did not change in any significant manner and this trend was further confirmed by actual fitting the PSD

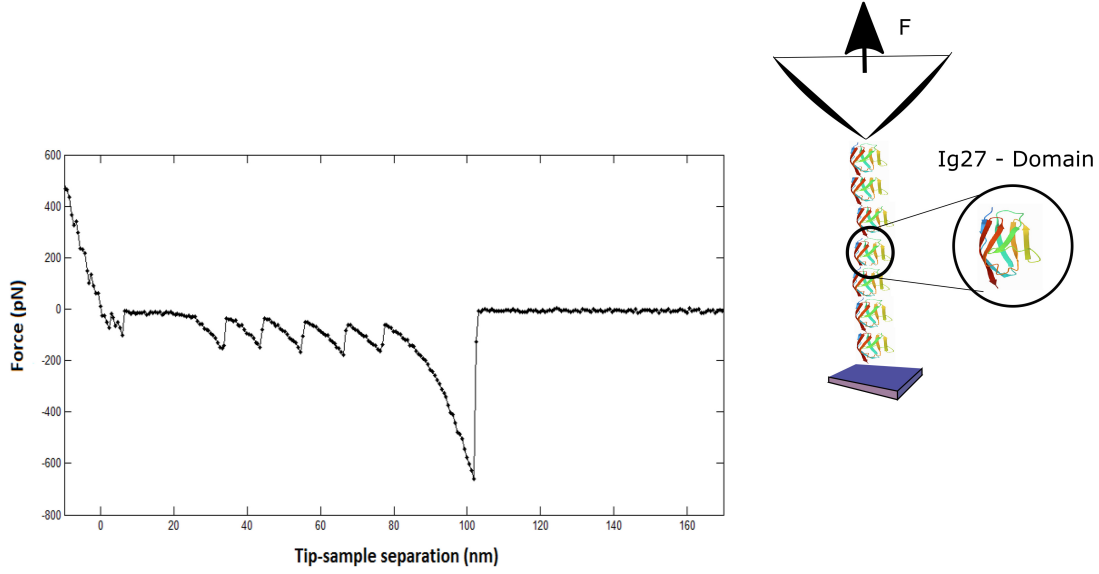


Figure 5.5: The pulling force-extension curve shows five unfolding events corresponding to unfolding of each I27 domain.

with equation 5.4 to extract k_p . Figure 5.7 depicts the changes in the peak as force is changed in a single I27 domain from 60 to 180 pN. No significant change was seen except for very large force close to 180 pN. This insensitivity to stiffness which is similar to what was observed for BR molecule needs explanation. In next section we try to explain the reasons for observed behavior.

5.3.3 Explanation

To explain the observed trend, we consider both time domain and frequency domain analysis for thermal fluctuations detected in AFM measurement.

Time Domain Analysis

In time domain analysis we look at the variance measure of fluctuation by writing the probability distribution for coupled cantilever-protein system. The energy in cantilever $k_c \delta^2/2$ and free energy F of protein effectively adds up to give probability distribution for the end-to-end distance $D = \delta + x$ as :

$$p(D) \sim e^{-\beta(F(D-\delta)+k_c\delta^2/2)} \quad (5.5)$$

Here $\beta = 1/k_B T$, x is extension of protein and δ is deflection of cantilever. By doing a Taylor expansion about D we get the following :

$$F(D - \delta) = F(D) - \frac{dF}{dD}\delta + \frac{1}{2} \frac{d^2F}{dD^2}\delta^2 \dots \quad (5.6)$$

$F(D)$ is a constant that can be set to zero since we are interested in fluctuation about mean behavior and system is in equilibrium which makes the the first derivative zero. Therefore, combining the Taylor expansion with probability distribution, we get the a Gaussian distribution in deflection δ or extension of protein x with variance:

$$(\Delta\delta)^2 = (\Delta x)^2 = \frac{k_B T}{k_c + \frac{d^2F}{dD^2}} \sim \frac{k_B T}{k_c + k_p} \quad (5.7)$$

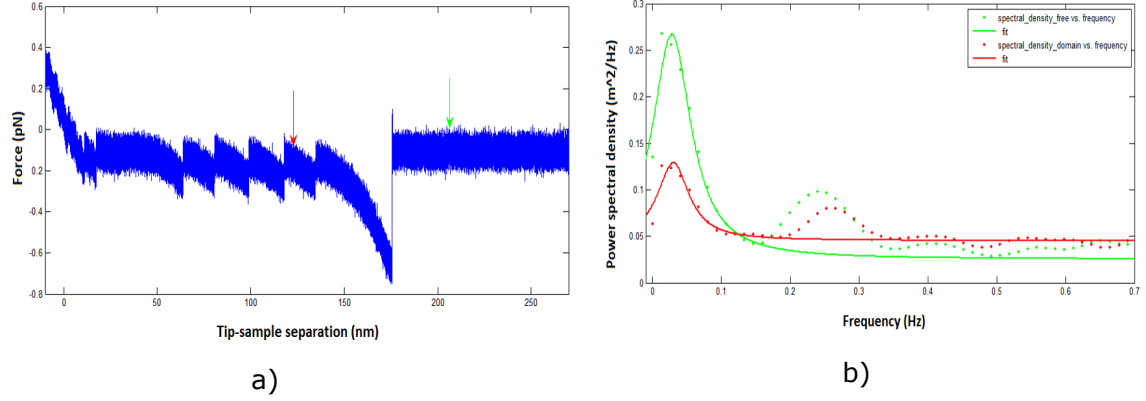


Figure 5.6: Time series for thermal deflection of cantilever are recorded as the protein is pulled and power spectral density was calculated for free cantilever (green arrow point) and cantilever plus protein (red arrow point)

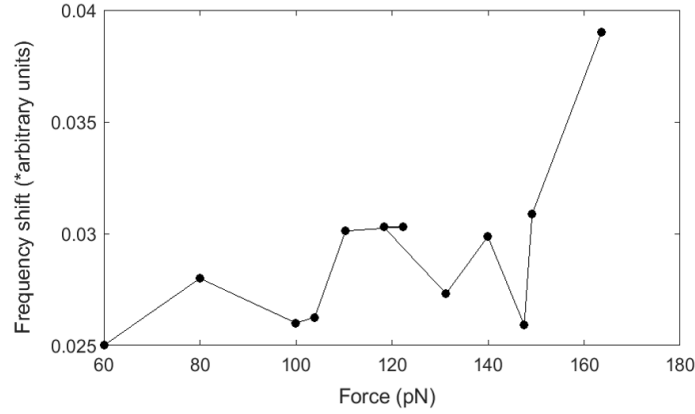


Figure 5.7: The changes in frequency of PSD peak as a function of force on the I27 domain.

The strength of fluctuation or variance in extension is same as in deflection because D relating them is a quantity that we control and hence not fluctuating. Importantly, we measure fluctuations in extension as a result of fluctuation in force whose strength is defined with Nyquist theorem $(\Delta f)^2 = 4k_B T \gamma B$. This is a special case for fluctuation-dissipation theorem where fluctuation are determined by damping γ of cantilever when measured for a finite bandwidth B . Therefore more accurate formula for describing fluctuations in extension x is :

$$(x - \bar{x})^2 = (\Delta x)^2 = \frac{4k_B T \gamma B}{k_c + k_p} \quad (5.8)$$

It is obvious from above equation that fluctuations in extension of protein molecule are determined by both cantilever and protein acting in a parallel or additive combination $k_c + k_p$. The stiffness of cantilever is constant but that of protein goes from zero to a maximum. At zero protein stiffness the fluctuations in extension are maximum, as commonly observed in flat regions of force-extension curve. It is generally the case that cantilever stiffness is either comparable or more than the stiffness of protein. And hence the thermal fluctuation in protein extension are limited by that of cantilever stiffness and are generally small. If we consider another experimental

scenario in which force on molecule is maintained constant, for instance with magnetic tweezers, the effect of cantilever is then averaged out and large fluctuations due to protein itself are being sampled. It is generally observed that fluctuation in magnetic tweezer setup are large due to constant force (effective zero stiffness $k_c = 0$) measurements. In this case the fluctuations in extension are given as :

$$(\Delta x)^2 = \frac{4k_B T \gamma B}{k_p} \quad (5.9)$$

In addition, damping factor of cantilever is also a major limiting factor in thermal fluctuation variance. The viscous damping factor for a huge cantilever is large compared to a small protein molecule attached at its end and in turn dominantly determines the fluctuation in extension. This will become more clear in frequency domain analysis. All this makes fluctuation measurement being limited by cantilever rather than a protein.

Frequency Domain Analysis

The effect of thermal fluctuations can be more vividly described in terms of PSD. It is easy to show using Parseval theorem that integration of PSD over all frequencies is just the average variance of eq 5.8. So a time domain analysis is merely an integrated measure of thermal fluctuations. Instead, PSD expresses fluctuation in its frequency component [20] and helps to elucidate the time scale dependent nature of randomness.

The physical meaning of Power Spectral Density is actually the power that is dissipated in fluctuations and therefore determined by out of phase dissipative response of system $\chi''(\omega)$. It can be written in terms of relaxation time $\tau = \gamma/k$ and resonance frequency ω_0 :

$$S_X(\omega) = \frac{1}{k} \frac{2k_B T \tau}{(1 - (\frac{\omega}{\omega_0})^2)^2 + (\omega\tau)^2} \quad (5.10)$$

At low frequency $\omega < 1/\tau$ the power spectral density is low and constant in frequency and given by :

$$S(\omega) = \frac{2k_B T \gamma}{k^2} \quad (5.11)$$

It is seen that the system stiffness k dominantly determines the PSD. These observations can be explained by considering the fact that for large timescales ($> \tau = \gamma/k > 1/\omega_0$) the Langevin equation 5.3, describing the response, is dominated by elasticity $kX(t) = f_b(t)$. In other words, large enough timescale greater than relaxation time τ allows the fluctuation to relax to equilibrium with autocorrelation $\langle X(0)X(t) \rangle$ being uncorrelated . Therefore, fluctuations are probing equilibrium elasticity and power dissipated is also small.

At high frequency $\omega > 1/\tau$, power spectral density decays as $1/\omega^2$ and depends on damping of cantilever as:

$$S(\omega) = \frac{2k_B T}{\gamma \omega^2} \quad (5.12)$$

It is because for frequencies $\omega > 1/\tau$ the system is not allowed to relax to equilibrium and hence response is dominated by dissipation. The Langevin equation becomes $\gamma X(t) = f_b(t)$ corresponding to free diffusion with characteristic $1/\omega_0^2$ dependence of diffusion dynamics. This means that as we keep on increasing the frequency,

fluctuations encapsulated in PSD are not probing elasticity but dissipation. The resonance peak of PSD at frequency ($\omega \sim \omega_0$) is critically determined by γ and defines a maximum in power dissipation. Therefore, damping of cantilever is more dominant factor for close to resonance operation which forms the basis of our stiffness analysis.

5.4 Comparison between Active and Passive Rheology

In conclusion, the overall fluctuation that are measured comes from the combined response of both cantilever and protein to brownian forces. Since cantilever is a massive object with large damping and relatively large stiffness, its response especially the damping/dissipative response limits us from measuring fluctuations from protein only. Coupling with AFM cantilever makes the measurement of protein elastic response from fluctuations less sensitive. This is true even when it is expected that fluctuations from softer protein molecule alone is either comparable or larger than cantilever. It is however important to note that there is a still a change in stiffness observed for fluctuation measurement in case of large/steep change in force as shown in figure 5.7. In previous work with polysaccharides, it was similarly observed that there is a change in stiffness only when there is sharp feature in the force-extension curve[21].

Insensitivity to fluctuations in force-extension curve was evident to some extent in section 4.4 chapter 4. Here we saw that simple force-extension curve showed no variations in fluctuations with size of polymer length. In contrast, active oscillations employed showed a clear dependence of fluctuations in measured stiffness on the size of polymer. Although active measurements are invasive and limited in time resolution but its measurement of average stiffness and its fluctuations makes it an important technique to probe polymer response and its elasticity.

5.5 Chapter Summary

In this chapter, we employed thermal fluctuations of AFM cantilever to extract the elastic response of I27 domain of protein Titin and membrane protein Bacteriorhodopsin. The thermal deflections of cantilever were converted into power spectral density estimate using fluctuation-dissipation theorem. Stiffness of protein molecule was extracted by modelling the fluctuation using simple harmonic oscillator in presence of Brownian forces. By working in both frequency and time domain we showed that fluctuations measured from the AFM cantilever comes dominantly from the cantilever itself because of its huge damping factor compared to protein molecule. As expected, only with sharp change in force did we saw a change in stiffness. Our work suggest the use of active oscillations as a more reliable rheological technique to probe the response of single polymer. In addition, we saw strong signature for non-stationarity especially for bacteriorhodopsin. This may include the possibility of different noise sources including finite sampling time. However, comparatively less non-stationarity observed in I27 may also reflect differences in unfolding landscapes of two functionally different proteins. Bacteriorhodopsin unfold through variety of intermediates while unfolding of I27 is all or none fashion.

Bibliography

- [1] Yalda Javadi, Julio M Fernandez, and Raul Perez-Jimenez. Protein folding under mechanical forces: a physiological view. *Physiology*, 2013.
- [2] Carlos Bustamante, Yann R Chemla, Nancy R Forde, and David Izhaky. Mechanical processes in biochemistry. *Annual review of biochemistry*, 73(1):705–748, 2004.
- [3] Jorge Alegre-Cebollada. Protein nanomechanics in biological context. *Biophysical Reviews*, pages 1–20, 2021.
- [4] Mariano Carrion-Vazquez, Andres F Oberhauser, Thomas E Fisher, Piotr E Marszalek, Hongbin Li, and Julio M Fernandez. Mechanical design of proteins studied by single-molecule force spectroscopy and protein engineering. *Progress in biophysics and molecular biology*, 74(1-2):63–91, 2000.
- [5] Ionel Popa and Ronen Berkovich. Mechanobiology: protein refolding under force. *Emerging Topics in Life Sciences*, 2(5):687–699, 2018.
- [6] Jörg Schönfelder, David De Sancho, and Raul Perez-Jimenez. The power of force: insights into the protein folding process using single-molecule force spectroscopy. *Journal of molecular biology*, 428(21):4245–4257, 2016.
- [7] Michael T Woodside and Steven M Block. Reconstructing folding energy landscapes by single-molecule force spectroscopy. *Annual review of biophysics*, 43: 19–39, 2014.
- [8] José Nelson Onuchic, Zaida Luthey-Schulten, and Peter G Wolynes. Theory of protein folding: the energy landscape perspective. *Annual review of physical chemistry*, 48(1):545–600, 1997.
- [9] S Walter Englander and Leland Mayne. The nature of protein folding pathways. *Proceedings of the National Academy of Sciences*, 111(45):15873–15880, 2014.
- [10] Matthias Rief, Mathias Gautel, Philipp Oesterhelt, Julio M Fernandez, and Hermann E Gaub. Reversible unfolding of individual titin immunoglobulin domains by afm. *science*, 276(5315):1109–1112, 1997.
- [11] Hongbin Li, Wolfgang A Linke, Andres F Oberhauser, Mariano Carrion-Vazquez, Jason G Kerkvliet, Hui Lu, Piotr E Marszalek, and Julio M Fernandez. Reverse engineering of the giant muscle protein titin. *Nature*, 418 (6901):998–1002, 2002.

- [12] Jaime Andrés Rivas-Pardo, Edward C Eckels, Ionel Popa, Pallav Kosuri, Wolfgang A Linke, and Julio M Fernández. Work done by titin protein folding assists muscle contraction. *Cell reports*, 14(6):1339–1347, 2016.
- [13] Daniel J Müller, Max Kessler, Philipp Oesterhelt, Clemens Möller, Dieter Oesterhelt, and Hermann Gaub. Stability of bacteriorhodopsin α -helices and loops analyzed by single-molecule force spectroscopy. *Biophysical Journal*, 83(6):3578–3588, 2002.
- [14] F Oesterhelt, D Oesterhelt, M Pfeiffer, A Engel, HE Gaub, and DJ Müller. Unfolding pathways of individual bacteriorhodopsins. *Science*, 288(5463):143–146, 2000.
- [15] Alexej Kedrov, Harald Janovjak, K Tanuj Sapra, and Daniel J Müller. Deciphering molecular interactions of native membrane proteins by single-molecule force spectroscopy. *Annu. Rev. Biophys. Biomol. Struct.*, 36:233–260, 2007.
- [16] H-J Butt and Manfred Jaschke. Calculation of thermal noise in atomic force microscopy. *Nanotechnology*, 6(1):1, 1995.
- [17] Shatruhan Singh Rajput, Surya Pratap S Deopa, Jyoti Yadav, Vikhyaat Ahlawat, Saurabh Talele, and Shivprasad Patil. The nano-scale viscoelasticity using atomic force microscopy in liquid environment. *Nanotechnology*, 32(8):085103, 2020.
- [18] Hongbin Li, Andres F Oberhauser, Susan B Fowler, Jane Clarke, and Julio M Fernandez. Atomic force microscopy reveals the mechanical design of a modular protein. *Proceedings of the National Academy of Sciences*, 97(12):6527–6531, 2000.
- [19] Toni Hoffmann and Lorna Dougan. Single molecule force spectroscopy using polyproteins. *Chemical Society Reviews*, 41(14):4781–4796, 2012.
- [20] Frederick Gittes and Christoph F Schmidt. Thermal noise limitations on micromechanical experiments. *European biophysics journal*, 27(1):75–81, 1998.
- [21] Christian A Bippes, Andrew DL Humphris, Martin Stark, Daniel J Müller, and Harald Janovjak. Direct measurement of single-molecule visco-elasticity in atomic force microscope force-extension experiments. *European Biophysics Journal*, 35(3):287–292, 2006.

Chapter 6

Conclusion

6.1 Summary and Conclusions

Fluctuations play a decisive role in understanding functioning of polymers including biological polymers such as proteins. Contrary to a macroscopic system, a single polymer chain undergoes entropic fluctuation in a thermal environment. The possession of entropy is due to vast number of configurations that a polymer chain can adopt under thermal environment. The sudden decrease of configuration space upon stretching under applied force give rise to its entropic elasticity. The aim of my work was to interpret this elasticity using Atomic Force Microscope (AFM).

A local length-scale called persistence length characterizes its elasticity. However, its measurement in conventional AFM pulling experiment is consistently low and nonphysical. To addresses this question, we propose a method to directly and locally measure the stiffness of a single polymer chain using AFM. We provided sub-nm oscillations to the chain by actively oscillating AFM cantilever probe at off-resonance frequencies. This ensured that overall response is linear and dominated by elastic response. From the oscillatory response, the stiffness of synthetic and neutral flexible polymer of PEG (polyethylene glycol) and polystyrene was investigated in good and poor solvent. It was found that stiffness deviated significantly from conventional AFM force-extension curves only in good solvents but polymer in poor solvent showed no deviation. The results were rationalized by considering a proper statistical mechanics of combined cantilever-polymer system. For good solvents, analysis with entropic model of WLC produced a large and physical value of persistence length that matched well with constant force magnetic tweezer experiments. Additional free energy contribution explains no deviation seen in case of poor solvents. In terms of fluctuation about the mean value, a short length polymer of PEG showed more fluctuations in contrast to long length polystyrene polymer. This is expected according to polymer physics but was not observed in conventional pulling experiments. We also performed similar measurements with home-built interferometer-based AFM. The fiber-interferometer assembly measures cantilever deflection directly at a local point in contrast to commercial beam deflection methods. This is important while oscillating the cantilever base in liquids. A local detection at a point provides a straightforward interpretation of stiffness, independent of complications from cantilever hydrodynamics. This independently confirmed our results and measurement methodology with that of commercial AFM.

We conclude from this that active rheology combined with a simple and artifact

free interpretation of observations is a tour de force in making quantitative measurement of polymer elasticity and assessing a bias in conventional pulling experiments. The results points to the importance of coupling between AFM-cantilever and intrinsic polymer response. A large and physical value of persistence length also suggest that WLC model, even though a phenomenological model, can satisfactorily describe the elasticity of single neutral flexible polymers. It, however, suggest caution at its applicability in poor solvent.

We also performed passive rheology measurements on proteins with mechanical role like titin I27 domain and membrane protein bacteriorhodopsin which has no clear mechanical function. Instead of actively oscillating the cantilever, we passively captured thermal fluctuation of cantilever as cantilever stretches a polymer. We performed spectral analysis on the time series of thermal fluctuations and used fluctuation-dissipation relation to obtain elasticity estimate. The results points to insensitivity of thermal fluctuation measurement to elastic response. The main reason include the fact that measurements are made with a macroscopic cantilever with large damping and comparatively large stiffness. This makes fluctuations less sensitive to polymer elasticity especially when there are no sharp changes in force-extension curve. Other sources like non-stationary time series are also a contributing factor. Although, differences in non-stationarity observed between I27 and Bacteriorhodopsin may also hint to a different unfolding landscape for two very functionally different proteins.

6.2 Future Direction

In the thesis, we showed that the bias in single molecule pulling experiment is due to the statistical convolution. However, there exist another possibility for bias. It is based on the fact that large hydrodynamic damping of AFM cantilever limits the time resolution of measurement. It means that non-equilibrium effects that may arise due to pulling of on polymer may not show up due to limited parameter space of the experiment. The non-equilibrium effects in pulling experiments have been considered in the past and analysis is also carried out using non-equilibrium relations like Jarzynski Equality[1, 2]. Based on analysis of Jarzynski relation and using principles from stochastic thermodynamics, it has been proposed[3, 4] that oscillatory loading may be a more accurate protocol to probe elastic free energy landscape. This is mainly due to the forward-reverse nature of oscillating protocol which makes it more equilibrium like protocol than a unidirectional pulling experiment. We considered such explanations for results obtained in our thesis but the precise mathematical assumptions underlying such a idea did not strictly obey our experimental conditions. In future, it is important to however consider such non-equilibrium effects of pulling experiments and devise optimal protocols based on stochastic thermodynamics[4]. In this regard, development of high speed AFM's is important since it extensions the time resolution of current AFMs significantly This allows for a large parameter space to view non-equilibrium effects.

Bibliography

- [1] Gerhard Hummer and Attila Szabo. Free energy reconstruction from nonequilibrium single-molecule pulling experiments. *Proceedings of the National Academy of Sciences*, 98(7):3658–3661, 2001.
- [2] Nolan C Harris, Yang Song, and Ching-Hwa Kiang. Experimental free energy surface reconstruction from single-molecule force spectroscopy using jarzynski’s equality. *Physical review letters*, 99(6):068101, 2007.
- [3] Oliver Braun, Andreas Hanke, and Udo Seifert. Probing molecular free energy landscapes by periodic loading. *Physical review letters*, 93(15):158105, 2004.
- [4] Tim Schmiedl and Udo Seifert. Optimal finite-time processes in stochastic thermodynamics. *Physical review letters*, 98(10):108301, 2007.